C.P. No. 798

C.P. No. 798

MINISTRY OF AVIATION

AERONAUTICAL RESEARCH COUNCIL

CURRENT PAPERS

Wind Tunnel Tests at Mach Numbers up to 1.8 on a Model with 1/36 Scale Wings and Nacelles of a Twin-Engined Supersonic Aircraft (Bristol 188)

by

E. P. Sutton, P. G. Hutton and L. C. Squire

LONDON: HER MAJESTY'S STATIONERY OFFICE

1965

PRICE 12s 6d NET

U.D.C. No. 533.6.011.35/5 Bristol 188

C.P. No. 798

February, 1958

WIND TUNNEL TESTS AT MACH NUMBERS UP TO 1.8 ON A MODEL WITH 1/36 SCALE WINGS AND NACELLES OF A TWIN-ENGINED SUPERSONIC AIRCRAFT (BRISTOL 188)

by

E.P. Sutton, P.G. Hutton, and L.C. Squire

SUMMARY

Tests have been made in the R.A.E. Bedford 3 foot tunnel on a model representing the exposed wing and nacelles of the Bristol 188 aircraft, mounted on an ogive-cylinder body. The wing was unswept inboard but had a swept-back leading edge outboard of the nacelles. Lift, drag, and pitching moment, and rolling moment due to aileron deflection, were measured at Mach numbers between 0.7 and 1.02 and between 1.4 and 1.8 at a Reynolds number of 1.7×10^6 based on mean aerodynamic chord.

At high subsonic speeds separations on the unswept inner wing dominate the characteristics of the model at incidence. Fitting leading edge vortex generators delays the effects of leading edge separation. The horn-balanced ailerons are effective throughout the test range.

The surface oil-flow technique was used as an aid to interpretation of the measurements.

Replaces R.A.E. Tech. Note No. Aero 2543 - A.R.C. 20303.

LIST OF CONTENTS

		Page
1	INTRODUCTION	6
2	DETAILS OF THE TESTS	6
	2.1 Description of the model	6
	2.2 Experimental technique	7
	2.3 Range of the tests	7
	2.4 Corrections applied and reduction of the results	8
	2.5 Accuracy	8
3	RESULTS AND DISCUSSION	9
	3.1 Lift, pitching moment, and drag of the basic model	9
	3.1.1 Lift and pitching moment	9
	3.1.2 Drag	11
	3.2 Contribution of the nacelles to lift, pitching moment, and drag	12
	3.2.1 Results of tests on the model without nacelles	12
	3.2.2 Results of tests on the model with no flow through the nacelles	13
	3.3 Lift, pitching moment, and drag of the model with leading edge vortex generators	14
	3.4 Effect of the aileron edge gaps on lift and pitching moment	14
	3.5 Results of aileron tests	15
	3.5.1 Rolling moment due to aileron deflection	15
	3.5.2 Normal force and pitching moment due to aileron deflection	15
4	CONCLUSIONS	16
	LIST OF SYMBOLS	17
	LIST OF REFERENCES	18
	APPENDIX 1	19
	TABLES 1 - 12	21-37
	ILLUSTRATIONS - Figs. 1 - 33	3-5
	DETACHABLE ABSTRACT CARDS	-

APPENDIX

1	Note on effects of mounting the wings on a non-representative body	19

LIST OF TABLES

Table		Page
1	Principal dimensions of the model	21
2	Wing sections	22
3	Measured aileron deflection angles	23
4	Aerodynamic coefficients of the basic model	24
5	Aerodynamic coefficients of the model with nacelles removed	27
6	Aerodynamic coefficients of the model with no flow through the nacelles	28
7	Aerodynamic coefficients of the model with leading edge vortex generators	29
8	Aerodynamic coefficients of the model with ailerons represented	31
9	Values of $\left(\frac{\partial C_L}{\partial \alpha}\right)_o$ for the tested configurations	36
10	Values of $\left(\frac{\partial C_m}{\partial C_L}\right)_o$ for the tested configurations	36
11	Values of $\left(C_D\right)_o$ for the tested configurations	37
12	Values of $\left(\frac{\partial C_L}{\partial \alpha}\right)_o$, $\left(\frac{\partial C_m}{\partial C_L}\right)_o$, $\left(C_D\right)_o$ for the body alone	37

LIST OF ILLUSTRATIONS

	Fig.
General arrangement of the model	1
Details of the wing and nacelles	2
Variation of lift coefficient with incidence for the basic model	3
Variation of pitching moment coefficient with lift coefficient for the basic model	4
Surface oil flow on the wing at a Mach number of 0.8	5
Comparison of the lift and pitching moment of the present model with those of the wing of Reference 5	6

LIST OF ILLUSTRATIONS (Contd)

	Fig.
Variation of lift coefficient with Mach number at constant incidence for the basic model	7
Variation of the lift curve slope, $\left(\frac{\partial C_L}{\partial \alpha}\right)_o$ with Mach number	8
Variation of pitching moment coefficient with Mach number at constant lift coefficient for the basic model	9
Variation of $\left(\frac{\partial C_m}{\partial C_L}\right)_o$ with Mach number	10
Variation of drag coefficient with lift coefficient for the basic model	11
Variation of drag coefficient with C_L^2 for the basic model	12
Variation of drag coefficient at zero lift with Mach number	13
Variation of drag coefficient at constant lift coefficient with Mach number	14
Variation of the induced drag factor with Mach number	15
Variation of lift coefficient with incidence for the model with and without nacelles	16
Variation of pitching moment coefficient with lift coefficient for the model with and without nacelles	17
Variation of drag coefficient with lift coefficient for the model with and without nacelles	18
Variation of lift coefficient with incidence for the model with and without flow through the nacelles	19
Variation of pitching moment coefficient with lift coefficient for the model with and without flow through the nacelles	20
Variation of drag coefficient with lift coefficient for the model with and without flow through the nacelles	21
Effect on lift coefficient of adding leading edge vortex generators	22
Effect on pitching moment coefficient of adding leading edge vortex generators	23
Effect on drag coefficient of adding leading edge vortex generators	24
Effect of aileron edge gaps on lift coefficient	25
Effect of aileron edge gaps on pitching moment coefficient	26
Variation of rolling moment coefficient with incidence at constant Mach number for various aileron settings	27(a) & (b)

LIST OF ILLUSTRATIONS (Contd)

	Fig.
Variation of rolling moment coefficient with Mach number at approximately constant incidence for various aileron settings.	
(a) at approximately 4° incidence	28(a)
(b) at approximately 7° incidence	28(b)
Variation with Mach number of the rolling moment due to constant deflection of one aileron	29
Change in normal force coefficient due to aileron deflection	30
Change in pitching moment coefficient due to aileron deflection	31
Variation with Mach number of ΔC_m due to aileron deflection at zero incidence	32
Comparison of the body-sizes of the scale aircraft and the tested model	33

1 INTRODUCTION

In order to obtain preliminary data on the aerodynamic characteristics of the wing of the Bristol 188 supersonic research aircraft a simple model has been tested. The aircraft design has two engines in long nacelles on the wing, which is unswept inboard of the nacelles and has a swept-back leading edge outboard of the nacelles. The fuselage is long and slender. The wing planform was designed to give a smaller and smoother transonic shift of aerodynamic centre than that of a simple unswept tapered wing of similar aspect ratio.

The model consisted of the exposed wing to 1/36 scale mounted on a body of about twice the scale diameter of the aircraft fuselage, in order to allow an existing strain gauge balance to be utilised for the tests. The effect of the large body on the results is discussed briefly in the Appendix.

The tests consisted mainly of measurements of lift, drag and pitching moment at high subsonic, transonic and supersonic speeds, including brief investigations of the contribution of the nacelles* and of the effect of adding leading edge vortex generators, which have been proposed as means of increasing the maximum usuable lift coefficient at low speeds. Measurements of the effectiveness of the horn-balanced aileron were also made.

Further tests on models of the Bristol 188 in the 3 foot tunnel, to be reported, include measurements of lift, pitching moment, side force, yawing moment and rolling moment on a complete model, exploratory measurements of downwash at the tailplane position, and measurements of aileron hinge moment on a partial model.

2 DETAILS OF THE TESTS

2.1 Description of the model

The general arrangement of the model is shown in Figure 1, and some dimensions of the model are listed in Table 1, and wing section data are given in Table 2.

The model was made of steel, with a very high standard of surface finish. The wing was mounted symmetrically** on an ogive-cylinder body, with long nacelles attached near mid-semispan and horn-balanced ailerons outboard of them.

The centre section of the wing, inboard of the nacelles, was unswept and untapered. Outboard of the nacelles, the leading edge was swept-back at an angle of 38° as far as the nose of the aileron horn (see below), and at 64° over the horn. The trailing edge was swept forward 3° outboard of the nacelles.

The wing section (Table 2) was a symmetrical 4% thick biconvex circular arc section inboard of the aileron horn, changing smoothly to a section with a rounded leading edge over the span of the horn; the trailing edge had a finite thickness of about 0.04% chord throughout the span.

---

* These tests included some with the nacelles blocked; they were made to find the possible effect of spillage on the wing flow, and also to investigate the technique of testing models with the nacelle entry shape correct but the nacelles blocked just inside the inlet.

** The wings of the aircraft design are set at 2° to the body.

The ailerons were integral with the wing, and were deflected by bending along grooves machined in the wings as shown in Figure 2. The gaps between the inboard end of the aileron and the wing and between the horn and the wing were cut 0.012 inch wide, whereas the scale width would have been 0.003 inch. The ailerons were not cut until the tests on the basic model had been completed. In later tests, with ailerons undeflected, the aileron hinge grooves and gaps were sealed rigidly with Araldite; in the aileron tests the hinge grooves only were faired with plasticene.

For some tests leading edge vortex generators, shown in Figure 2, were fitted in the corners between the inner wing leading edge and the body and nacelles. They were made of 0.002 inch thick metal sheet attached in the wing chord plane, and were faired to the wing with Araldite.

The nacelles were cylindrical over the greater part of their length, mounted in a mid-wing position at an angle of 2°, nose-down relative to the chord plane. They had centre-body intakes with sharp lips. Figure 2 shows the shape of the ducts and the distribution of cross section area along them. The nacelles could be removed for tests of the plain wing and body combination.

2.2 Experimental technique

The tests were carried out in the R.A.E. (Bedford) 3 ft tunnel, using the supersonic working section[1] and the transonic working section with slotted side liners[2]. The model was mounted on a sting. A five-component internal strain gauge balance was used to measure normal force, pitching moment, rolling moment, yawing moment and side force, or, alternatively, a three-component balance to measure normal force, pitching moment, and axial force. The latter balance was limited by strength to use over an incidence range up to about 10° and in some cases the five-component balance was used to extend the measurements of normal force and pitching moment to higher incidences.

Base pressure was measured by means of a pressure lead to a point inside the model. No measurements were made of the flow through the nacelles.

To ensure that the boundary layer was turbulent, the leading edge of the wing was roughened by the application of a mixture of fine carborundum powder in aluminium paint, back to 10% chord on both surfaces.

For the transonic tests the roughness band had a base of paint about 0.001 inch thick from which the carborundum grains formed projections about 0.0015 inch high. A coarser powder was used for the supersonic tests, making the height of the projections about 0.0025 inch. A similar roughness band 0.5 inch wide was applied to each nacelle 1.5 inches aft of the lip, and a wire of diameter 0.005 inch was attached to the body 2.5 inches from the nose.

Some observations were made of the flow of oil on the wing using the technique described in Reference 3 and further discussed and illustrated in References 4 and 5.

2.3 Range of the tests

The Mach numbers at which tests were done were 0.70, 0.80, 0.85, 0.90, 0.94, 0.98, 1.02, 1.42, 1.61 and 1.82. The Reynolds number based on aerodynamic mean chord was 1.7×10^{6}.

In general, normal force, axial force and pitching moment were measured on the complete model at angles of incidence up to between 9° and 14°. Some of these measurements were repeated with the nacelle flow blocked and with the nacelles removed.

For the aileron tests the ailerons were bent to combinations of approximately 0, 5°, and 10° down on the port wing with 0, 5°, and 10° up on the starboard wing. The actual angles and combinations are listed in Table 3. Measurements of normal force, pitching moment, rolling moment, yawing moment and side force were made with the ailerons deflected, at several subsonic and supersonic Mach numbers, at angles of incidence up to 7°.

Observations of surface oil flow were made at various angles of incidence at Mach numbers of 0.80, 0.90, and 1.61.

2.4 Corrections applied and reduction of results

The angle of incidence was corrected for balance and sting deflections throughout, but no correction was made for changes in aileron angle due to aerodynamic loading, except in the derivation of the curves of rolling moment due to constant aileron deflection against Mach number (Figure 29). The deflection of the aileron as calculated from estimated hinge moments and the known flexibility of the spring centre hinges did not exceed 0.15°.

The measurements of axial force were corrected to a body base pressure equal to free stream static, but no corrections were made for the internal drag of the nacelles.

No tunnel interference corrections have been applied. In the supersonic tests at Mach numbers of 1.42, 1.61 and 1.82 the reflection of the model bow-wave from the tunnel walls always passed behind the model. For the transonic and subsonic tests small corrections may be needed to Mach number and incidence, but insufficient data is available to make reliable corrections.

The balance measurements have been reduced to coefficient form in the usual way. The reference dimensions were those of the basic gross wing, neglecting the leading edge vortex generators when present. The pitching moment coefficients were referred to the aerodynamic mean chord $\bar{c}$ and a moment centre at the mean quarter chord point.

Whenever possible normal force and axial force measurements have been resolved to lift and drag coefficients. Axial force measurements with the three component balance were extrapolated to enable some of the normal force measurements with the five component balance at the higher incidences to be reduced to lift coefficients. The accuracy of determining C_L is not greatly impaired by the extrapolation, since the contribution of axial force to lift did not exceed 2%.

2.5 Accuracy

Apart from the possible effects of tunnel interference mentioned above, the experimental accuracy is estimated to have been:-

lift coefficient	± 0.005
pitching moment coefficient	± 0.002
drag coefficient	± 0.001
rolling moment coefficient	± 0.001
side force coefficient	± 0.001
yawing moment coefficient	± 0.001
incidence	± 0.1°
aileron deflection	± 0.08°
Mach number	± 0.005

3 RESULTS AND DISCUSSION

3.1 Lift, pitching moment and drag of the basic model

The lift, pitching moment and drag of the basic model (with nacelles) are tabulated in Table 4 and plotted in Figures 3, 4 and 11.

3.1.1 Lift and pitching moment

Figure 3 shows the variation of lift coefficient with incidence and Figure 4 the variation of pitching moment coefficient with lift coefficient for the basic wing, body and nacelle combination over the Mach number range.

The results at subsonic and transonic speeds will be considered first, and the main features of the lift and pitching moment curves summarised.

At zero incidence there is a small negative lift, due to the asymmetric setting of the nacelles on the wing. Except at M = 1.02, the lift curve slope increases at an angle of incidence of about 2°. At Mach numbers 0.70 to 0.85 a decrease in lift curve slope occurs at an angle of incidence 5° to 7° (C_L = about 0.4 or 0.5), above which the slope remains roughly constant at about two thirds of its value at zero incidence. At Mach numbers 0.90 to 1.02 a decrease in lift curve slope begins at an incidence which falls from 5° (C_L = about 0.4) at M = 0.90 to 2° (C_L = about 0.2) at M = 1.02. This is followed by a sharp loss of lift (or stall) at M = 0.90 at an incidence of 9° (C_L = 0.7) and at M = 0.94 at an incidence of 10° (C_L = 0.85), beyond which there is a substantial recovery to a lift curve slope of the order of three quarters of its initial value. There is a hysteresis effect at the stall; lower values of C_L were recorded when the angle of incidence was being decreased from above the stall than when the incidence was being increased from below. At Mach numbers of 0.98 and 1.02 there is no stall within the incidence range, but there is a gradual decrease in lift curve slope at the higher incidences.

At Mach numbers of 0.70 to 0.85, Figure 4, shows a rearward movement of the aerodynamic centre (decrease in the slope $\left(\frac{\partial C_m}{\partial C_L}\right)_M$), beginning at a low lift coefficient of about 0.15, followed by a more rapid rearward movement at lift coefficients of about 0.4 to 0.5. Above a lift coefficient between 0.5 and 0.6 the aerodynamic centre moves forward again. At Mach numbers 0.90 to 0.98, there is a well defined reduction in $\left(\frac{\partial C_m}{\partial C_L}\right)_M$ at a lift coefficient somewhat below that at which a decrease in lift curve slope was noted - C_L = 0.35 at M = 0.90, falling to C_L = 0.2 at M = 0.98. The magnitude of the rearward aerodynamic centre movement increases with increasing Mach number. A smaller and more gradual rearward shift begins at a lift coefficient of about 0.2 at a Mach number of 1.02. There is a large nose-down change in pitching moment at the stall at Mach numbers of 0.90 and 0.94; after the stall the aerodynamic centre position is further back than before. At M = 0.98 and 1.02 the stability remains roughly constant at the higher lift coefficients.

The results at Mach numbers up to 0.85 resemble those of the low speed tunnel tests[6,7]; this suggests that leading edge separations of the long bubble type occur at incidence in this Mach number range, as in the low speed tests. This was verified by observations of surface oil flow on the model at a Mach number of 0.8. Photographs of upper surface oil flow patterns obtained are reproduced in Figure 5. Figure 5(b) shows attached chordwise flow over

the inner wing at an incidence of 2.1°. As incidence is increased, the appearance and growth of a region of undisturbed oil behind the roughness band at the leading edge of the inner wing show that a leading edge separation bubble begins to grow rapidly here at an incidence of about 4°, extends to near mid-chord at an incidence of 5.4°, and does not close on the wing at all at an incidence of 8.5°. (The oil pattern on the inner wing at 6.4° in Figure 5(d) is imperfectly developed.) At 8.5°, the oil lines near the trailing edge of the inner wing indicate forward flow. The oil flow lines on the side of the nacelle give some indication of the growth of the bubble. Leading edge separation occurs also on the outer wing, but develops in a way more typical of swept wings[8]. In Figure 5(c) at an incidence of 4.3° a region of spanwise oil flow near the leading edge, outboard of the nacelle but inboard of the horn, is taken as evidence of leading edge separation; over the horn, spiral lines in the surface pattern of flow, typical of a leading edge vortex separation can be seen. By 6.4° incidence (Figure 5(d)) a single spiral vortex sheet appears to be formed by separation from the leading edge of the whole of the outer wing; a dividing line between spanwise surface flow under the vortex sheet and chordwise surface flow downstream of it extends from the junction of leading edge and nacelles. As the incidence is further increased, the region of strongest influence of the vortex sheet on the surface flow swings inboard, and the area of undisturbed oil at the tip grows; the oil flow pattern at the tip is not fully developed, but suggests a rear or secondary separation line under the vortex sheet moving inboard with increasing incidence.

A probable explanation of the lift and pitching moment characteristics at a Mach number of 0.8 and, in view of the similarity of the curves, at 0.70 and 0.85 also, is as follows. The increase in lift curve slope at low incidence and the beginning of the rearward movement of the aerodynamic centre are due mainly to the development of the leading edge separation vortex sheet over the outer wing, first at the tips and then in towards the nacelles. The acceleration of the rearward movement of the aerodynamic centre and the reduction in lift curve slope occur as the separation bubble on the inner wing spreads towards the trailing edge, until re-attachment no longer takes place and the inner wing stalls[9]. At higher incidences, the outer wing supplies an increasing fraction of the lift, and the gradual reduction in stability that is observed is due to loss of lift at the tip as the core of the leading edge separation vortex sheet moves inboard[4].

A few oil observations that were made at a Mach number of 0.90, but not photographed, showed that a shock-induced separation occurs on the inner wing before the leading edge separation as incidence is increased, as on the wing of Reference 5. The flow pattern over the outer wing is broadly similar to that at M = 0.8 in Figure 5. For example, at 7° incidence (C_L = 0.6) shock-induced separation occurs at about 25% chord, with re-attachment at 42% chord. Following Scott-Wilson's analysis[5], it may reasonably be supposed that the reduction in lift curve slope and the increase in stability observed at progressively lower angles of incidence at Mach numbers of 0.90 to 0.98 are due to the onset of shock-induced separation on the inner wing, and that the sudden stall at higher incidences, accompanied by a nose-down change of pitching moment, are due to a sudden forward movement of the separation point to the leading edge. The hysteresis effect at the stall is probably associated with differences in the transition between shock-induced separation and leading edge separation as incidence is increased and the change back to shock-induced separation as incidence is decreased. The relatively greater lift curve slope after the stall than that of the unswept tapered wing of Reference 5 is undoubtedly due to the maintenance of lift over the outer wing after the stall on the inner wing. It is not clear, without further evidence, whether shock-induced separation occurs at a Mach number of 1.02 or not.

Thus it may be said that the aerodynamic characteristics of the model at incidence at high subsonic speeds are dominated to some extent by those of the straight inner wing, on which a long bubble type of leading edge separation occurs first, at Mach numbers of up to 0.80 at least, and shock induced separation further aft occurs before leading edge separation at Mach numbers of 0.90 and above. To illustrate this, some comparisons are shown in Figure 6 between the lift and pitching moment of the present model and of the tapered unswept wing of Reference 5, on which wing flow patterns of this type are known to occur.

At supersonic speeds the curves of lift coefficient against incidence are almost linear, but reductions in stability occur at lift coefficients above about 0.4 at M = 1.42 and 0.3 at M = 1.82. At the latter Mach number, the aerodynamic centre moves forward by about 2% chord between $C_L = 0$ and 0.5 and by a further 2% chord between $C_L = 0.5$ and 0.8. Similar changes in stability, thought to be due to relatively small areas of shock-induced separation near the trailing edge, are observed on the tapered straight wing[10] referred to above and on a delta wing with attached flow at the leading edge[8] at supersonic speeds. The reason why there is no loss of stability at 1.61 is not fully understood.

Figure 7 shows curves of variation of lift coefficient at constant angles of incidence of 0°, 3° and 6° over the Mach number range. The lift coefficient at zero incidence varies between -0.02 and -0.032, and the angle of incidence for zero lift between 0.3° at high subsonic speed and 0.55° at M = 1.8. The variation of lift curve slope (averaged between -2° and +2° incidence) with Mach number is shown in Figure 8. For the complete model the lift curve slope increases from 0.071 per degree at M = 0.70 to 0.101 at M = 1.02. At M = 1.42 it has fallen to 0.071 again, and at M = 1.82 it is 0.059 per degree.

The lift curve slope for the body alone is also included in Figure 8 and is almost constant throughout the Mach number range.

Curves of the pitching moment coefficient at lift coefficients of 0 and 0.3 against Mach number are given in Figure 9. The value of C_m at zero lift varies between -0.003 and -0.009. The variation of aerodynamic centre position at zero incidence (again averaged between -2° and +2°) is shown in Figure 10 for the complete model. There is a gradual rearward shift from 5% to 9% aerodynamic mean chord between M = 0.70 and 0.94, followed by a more rapid shift to 21% chord at M = 1.02. At a Mach number of 1.42 the aerodynamic centre of the model is at the mean quarter-chord point of the wing, and there is a further small rearward movement to about 27% aerodynamic mean chord between M = 1.42 and 1.82. Thus the total rearward shift of the aerodynamic centre over the Mach number range of the tests is 22% aerodynamic mean chord.

Values of $\frac{\partial C_L}{\partial \alpha}$ and $\frac{\partial C_m}{\partial C_L}$ for the basic model, and for all the other tested configurations, are tabulated in Tables 9 and 10.

3.1.2 Drag

Figure 11 shows the drag coefficient plotted against lift coefficient, C_L, and Figure 12 the drag coefficient plotted against C_L^2 over the Mach number range of the tests. At subsonic and transonic speeds the slope $\frac{\partial C_D}{\partial C_L^2}$

begins to increase at about the same lift coefficient as that at which there is a marked increase in stability (Figure 4). Like the increase in stability, the changes in $\frac{\partial C_D}{\partial C_L^2}$ are probably due to flow separations at the leading edge, as described in the previous section.

The variation of $\left(C_D\right)_o$ with Mach number is plotted in Figure 13, and the variation of C_D at $C_L = 0$, 0.2 and 0.4 with Mach number in Figure 14. $\left(C_D\right)_o$ is tabulated in Table 11 for all the configurations tested.

For the complete model the zero-lift drag coefficient remains almost constant at 0.031 up to M = 0.90, after which it increases gradually to 0.032 at M = 0.94. Beyond this the drag coefficient rises sharply to 0.041 at M = 1.02. At supersonic speeds the drag coefficient for the complete model is greater than at M = 1.0, being 0.047 at M = 1.4 and falling to 0.042 at M = 1.8.

In Figure 15 the induced drag factor at zero lift, $\left(\pi A \frac{\partial C_D}{\partial C_L^2}\right)_o$, and a mean induced drag factor for the range of lift coefficient from 0 to 0.3, $\left(\pi A \left\{\left(C_D\right)_{0.3} - \left(C_D\right)_o\right\} \Big/ 0.09\right)$, are plotted against Mach number. This figure also shows the induced drag factor (1.0) for a wing with elliptic loading and full leading edge suction at subsonic speeds and $\pi A \Big/ \frac{\partial C_L}{\partial \alpha}$, which would be the induced drag factor for the measured lift curve slope in the absence of leading edge suction. It will be seen from the figure that below M = 0.95 the measured induced drag factor lies about half way between these two values, but that between M = 0.97 and 1.02 it rapidly approaches the case with no leading edge suction. At supersonic speeds the measured value is again close to the no-leading-edge-suction value.

The variation of $\left(C_D\right)_o$ due to the body alone is also plotted in Figure 13.

3.2 Contribution of the nacelles to lift, pitching moment and drag

3.2.1 Results of tests on the model without nacelles

Values of lift coefficient, pitching moment coefficient, and drag coefficient for the body and wing without nacelles, at Mach numbers of 0.80, 0.90, 1.02, and 1.61, are presented in Table 5, and in Figures 16, 17 and 18 they are compared with those for the complete model.

Without the nacelles, the model was nominally symmetrical and the small positive lift and negative pitching moment recorded must be due to accidental asymmetries of the model or the flow. It will be seen that in general the nacelles contribute a small negative lift and a reduction in stability. Their

effect on the lift curve slope at low incidences is small, except at a Mach number of 1.02, (see Table 9). The lift curve slope of the complete model varies rapidly with Mach number near M = 1.02, as was seen above, and the difference in lift curve slope could be due to a relatively small increase in local Mach number at the wings when the nacelles are added. The reduction in stability at low incidences due to adding the nacelles corresponds to a forward movement of the aerodynamic centre by about 7% of the aerodynamic mean chord, except at M = 1.02, where again the change in local Mach number due to adding the nacelles may account for the inconsistency.

The effects of the nacelles on lift and stability at the higher incidences at subsonic speeds correspond to earlier occurrence or development of leading edge separation on the inner wing in the presence of the nacelles. Thus at a Mach number of 0.80 the rapid rearward movement of the aerodynamic centre, associated above with the growth of the separation bubble on the inner wing towards and beyond the trailing edge, begins at an incidence of about 5° for the complete model but 7° for the model without nacelles. At a Mach number of 0.90 the complete model stalls, when separation occurs at the leading edge, at about 9° incidence, while the model without nacelles has not stalled at an incidence of 9.6° (the highest at which it was tested at this Mach number). These differences are presumed to be caused mainly by the increase in upwash angle at the leading edge of the inner wing due to the flow about the nacelles at incidence. At a Mach number of 1.02, on the other hand, the differences between the shapes of the lift and pitching moment curves with and without nacelles appear to be due principally to the effect of the nacelles on the local Mach number at the wing, for the increase in the lift curve slope and stability of the model without nacelles at a lift coefficient of about 0.2 resemble those of the complete model at a Mach number of 0.98 (Figure 4). It is interesting to see that at M = 1.61 a decrease in stability occurs at a lift coefficient of 0.35, similar to those observed on the complete model at Mach numbers of 1.42 and 1.82 but not 1.61, and attributed above to shock-induced separation near the trailing edge.

The increment in drag coefficient due to the nacelles is relatively constant over the whole range of the tests (Figure 18). It amounts to nearly a half of the drag coefficient at zero lift at a Mach number of 0.80 and one third at a Mach number of 1.61. A large part of this increment is likely to be the internal drag of the flow through the nacelles.

3.2.2 Results of tests on the model with no flow through the nacelles

The results of tests with the nacelle ducts blocked, at Mach numbers of 0.80, 0.90, 1.02 and 1.61 are tabulated in Table 6 and compared with the results of tests on the model with the nacelle ducts open in Figures 19 to 21.

The differences in lift and pitching moment are small, except at lift coefficients above 0.5 at M = 1.02 where the stability of the model is increasing with flow through the nacelles, but decreasing without flow through (Figure 20). The drag of the model (Figure 21) is almost the same at subsonic speeds with and without internal flow, but at a Mach number of 1.61 blocking the nacelles increases the drag coefficient by 0.014, more than a third of the drag coefficient at zero lift of the model with internal flow through the nacelles. Expressed in terms of the combined inlet area of the two nacelles, the incremental drag coefficient at this Mach number is 0.9.

From the testing-technique point of view these results suggest that flow through the nacelles in configurations of this type is not essential for accuracy of lift and pitching moment measurements.

3.3 Lift, pitching moment, and drag of the model with leading edge vortex generators

In Table 7 and Figures 22 to 24 the results of lift and pitching moment measurements over the whole Mach number range with and without leading edge vortex generators on the inner wing are compared.

The effects of the vortex generators on lift and pitching moment at low angles of incidence barely exceed the limits of experimental error, but they produce a small forward movement of the aerodynamic centre of about 1% chord. Their chief influence is at higher incidences at subsonic speeds. Thus at Mach numbers of 0.7 to 0.85 they reduce the loss in lift curve slope and rearward shift of aerodynamic centre at lift coefficients above 0.4. In this Mach number range, as at low speeds[6], vortices shed from the highly swept edges of the vortex generators and passing downstream above the upper surface of the inner wing retard the growth of the long bubble separation from the leading edge; this was confirmed by surface oil flow observations. At a Mach number of 0.90, the vortex generators delay the sudden stall associated with leading edge separation from an incidence of 9° to at least 9.7°, the highest incidence at which they were tested. They have no significant effect on the rearward shift of aerodynamic centre with increasing incidence at lower lift coefficients at Mach numbers of 0.90 to 0.98, attributed in section 3.1.1 to the onset of shock-induced separation on the inner wing. Surface oil flow observations appear to show that no separation occurs at the shock at a lift coefficient as high as 0.77 at M = 0.90 with the vortex generators on, however, while in the absence of vortex generators the occurrence of shock-induced separation has been confirmed at a lift coefficient of 0.6. Some similar results have been found by Pearcey in some unpublished work at the National Physical Laboratory. It is believed that they are due to the fact that the shock may be stronger, and followed by an expansion, when vortex generators have led to unseparated flow. The pressure distribution is then qualitatively similar to that on the wing with separation, and the overall forces will also be similar.

At supersonic speeds the main effect of the vortex generators on lift and pitching moment is the small forward movement of aerodynamic centre referred to above. In addition, a somewhat sharper reduction in stability at M = 1.82 near C_L = 0.3 is observed with vortex generators present than without them.

The effect on drag coefficient, shown in Figure 24, is small, except where at the higher angles of incidence at Mach numbers between 0.8 and 0.9 they increase the lift coefficient and reduce the drag due to lift.

It may be expected that the vortex generators will give an increase in the maximum usable lift coefficients at subsonic Mach numbers up to 0.85 at least, without having any adverse effect on performance or stability at subsonic or supersonic speeds.

3.4 Effect of the aileron edge gaps on lift and pitching moment

Measurements were made, at Mach numbers of 0.80, 0.90, 0.98, 1.42, and 1.82 of the lift and pitching moment on the model with the ailerons undeflected but with the chordwise gaps at the inboard end of the aileron and at the inboard edge of the aileron horn unsealed. The results are included in Table 8, and are compared with the results obtained with the gaps sealed in Figures 25 and 26.

The effect of the aileron gaps is very small throughout. It should be borne in mind however that the Reynolds number based on gap width is very small, so that quite different effects might be obtained in full scale conditions.

3.5 Results of aileron tests

Rolling moment, normal force and pitching moment, and side force and yawing moment were measured for each of five aileron settings, listed in Table 3, over a range of incidence at Mach numbers of 0.80, 0.90, 0.98, 1.42 and 1.82. The results are tabulated in Table 8. Curves of rolling moment coefficient are presented in Figures 27(a) and (b), and curves of incremental normal force and pitching moment coefficients due to aileron deflection in Figures 30 and 31. These results are discussed in sections 3.5.1 and 3.5.2. The side force and yawing moment due to aileron deflection were small throughout, and are not discussed further.

3.5.1 Rolling moment due to aileron deflection

As the aileron tests were carried out at steps of approximately 5° in aileron deflection angle, and as the results were not linear with this deflection it is not possible to give accurate curves of aileron effectiveness, $\frac{\partial C_\ell}{\partial \xi}$. Instead, curves of C_ℓ at constant aileron angles are plotted; these curves give the average aileron effectiveness. However, the variation of the rolling moment coefficient with incidence at fixed Mach number (Figures 27(a) and 27(b)) is considered first. At high subsonic speeds the rolling moment varies slightly throughout the incidence range but some general trends can be distinguished. There is a small increase in the rolling moment due to upward aileron deflection as the incidence is increased above 3° or 4°, and a slightly earlier increase in the rolling moment due to downward aileron deflection, followed by a steady rise as the incidence is further increased. At supersonic speeds the rolling moment is almost independent of wing incidence.

Figures 28(a) and 28(b) show the variation with Mach number of the rolling moment due to approximately equal, and opposite, aileron deflections. These curves were obtained by varying the Mach number in small steps with the model at 4° and 7° incidence. Owing to sting deflections the actual angles of incidence varied between 4.2° and 4.4° and between 7.4° and 7.7° respectively.

The aileron effectiveness falls by more than half between subsonic and supersonic speeds and there is a further fall between $M = 1.4$ and $M = 1.8$. At 7° incidence there is a sharp reduction in rolling moment at Mach numbers between 0.9 and 0.94, followed by a partial recovery before the decline to the supersonic value continues. This temporary reduction is presumably due to shock-induced separations on the aileron.

In Figure 29 interpolated curves are presented showing the variation with Mach number of the rolling moment due to constant deflection of one aileron; these curves, as mentioned earlier, are a measure of the average aileron effectiveness. The curves are given for constant values of normal force coefficient, C_N, before aileron deflection. They show the relative effectiveness of the upward and downward deflected aileron but there are insufficient points to show up the loss of rolling moment at 0.94 referred to above.

3.5.2 Normal force and pitching moment due to aileron deflections

In Figures 30 and 31 the increments of normal force and pitching moment due to differential aileron settings of $\pm 5^\circ$ and $\pm 10^\circ$ (nominal), and also due to setting one aileron about 5° up, are plotted against incidence for three Mach numbers. These results show that the differential aileron settings have a very small effect on normal force and pitching moment. From the

increments due to deflection of one aileron it is calculated that the normal force increment acts about 10% $\bar{c}$ ahead of the hinge line. Interpolated curves of ΔC_m due to one aileron deflection are plotted in Figure 32.

The lateral position of the normal force increment due to aileron deflection has been obtained by dividing this increment into the corresponding increment in rolling moment. The centre of pressure so obtained lies well inboard on the aileron at subsonic speeds; in some cases it appears to be inboard of the inner aileron edge. This result is also true at low speeds as shown by integration of pressure distributions obtained by the Bristol Aeroplane Company in low speed tunnel tests. At supersonic speeds the normal force increment acts closer to the aileron centre of area.

4 CONCLUSIONS

A model with wings and nacelles similar to those of the Bristol 188 aircraft to 1/36 scale, but with a larger body, has been tested in the R.A.E. (Bedford) 3 foot tunnel at Mach numbers between 0.70 and 1.02 and at 1.42, 1.61 and 1.82.

The lift curve slope of the model near zero incidence increases from 0.072 per degree at M = 0.70 to 0.101 per degree at M = 1.02, and falls to 0.071 at M = 1.42 and 0.059 at M = 1.82. The aerodynamic centre position moves back from 5% aerodynamic mean chord at M = 0.7 to 9% at M = 0.94, 21.5% at M = 1.02, and 26.5% at M = 1.82.

The aerodynamic characteristics of the wing at incidence at subsonic speeds are dominated by those of the unswept inner wing, on which a long bubble type of leading edge separation occurs at Mach numbers up to 0.80 or 0.85, and shock induced separation aft of the leading edge at higher Mach numbers. Slight reductions in stability with increasing incidence, possibly due to separations near the trailing edge, are observed at lift coefficients of 0.4 at M = 1.42 and 0.3 at M = 1.82.

Leading edge vortex generators fitted to the inner wing delay the development of the leading edge separation at Mach numbers up to 0.85 as they do at low speeds, and are likely to increase the maximum usable lift coefficient in this range. It is not clear from the results whether or not they delay shock-induced separation on the inner wing at higher subsonic speeds. Their effects on lift, drag, and stability at low lift coefficients are small, and they have no adverse effects within the range of the tests.

The horn balanced ailerons are effective throughout the range of the tests. The effects of aileron deflection on longitudinal stability are small.

LIST OF SYMBOLS

b	Span
$\bar{\bar{c}}$	Aerodynamic mean chord
M	Mach number
q	free stream dynamic pressure
R	Reynolds number based on aerodynamic mean chord
S	gross wing area
C_D	drag coefficient $= \frac{\text{drag}}{qS}$
C_L	lift coefficient $= \frac{\text{lift}}{qS}$
C_N	normal force coefficient $= \frac{\text{normal force}}{qS}$
C_Y	side force coefficient $= \frac{\text{side force}}{qS}$
C_ℓ	rolling moment coefficient $= \frac{\text{rolling moment}}{qSb}$
C_m	pitching moment coefficient $= \frac{\text{pitching moment}}{qS\bar{\bar{c}}}$
C_n	yawing moment coefficient $= \frac{\text{yawing moment}}{qSb}$

C_m and C_n refer to moments about the mean quarter chord point.

α	angle of incidence
ξ	aileron angle

LIST OF REFERENCES

No.	Author	Title, etc
1	Morris, D.E.	Calibration of the flow in the working section of the 3 ft x 3 ft tunnel, National Aeronautical Establishment. AGARD AG17/P7 A.R.C. C.P. 261. September, 1954.
2	Sutton, E.P.	The development of slotted working section liners for transonic operation of the N.A.E. 3 foot wind tunnel. A.R.C. R. & M. 3085. March, 1955.
3	Winter, K.G. Scott-Wilson, J.B. Davies, F.V.	Methods of determination and of fixing boundary layer transition on wind tunnel models at supersonic speeds. A.R.C. C.P. 212. September, 1954.
4	O'Hara, F. Scott-Wilson, J.B.	An investigation of the flow on a half wing model with 60.5° leading-edge sweep-back at high subsonic and supersonic speeds. A.R.C. C.P. 471. November, 1955.
5	Scott-Wilson, J.B.	An experimental investigation of the transonic flow over an unswept wing of aspect ratio 3.5, taper ratio 0.5 with a 4% biconvex section. A.R.C. R. & M. 3209. November, 1955.
6	Leathers, J.W.	Low speed wind tunnel tests on a 1/10th scale model of a twin jet-engined aircraft. (Bristol 188). R.A.E. Tech. Note No. Aero 2515. A.R.C. 20047. July, 1957.
7	Williams, T.J.	Type 188, low speed wind tunnel tests on a 1/10 scale model, lift, drag and pitching moment measurements. Bristol Aeroplane Co. Wind Tunnel Report 244.
8	Sutton, E.P.	Some observations of the flow over a delta winged model with 55° leading edge sweep, at Mach numbers between 0.4 and 1.8. A.R.C. R. & M. 3190. November, 1955.
9	McCullough, G.D. Gault, D.E.	Boundary layer and stalling characteristics of the N.A.C.A. 64A006 Airfoil Section. N.A.C.A. Tech. Note No. 1923 August 1949. A.R.C. 12781.
10	Scott-Wilson, J.B.	The lift, drag and pitching moments of three unswept wings of aspect ratio 3.5 and taper ratio 0.5, with different wing sections at transonic and supersonic speeds. R.A.E. Tech. Note No. Aero 2387 Sept. 1955.

APPENDIX 1

NOTE ON EFFECTS OF MOUNTING THE WING ON A NON-REPRESENTATIVE BODY

The tests described in this note were made to provide information about the aerodynamic characteristics of the Bristol 188 aircraft, which, as stated in the Introduction, will have exposed wings similar to those of the model tested, mounted on a more slender body. The body length of the aircraft design is about the same, but its cross-section in the neighbourhood of the wing is roughly elliptical, with scaled height 1.63 inch and width 1.23 inch, while the present model is of circular section with diameter 2.50 inches (see Figure 33). No attempt will be made here to correct the results for the difference in body shape, but some of the more important consequences of the difference will be considered briefly.

Near zero incidence, the lift on the body alone acts almost entirely ahead of the wing position, and can be considered as "body nose lift". The larger body will have more nose lift, which will make a bigger contribution to lift curve slope and a bigger nose-up (positive) contribution to $\frac{\partial C_m}{\partial C_L}$ at low incidence throughout the Mach number range. To enable these to be assessed, values of $\frac{\partial C_L}{\partial \alpha}$ and $\frac{\partial C_m}{\partial C_L}$ at zero incidence for an identical body alone, from unpublished 3 foot tunnel tests, are given in Table 12. The coefficients are based on the wing reference dimensions. Values of $\frac{\partial C_L}{\partial \alpha}$ for the body alone are plotted together with those for the complete model in Figure 8.

An indication of the aerodynamic centre movement attributable to the complete model minus the body alone is given by the ratio of the increments of $\frac{\partial C_m}{\partial \alpha}$ and $\frac{\partial C_L}{\partial \alpha}$. This ratio is given by:

$$\frac{\left(\frac{\partial C_m}{\partial \alpha}\right)_{\substack{\text{complete}\\\text{model}}} - \left(\frac{\partial C_m}{\partial \alpha}\right)_{\substack{\text{body}\\\text{alone}}}}{\left(\frac{\partial C_L}{\partial \alpha}\right)_{\substack{\text{complete}\\\text{model}}} - \left(\frac{\partial C_L}{\partial \alpha}\right)_{\substack{\text{body}\\\text{alone}}}} \qquad (1)$$

and neglecting $\left(\frac{\partial C_L}{\partial \alpha}\right)_{\substack{\text{body}\\\text{alone}}}$ since this is shown to be small in Figure 8, it becomes:

$$\left(\frac{\partial C_m}{\partial C_L}\right)_{\substack{\text{complete}\\\text{model}}} - \left(\frac{\partial C_m}{\partial \alpha}\right)_{\text{body}} \Bigg/ \left(\frac{\partial C_L}{\partial \alpha}\right)_{\substack{\text{complete}\\\text{model}}} \qquad (2)$$

This ratio is plotted in Figure 10 (labelled "model - body alone"). It will be seen that the change in aerodynamic centre position due to the body is

large, and varies between 10% mean chord at M = 0.8, 7% at M = 1.0, and 17% at M = 1.6. (The reason why this is so, although the pitching moment slope of the body is relatively independent of Mach number, is to be seen in the second term of (2), for the lift curve slope of the complete model varies rapidly with Mach number, particularly near M = 1).

The change in loading on the wing due to the presence of the body and on the body due to the presence of the wing have not so far been considered. The reduction in the total rearward movement of the aerodynamic centre over the Mach number range due to the contribution of the body nose lift will be partly offset by a rearward shift of the centre of the loading induced on the body by the wing at transonic and supersonic speeds. It must be concluded that the transonic and supersonic movement of the aerodynamic centre depends on the body shape.

The body makes a large direct contribution to the drag of the model. The drag at zero incidence of the body alone is given in Table 12, and a curve of drag at zero lift coefficient for the body alone at zero incidence has been plotted in Figure 13. The body contributes about a third of the drag at subsonic speeds and a little over a half of the drag rise to supersonic speeds. Since the body used in the tests was cylindrical and the fuselage of the aircraft design not far from the same cylindrical shape in the neighbourhood of the wing root, no large error will be made if it is assumed that, except perhaps near M = 1, the curve of the difference between the complete model drag and the body alone drag is applicable to the exposed wings and nacelles of the aircraft design. (Near M = 1 the difference is very sensitive to the accuracy with which the shape of the steeply rising part of the drag curve is located, and tunnel interference may have a disproportionately large effect).

A second way in which the change in body shape may have an important effect on the aerodynamic characteristics of the wing tested is by changing the angle of upwash at the wing leading edge at incidence. It has been shown that at subsonic speeds flow separation from the leading edge of the inner wing plays an important part in the behaviour of the wing at incidence. The angle of upwash will be greater at a given wing incidence on the model, and leading edge separation will develop at a slightly lower incidence, because of its greater body diameter and also because its axis lies in the wing chord plane while the fuselage of the aircraft design is set at 2° nose down to the chord plane. The lift coefficient at which a separation bubble begins to grow rapidly from the leading edge of the inner wing without vortex generators is estimated to be 0.05 to 0.1 higher with a scale fuselage than with the fuselage used in the tests.

The use of a body which is broader than the scale body increases the span, area, aspect ratio and mean chord of the gross wing. It also increases the moment arm of the aileron. If it is assumed that the lift increment due to deflection of an aileron acts near the aileron centre of area, it is found that a reduction of about 5% in the rolling moment coefficient due to aileron deflection is required to correct the results obtained to apply them to the scale aircraft shape. (The correction to C_{ℓ} is only so small because the span changes as well as the moment arm). However, as was pointed out in section 3.5.1, the centre of lift due to aileron deflection appears to be inboard of these ailerons at subsonic and transonic speeds, and the correction required may be of the order of 10%. Apart from this, the results of the aileron tests should be little affected.

The change in body shape will not invalidate the comparisons made between results with and without nacelles, vortex generators, aileron edge gaps, etc.

TABLE 1

Principal Dimensions of the Model

Wing

Span	13.03 ins
Gross area (excluding vortex generators)	48.35 sq ins
Aerodynamic mean chord	3.992 ins
Aspect ratio	3.51
Chord of unswept part of wing inboard of the nacelles	4.44 ins
Chord immediately outboard of nacelle	4.12 ins
Chord at inboard edge of aileron horn	2.50 ins
Tip chord	0.67 ins
Sweepback of leading edge between nacelle and aileron horn	38.1°
Sweepback of aileron horn leading edge	64.5°
Sweepforward of trailing edge outboard of the nacelle	2.7°
Dihedral	0°
Twist	0°

Wing, excluding part enclosed by body

Span	10.53 ins
Area (excluding vortex generators)	37.24 sq ins
Aerodynamic mean chord	3.86 ins
Aspect ratio	2.98

Ailerons

Span; each side	2.82 ins
Area aft of hinge line; each side	2.07 sq ins
Aileron chord: wing chord, at inboard end of hinge	0.192
Aileron chord: wing chord, at outboard end of hinge	0.284
Distance of inboard edge of aileron horn from model centre line	5.65 ins

Nacelles

Length, from lip of centre body to exit	10.29 ins
Length, from lip to exit	9.92 ins
Lip diameter	0.77 ins
Maximum diameter	1.22 ins
Exit diameter	0.90 ins
Distance of nacelle centre line from body centre line	3.08 ins
Distance of lip ahead of inner wing leading edge	3.59 ins
Nacelle-wing chord angle (nacelle nose down)	2°

Body

Length	25 ins
Diameter of cylindrical part	2.5 ins
Length of tangent circular arc ogival nose	9 ins
Radius of nose tip	0.063 ins
Distance of the base behind the inner wing leading edge	12.49 ins

Further details of the wing planform, ailerons, vortex generators and the nacelles are given in Figure 2. Details of the wing sections are given in Table 2.

TABLE 2

Wing Sections

From the root to inner edge of aileron horn

Biconvex circular arc section, symmetrical, 4% thick, shortened for finite trailing edge thickness.

At the tip

Section formed by fairing part of 8% RAE 103 section, used over first 24% chord to above biconvex section used over rear 50% chord (table of ordinates below).

Over the aileron horn

Sections defined by straight lines joining points of equal slope at the tip and the inboard edge of the horn.

	Root chord	Chord at inboard edge of aileron horn	Tip chord
Chord length	4.444 ins	2.500 ins	0.667 ins
Max. thickness	0.178 ins = 4.01%	0.101 ins = 4.04%	0.052 ins = 7.8%
Position of max. thickness	51.3% chord	51.3% chord	34.2% chord
Trailing edge thickness	0.017 ins = 0.39% chord	0.010 ins = 0.39% chord	0.007 ins = 1.08% chord
Leading edge radius	0.001 inch	0.001 inch	0.0035 ins

Ordinates of tip chord

RAE 103 8%

$\frac{x}{c}$	0	0.005	0.025	0.075	0.160	0.200	0.240
$\frac{z}{c}$	0	0.0063	0.0139	0.0234	0.0322	0.0348	0.0367

$\frac{x}{c}$	0.266	0.290	0.300	0.314	0.342	0.378	0.396
$\frac{z}{c}$	0.0378	0.0384	0.0387	0.0388	0.0390	0.0387	0.0386

$\frac{x}{c}$	0.413	0.446	0.478
$\frac{z}{c}$	0.0381	0.0373	0.0361

Faired curve.

$\frac{x}{c}$	0.571	0.734	0.927	1.000
$\frac{z}{c}$	0.0319	0.0222	0.0105	0.0052

Outer wing 4% biconvex continued.

TABLE 3

Measured Aileron Deflection Angles

Port (down)	Starboard (up)	Nominal	Port (down)	Starboard (up)
0	0	(0,0)	0	0
0	5.8°	(0,5)	0	4.6°
5.9°	5.8°	(5,5)	5.1°	4.6°
5.9°	9.9°	(5,10)	5.1°	9.9°
10.1°	9.9°	(10,10)	10.1°	9.9°
Subsonic			Supersonic	

TABLE 4

Aerodynamic Coefficients of the Basic Model

	3 Component Balance				5 Component Balance		
M	α^o	C_L	C_m	C_D	α^o	C_L	C_m
0.70	-2.14	-0.177	-0.038	+0.0355	+11.58	+0.765	+0.044
	-1.08	-0.096	-0.024	+0.032	+13.66	+0.855	+0.049
	-0.02	-0.020	-0.007	+0.031			
	+1.04	+0.055	+0.009	+0.0315			
	+2.11	+0.131	+0.023	+0.0335			
	+3.17	+0.213	+0.039	+0.0375			
	+4.24	+0.295	+0.053	+0.0465			
	+5.30	+0.379	+0.066	+0.058			
	+6.37	+0.466	+0.073	+0.0735			
	+7.43	+0.545	+0.070	+0.092			
	+8.47	+0.612	+0.057	+0.1135			
	+9.51	+0.663	+0.050	+0.133			
0.80	-2.17	-0.183	-0.042	+0.037	+ 9.55	+0.647	+0.039
	-1.09	-0.100	-0.026	+0.0325	+10.58	+0.687	+0.040
	-0.56	-0.061	-0.018	+0.0315	+11.62	+0.734	+0.042
	-0.02	-0.019	-0.010	+0.031	+12.68	+0.796	+0.042
	+0.52	+0.022	-0.001	+0.0315	+13.89	+0.844	+0.053
	+1.05	+0.061	+0.007	+0.0315			
	+2.13	+0.142	+0.022	+0.034			
	+4.28	+0.315	+0.053	+0.0475			
	+5.36	+0.407	+0.066	+0.0605			
	+6.43	+0.488	+0.063	+0.0765			
	+7.47	+0.548	+0.048	+0.096			
	+8.50	+0.588	+0.043	+0.1135			
	+9.54	+0.633	+0.043	+0.1335			
0.85	-2.18	-0.189	-0.042	+0.0365			
	-0.02	-0.022	-0.009	+0.031			
	+2.13	+0.146	+0.023	+0.034			
	+4.30	+0.327	+0.054	+0.0485			
	+5.38	+0.414	+0.070	+0.061			
	+6.45	+0.505	+0.062	+0.079			
	+7.48	+0.544	+0.043	+0.0965			
	+8.51	+0.584	+0.039	+0.115			
	+9.55	+0.631	+0.038	+0.135			
0.90	-2.20	-0.198	-0.043	+0.037	+ 9.59	+0.651	+0.030
	-1.11	-0.108	-0.027	+0.033	+10.65	+0.709	+0.028
	-0.57	-0.064	-0.019	+0.032	+11.71	+0.775	+0.024
	-0.02	-0.020	-0.010	+0.031	+12.76	+0.835	+0.025
	+0.52	+0.026	-0.003	+0.0315	+13.83	+0.897	+0.032
	+1.06	+0.069	+0.005	+0.032			
	+2.15	+0.156	+0.020	+0.0345			
	+4.33	+0.350	+0.055	+0.0495			
	+5.43	+0.454	+0.067	+0.064			
	+6.52	+0.552	+0.073	+0.083			
	+7.59	+0.631	+0.077	+0.104			
	+8.66	+0.707	+0.080	+0.128			
	+9.06	+0.618	+0.033	+0.129			
	+9.59	+0.653	+0.029	+0.142			
	α decreasing						
	+8.54	+0.597	+0.032	+0.119			
	+8.02	+0.572	+0.035	+0.1085			
	+7.53	+0.572	+0.054	+0.100			
	+7.06	+0.597	+0.074	+0.094			

TABLE 4 (Contd)

	3 Component Balance				5 Component Balance		
M	α	C_L	C_m	C_D	α	C_L	C_m
0.94	-2.21	-0.207	-0.044	+0.038	+ 9.80	+0.843	+0.041
	-1.12	-0.112	-0.027	+0.0335	+10.74	+0.782	+0.014
	-0.02	-0.017	-0.012	+0.032	+11.80	+0.845	+0.010
	+1.07	+0.073	+0.002	+0.0325	+12.88	+0.925	+0.005
	+2.16	+0.166	+0.017	+0.0355	+13.96	+1.006	+0.003
	+3.26	+0.268	+0.034	+0.0415	α decreasing		
	+4.37	+0.378	+0.041	+0.053	+ 9.70	+0.744	+0.020
	+5.46	+0.478	+0.043	+0.070	+ 8.74	+0.776	+0.036
	+6.55	+0.576	+0.046	+0.0895			
	+7.63	+0.668	+0.045	+0.1135			
	+8.72	+0.764	+0.043	+0.141			
	+9.79	+0.842	+0.043	+0.1695			
0.98	-2.23	-0.231	-0.030	+0.0465	+ 9.86	+0.897	-0.003
	-1.13	-0.124	-0.020	+0.041	+10.94	+0.979	-0.004
	-0.03	-0.025	-0.010	+0.040	+12.01	+1.054	-0.013
	+1.07	+0.072	0	+0.0395	+13.08	+1.128	-0.014
	+2.16	+0.170	+0.011	+0.043			
	+3.27	+0.282	+0.017	+0.0495			
	+4.38	+0.398	+0.013	+0.063			
	+5.48	+0.509	+0.008	+0.080			
	+6.57	+0.610	+0.005	+0.1015			
	+7.66	+0.708	+0.004	+0.127			
	+8.75	+0.808	-0.003	+0.155			
	+9.84	+0.896	-0.004	+0.186			
1.02	-2.25	-0.253	-0.017	+0.0525	+ 9.86	+0.878	+0.004
	-1.14	-0.144	-0.013	+0.0445	+10.94	+0.950	+0.008
	-0.04	-0.033	-0.008	+0.042	+12.01	+1.023	-0.001
	+1.08	+0.085	-0.005	+0.0415	+13.08	+1.095	0
	+2.18	+0.193	+0.001	+0.0465			
	+3.29	+0.301	+0.004	+0.056			
	+4.39	+0.405	+0.006	+0.069			
	+5.48	+0.502	+0.008	+0.085			
	+6.57	+0.595	+0.008	+0.105			
	+7.66	+0.690	+0.006	+0.129			
	+8.75	+0.792	+0.005	+0.1555			
	+9.84	+0.868	+0.005	+0.1845			
1.42	-2.39	-0.199	-0.007	+0.056	- 2.34	-0.202	-0.008
	-1.34	-0.127	-0.008	+0.0505	- 1.25	-0.124	-0.008
	-0.27	-0.049	-0.007	+0.0475	- 0.17	-0.047	-0.007
	+0.79	+0.025	-0.006	+0.047	+ 0.91	+0.027	-0.007
	+1.85	+0.102	-0.007	+0.0495	+ 1.99	+0.105	-0.007
	+2.90	+0.174	-0.006	+0.054	+ 3.07	+0.184	-0.007
	+3.96	+0.243	-0.006	+0.062	+ 4.15	+0.262	-0.008
	+5.02	+0.321	-0.007	+0.072	+ 5.23	+0.337	-0.009
					+ 6.32	+0.418	-0.009
					+ 7.40	+0.491	-0.007
					+ 8.48	+0.563	-0.004

TABLE 4 (Contd)

	3 Component Balance				5 Component Balance		
M	α	C_L	C_m	C_D	α	C_L	C_m
1.61	-2.58	-0.190	-0.002	+0.055	-2.52	-0.189	-0.001
	-0.48	-0.054	-0.004	+0.0465	-1.45	-0.119	-0.002
	+1.63	+0.075	-0.004	+0.0475	-0.38	-0.052	-0.003
	+3.73	+0.208	-0.006	+0.0575	+0.69	+0.014	-0.002
	+5.84	+0.342	-0.007	+0.078	+1.77	+0.082	-0.003
	+7.95	+0.475	-0.008	+0.1075	+2.84	+0.150	-0.004
	+9.01	+0.545	-0.008	+0.1265	+3.92	+0.222	-0.005
					+4.99	+0.289	-0.006
					+6.06	+0.358	-0.005
					+7.14	+0.427	-0.006
					+8.21	+0.499	-0.006
					+9.29	+0.565	-0.008
					+10.36	+0.631	-0.008
					+11.44	+0.702	-0.011
					+12.50	+0.761	-0.010
1.82	-2.25	-0.162	0	+0.049	-2.17	-0.159	+0.001
	-0.16	-0.040	-0.001	+0.042	-1.11	-0.096	-0.001
	+1.93	+0.083	-0.004	+0.044	-0.05	-0.036	-0.001
	+4.01	+0.202	-0.007	+0.054	+1.00	+0.024	-0.003
	+6.10	+0.323	-0.008	+0.0735	+2.06	+0.086	-0.004
	+8.19	+0.442	-0.008	+0.1015	+3.12	+0.148	-0.005
	+10.27	+0.559	-0.008	+0.1375	+4.18	+0.211	-0.007
					+5.24	+0.272	-0.008
					+6.30	+0.335	-0.010
					+7.36	+0.398	-0.009
					+8.42	+0.460	-0.010
					+9.48	+0.523	-0.011
					+10.54	+0.582	-0.009
					+11.60	+0.641	-0.008
					+12.66	+0.700	-0.006
					+13.73	+0.762	-0.003
					+14.79	+0.817	0

TABLE 5

Aerodynamic Coefficients of Model with the Nacelles removed

	3 Component Balance								
M	α^o	C_L	C_m	C_D	M	α^o	C_L	C_m	C_D
0.80	-2.13	-0.149	-0.020	+0.0225	1.02				
	-1.06	-0.069	-0.010	+0.0195					
	+0.01	+0.011	0	+0.019		-2.17	-0.177	-0.005	+0.0355
	+1.08	+0.091	+0.010	+0.0205		-1.08	-0.083	-0.002	+0.0315
	+2.15	+0.170	+0.020	+0.0235		+0.01	+0.012	-0.001	+0.0305
	+3.22	+0.256	+0.031	+0.0295		+1.10	+0.106	0	+0.032
	+4.29	+0.342	+0.041	+0.038		+2.19	+0.200	+0.005	+0.036
	+5.37	+0.425	+0.051	+0.051		+3.29	+0.308	+0.002	+0.0445
	+6.44	+0.511	+0.054	+0.068		+4.39	+0.415	-0.005	+0.0575
	+7.49	+0.586	+0.051	+0.087		+5.48	+0.518	-0.014	+0.0745
	+8.53	+0.641	+0.031	+0.109		+6.57	+0.615	-0.020	+0.094
	+9.55	+0.676	+0.019	+0.129		+7.66	+0.709	-0.026	+0.118
						+8.74	+0.798	-0.027	+0.145
						+9.82	+0.880	-0.030	+0.174
0.90	-2.15	-0.167	-0.020	+0.023	1.61	-2.54	-0.153	+0.011	+0.0365
	-1.07	-0.077	-0.009	+0.020		-1.50	-0.089	+0.006	+0.032
	+0.01	+0.012	0	+0.019		-0.45	-0.027	+0.002	+0.0305
	+1.09	+0.097	+0.010	+0.020		+0.60	+0.036	-0.004	+0.0305
	+2.17	+0.186	+0.021	+0.0235		+1.64	+0.094	-0.007	+0.033
	+3.26	+0.283	+0.031	+0.0305		+2.69	+0.160	-0.013	+0.038
	+4.36	+0.388	+0.043	+0.041		+3.74	+0.223	-0.018	+0.0445
	+5.45	+0.490	+0.046	+0.0565		+4.78	+0.285	-0.023	+0.054
	+6.53	+0.588	+0.046	+0.0775		+5.83	+0.350	-0.028	+0.0655
	+7.60	+0.666	+0.045	+0.0995		+6.88	+0.412	-0.030	+0.0795
	+8.63	+0.705	+0.040	+0.121		+7.93	+0.472	-0.033	+0.0955
	+9.68	+0.757	+0.034	+0.145		+8.98	+0.535	-0.036	+0.114

TABLE 6

Aerodynamic Coefficients of Model with no Flow through the Nacelles

3 Component Balance									
M	α	C_L	C_m	C_D	M	α	C_L	C_m	C_D
0.80	-2.16	-0.177	-0.041	0.0375	1.02	-2.31	-0.264	-0.012	0.053
	-1.09	-0.097	-0.024	0.0335		-1.15	-0.148	-0.010	0.046
	-0.02	-0.017	-0.009	0.0315		-0.04	-0.034	-0.007	0.0425
	+1.05	+0.062	+0.006	0.032		+1.07	+0.079	-0.004	0.0435
	+2.12	+0.141	+0.021	0.034		+2.18	+0.190	-0.003	0.0485
	+4.28	+0.312	+0.052	0.0485		+3.29	+0.305	-0.002	0.0575
	+5.35	+0.396	+0.063	0.0605		+4.39	+0.410	0	0.070
	+6.43	+0.491	+0.066	0.079		+5.49	+0.518	-0.001	0.089
	+7.48	+0.564	+0.053	0.0995		+6.59	+0.619	+0.002	0.111
	+8.52	+0.620	+0.045	0.121		+7.68	+0.712	+0.006	0.1365
	+9.56	+0.670	+0.042	0.142		+8.77	+0.801	+0.011	0.1645
						+9.85	+0.877	+0.014	0.194
0.90	-2.19	-0.194	-0.043	0.0375					
	-0.02	-0.017	-0.011	0.031	1.61	-2.58	-0.180	-0.003	0.0685
	+2.15	+0.155	+0.020	0.034		-0.48	-0.055	-0.002	0.0605
	+4.33	+0.345	+0.052	0.049		+1.63	+0.075	-0.002	0.0615
	+6.52	+0.547	+0.072	0.0845		+3.73	+0.205	-0.004	0.0715
	+7.05	+0.591	+0.074	0.096		+5.84	+0.335	-0.004	0.091
	+7.59	+0.628	+0.076	0.107		+7.95	+0.465	-0.005	0.122
	+8.13	+0.669	+0.078	0.119		+9.00	+0.530	-0.005	0.1405
	+8.60	+0.659	+0.040	0.130					
	+9.12	+0.683	+0.037	0.1405					
	+9.65	+0.717	+0.033	0.1545					
	α decreasing								
	+8.60	+0.656	+0.040	0.129					
	+8.07	+0.627	+0.044	0.117					
	+7.56	+0.605	+0.061	0.1055					
	+7.05	+0.585	+0.075	0.095					

TABLE 7

Aerodynamic Coefficients of Model with Vortex Generators

3 Component Balance									
M	α	C_L	C_m	C_D	M	α	C_L	C_m	C_D
0.7	-2.14	-0.175	-0.041	+0.036	0.94	-2.22	-0.218	-0.045	+0.0385
	-1.08	-0.099	-0.025	+0.032		-1.13	-0.121	-0.027	+0.0335
	-0.02	-0.023	-0.009	+0.030		-0.03	-0.027	-0.012	+0.0305
	+1.04	+0.052	+0.009	+0.0305		1.06	+0.064	+0.003	+0.0315
	+2.10	+0.127	+0.025	+0.0325		2.15	+0.157	+0.018	+0.035
	+3.17	+0.207	+0.040	+0.0375		3.25	+0.255	+0.037	+0.041
	+4.24	+0.293	+0.055	+0.046		4.36	+0.367	+0.043	+0.0525
	+5.30	+0.375	+0.070	+0.0575		5.45	+0.470	+0.048	+0.068
	+6.36	+0.452	+0.082	+0.071		6.55	+0.570	+0.045	+0.089
	+7.43	+0.530	+0.090	+0.090		7.63	+0.659	+0.046	+0.112
	+8.48	+0.600	+0.098	+0.108		8.71	+0.747	+0.044	+0.138
	+9.53	+0.666	+0.096	+0.1305		9.79	+0.829	+0.045	+0.166
0.8	-2.17	-0.183	-0.042	+0.0365	0.98	-2.24	-0.241	-0.030	+0.0465
	-1.10	-0.106	-0.024	+0.032		-1.13	-0.131	-0.020	+0.041
	-0.03	-0.028	-0.009	+0.0305		-0.59	-0.085	-0.014	+0.040
	1.05	+0.053	+0.008	+0.031		-0.04	-0.036	-0.008	+0.039
	2.12	+0.131	+0.024	+0.0335		+0.51	+0.013	-0.003	+0.039
	3.20	+0.221	+0.039	+0.0385		1.06	+0.060	+0.003	+0.039
	4.28	+0.309	+0.055	+0.0475		2.15	+0.157	+0.013	+0.0425
	5.35	+0.395	+0.069	+0.0595		3.27	+0.273	+0.021	+0.054
	6.42	+0.474	+0.081	+0.075		4.37	+0.390	+0.017	+0.0655
	7.49	+0.553	+0.088	+0.0935		5.47	+0.503	+0.013	+0.0805
	8.55	+0.622	+0.090	+0.114		6.57	+0.601	+0.011	+0.101
	9.60	+0.680	+0.088	+0.136		7.66	+0.699	+0.007	+0.125
						8.74	+0.791	+0.005	+0.1525
						9.83	+0.881	+0.002	+0.183
0.85	-2.19	-0.195	-0.044	+0.037	1.02	-2.26	-0.263	-0.017	+0.053
	-1.10	-0.109	-0.026	+0.0325		-1.15	-0.153	-0.013	+0.046
	-0.03	-0.027	-0.010	+0.0305		-0.60	-0.099	-0.009	+0.0435
	1.05	+0.056	+0.007	+0.031		-0.04	-0.043	-0.005	+0.042
	2.13	+0.137	+0.024	+0.0335		+0.51	+0.015	-0.005	+0.042
	3.21	+0.230	+0.040	+0.039		1.06	+0.068	-0.001	+0.043
	4.30	+0.322	+0.056	+0.048		2.17	+0.179	+0.005	+0.047
	5.38	+0.408	+0.072	+0.061		4.39	+0.399	+0.009	+0.069
	6.45	+0.487	+0.080	+0.0765		6.57	+0.588	+0.011	+0.1045
	7.53	+0.576	+0.086	+0.097		8.74	+0.770	+0.009	+0.1565
	8.59	+0.645	+0.085	+0.1185		9.83	+0.858	+0.006	+0.1835
	9.63	+0.701	+0.082	+0.141					
0.90	-2.20	-0.203	-0.045	+0.037	1.42	-4.51	-0.341	-0.011	+0.074
	-1.11	-0.114	-0.028	+0.033		-3.45	-0.266	-0.010	+0.063
	-0.03	-0.029	-0.011	+0.0315		-2.39	-0.185	-0.010	+0.0545
	+1.05	+0.060	+0.005	+0.031		-1.33	-0.114	-0.008	+0.049
	+2.14	+0.145	+0.022	+0.034		-0.27	-0.041	-0.008	+0.0465
	+3.23	+0.240	+0.039	+0.040		+0.79	+0.033	-0.007	+0.0465
	+4.33	+0.340	+0.056	+0.049		+1.85	+0.108	-0.007	+0.049
	+5.42	+0.439	+0.068	+0.063		+2.91	+0.184	-0.006	+0.054
	+6.52	+0.548	+0.071	+0.083		+3.97	+0.260	-0.006	+0.0615
	+7.58	+0.624	+0.076	+0.103		+5.04	+0.338	-0.005	+0.072
	+8.65	+0.692	+0.080	+0.1265					
	+9.72	+0.766	+0.081	+0.153					

TABLE 7 (Contd)

3 Component Balance									
M	α	C_L	C_m	C_D	M	α	C_L	C_m	C_D
1.61	-4.69	-0.315	-0.003	0.0705	1.82	-2.25	-0.158	-0.002	+0.047
	-2.58	-0.182	-0.004	0.0525		-1.20	-0.097	-0.002	+0.0445
	-1.53	-0.115	-0.004	0.047		-0.16	-0.035	-0.002	+0.042
	-0.47	-0.051	-0.004	0.0445		+0.89	+0.023	-0.002	+0.042
	+0.58	+0.013	-0.004	0.040		+1.93	+0.083	-0.002	+0.044
	+1.63	+0.078	-0.003	0.045		+4.01	+0.204	-0.004	+0.0545
	+3.74	+0.214	-0.003	0.056		+5.06	+0.263	-0.004	+0.063
	+5.85	+0.351	-0.004	0.076		+6.10	+0.324	-0.003	+0.0735
	+7.96	+0.488	-0.004	0.107		+7.15	+0.386	-0.003	+0.087
	+9.02	+0.556	-0.003	0.126		+8.19	+0.446	-0.003	+0.102
						+9.24	+0.506	-0.005	+0.1195
						+10.28	+0.567	-0.005	+0.139

TABLE 8(a)

Aerodynamic Coefficients of the Model with Ailerons Represented

(Nominal settings Port 0°, Starboard 0°)

M	α	C_N	C_m	C_Y	C_n	C_ℓ
0.80	-1.09	-0.103	-0.026	+0.001	+0.001	-0.0005
	-0.02	-0.024	-0.010	+0.001	+0.001	-0.0005
	+1.05	+0.058	+0.006	+0.001	+0.001	0
	+2.12	+0.141	+0.022	+0.001	+0.001	0
	+3.19	+0.225	+0.038	+0.001	+0.001	0
	+4.28	+0.319	+0.051	+0.001	+0.001	0
	+5.35	+0.408	+0.063	+0.001	+0.001	0
	+6.42	+0.499	+0.065	+0.001	+0.001	0
	+7.47	+0.567	+0.047	+0.002	+0.001	0
0.90	-1.11	-0.113	-0.027	+0.002	+0.001	-0.0005
	-0.03	-0.026	-0.011	+0.002	0	-0.0005
	+1.06	+0.062	+0.005	+0.002	0	-0.0005
	+2.14	+0.152	+0.021	+0.002	0	0
	+3.23	+0.246	+0.038	+0.002	0	0
	+4.33	+0.357	+0.054	+0.002	0	0
	+5.42	+0.460	+0.064	+0.002	0	0
	+6.52	+0.563	+0.068	+0.002	0	0
	+7.59	+0.648	+0.073	+0.002	0	0
0.98	-1.11	-0.128	-0.021	+0.002	+0.001	-0.0005
	-0.03	-0.032	-0.009	+0.002	0	-0.0005
	+1.05	+0.063	0	+0.002	0	-0.0005
	+2.14	+0.165	+0.012	+0.002	0	-0.0005
	+3.23	+0.278	+0.017	+0.002	0	-0.0005
	+4.33	+0.404	+0.013	+0.002	0	0
	+5.42	+0.514	+0.009	+0.002	0	0
	+6.51	+0.621	+0.005	+0.002	0	0
	+7.59	+0.718	+0.005	+0.002	+0.001	0

M	α	C_N	C_m	C_Y	C_n	C_ℓ
1.42	-2.33	-0.197	-0.008	+0.001	0	+0.0005
	-0.17	-0.043	-0.008	+0.001	0	+0.0005
	+1.99	+0.104	-0.007	0	0	+0.0005
	+4.15	+0.259	-0.006	0	0	+0.0005
	+6.31	+0.416	-0.006	0	0	+0.0005
	+8.47	+0.565	-0.003	+0.001	0	+0.0005
1.82	-2.17	-0.161	+0.002	0	0	0
	-0.05	-0.035	0	+0.001	0	0
	+2.06	+0.082	-0.003	+0.001	0	0
	+4.17	+0.205	-0.005	+0.001	0	0
	+6.29	+0.326	-0.006	+0.001	0	0

Actual settings Port 0°; Starboard 0°.

TABLE 8(b)

Aerodynamic Coefficients of the Model with Ailerons Represented

(Nominal settings Port 0, Starboard 5.0° up)

M	α	C_N	C_m	C_Y	C_n	C_ℓ
0.80	-1.13	-0.156	-0.010	0	+0.002	+0.0125
	-0.06	-0.073	+0.006	+0.001	+0.002	+0.012
	+1.02	+0.009	+0.021	+0.001	+0.001	+0.012
	+2.09	+0.091	+0.038	+0.001	+0.001	+0.012
	+3.16	+0.172	+0.053	+0.002	+0.001	+0.0125
	+4.24	+0.260	+0.070	+0.002	+0.001	+0.013
	+5.31	+0.351	+0.080	+0.002	+0.001	+0.014
	+6.39	+0.450	+0.081	+0.003	+0.001	+0.014
	+7.44	+0.516	+0.064	+0.003	+0.001	+0.0125
0.90	-1.15	-0.169	-0.007	+0.001	+0.002	+0.013
	-0.06	-0.079	+0.009	+0.001	+0.002	+0.0125
	+1.02	+0.009	+0.024	+0.002	+0.001	+0.0125
	+2.10	+0.099	+0.041	+0.001	+0.001	+0.0135
	+3.19	+0.187	+0.058	+0.002	+0.001	+0.014
	+4.28	+0.287	+0.073	+0.003	+0.001	+0.0145
	+5.36	+0.396	+0.087	+0.003	+0.001	+0.0155
	+6.47	+0.502	+0.092	+0.004	+0.001	+0.0145
	+7.54	+0.583	+0.096	+0.005	+0.001	+0.0165
0.98	-1.16	-0.170	+0.002	0	+0.002	+0.013
	-0.06	-0.069	+0.011	+0.001	+0.002	+0.0125
	+1.03	+0.026	+0.020	+0.001	+0.002	+0.012
	+2.13	+0.127	+0.032	+0.002	+0.002	+0.012
	+3.24	+0.240	+0.039	+0.002	+0.001	+0.013
	+4.35	+0.364	+0.036	+0.004	+0.001	+0.0135
	+5.45	+0.474	+0.032	+0.004	+0.001	+0.0135
	+6.55	+0.583	+0.029	+0.005	+0.001	+0.0135
	+7.64	+0.686	+0.027	+0.005	0	+0.013

M	α	C_N	C_m	C_Y	C_n	C_ℓ
1.42	-2.34	-0.212	0.003	-0.001	0.001	0.0055
	-0.18	-0.057	0.004	0	0.001	0.0055
	1.97	+0.088	0.004	0	0	0.0055
	4.14	0.243	0.005	+0.001	0	0.006
	6.30	0.400	0.007	+0.002	0	0.006
	8.42	0.550	0.010	+0.002	0	0.006
1.82	-2.17	-0.164	0.009	-0.001	0.001	0.0035
	-0.06	-0.042	0.006	0	0.001	0.0035
	2.05	+0.076	0.004	0	0	0.0035
	4.17	0.197	0.002	0.001	0	0.004
	6.29	0.323	0.001	0.002	0	0.004
	8.41	0.451	0.001	0.002	-0.001	0.004
	9.46	0.515	0.001	0.003	-0.001	0.004

Actual settings M = 0.8, 0.9, 0.98 Port 0; Starboard 5.8° up.
M = 1.42, 1.82 Port 0°; Starboard 4.6° up.

TABLE 8(c)

Aerodynamic Coefficients of the Model with Ailerons Represented

(Nominal settings Port 5° down, Starboard 5° up)

M	α	C_N	C_m	C_Y	C_n	C_ℓ
0.80	-1.09	-0.103	-0.028	-0.001	+0.002	+0.025
	-0.02	-0.021	-0.012	-0.001	+0.002	+0.025
	+1.06	+0.069	+0.001	0	+0.001	+0.0245
	+2.13	+0.149	+0.017	+0.001	+0.001	+0.026
	+3.20	+0.234	+0.033	+0.002	0	+0.027
	+4.23	+0.323	+0.048	+0.003	0	+0.0275
	+5.35	+0.412	+0.061	+0.004	-0.001	+0.027
	+6.43	+0.505	+0.061	+0.005	-0.001	+0.027
	+7.47	+0.567	+0.044	+0.005	-0.001	+0.0255
0.90	-1.11	-0.113	-0.029	-0.002	+0.002	+0.026
	-0.02	-0.021	-0.014	-0.001	+0.002	+0.026
	+1.06	+0.069	+0.001	+0.002	+0.001	+0.026
	+2.15	+0.161	+0.016	+0.001	+0.001	+0.028
	+3.24	+0.257	+0.033	+0.002	0	+0.0295
	+4.33	+0.357	+0.051	+0.004	0	+0.029
	+5.42	+0.451	+0.062	+0.006	-0.001	+0.028
	+6.51	+0.554	+0.066	+0.006	-0.001	+0.025
	+7.57	+0.623	+0.075	+0.006	-0.001	+0.025
0.98	-1.13	-0.128	-0.022	-0.002	+0.002	+0.0245
	-0.03	-0.029	-0.014	-0.001	+0.002	+0.0245
	+1.06	+0.073	-0.005	0	+0.001	+0.025
	+2.16	+0.176	+0.005	+0.001	+0.001	+0.026
	+3.27	+0.294	+0.010	+0.003	0	+0.026
	+4.38	+0.409	+0.009	+0.004	-0.001	+0.026
	+5.48	+0.522	+0.006	+0.006	-0.001	+0.0255
	+6.57	+0.626	+0.003	+0.007	-0.002	+0.0245
	+7.59	+0.727	+0.002	+0.008	-0.002	+0.023

M	α	C_N	C_m	C_Y	C_n	C_ℓ
1.42	-2.33	-0.192	-0.010	-0.002	+0.002	0.0115
	-0.17	-0.041	-0.010	-0.001	+0.001	0.011
	1.99	0.107	-0.009	0	0.001	0.0115
	4.15	0.263	-0.007	0.001	0	0.012
	6.32	0.419	-0.007	0.002	-0.001	0.012
	8.47	0.568	-0.003	0.004	-0.002	0.012
1.82	-2.18	-0.154	-0.001	-0.002	+0.001	0.008
	-0.05	-0.031	-0.003	-0.001	0.001	0.008
	2.06	0.089	-0.005	0	0	0.008
	4.18	0.211	-0.008	+0.001	-0.001	0.008
	6.29	0.337	-0.008	+0.002	-0.001	0.008
	8.42	0.464	-0.009	+0.004	-0.002	0.008
	9.47	0.526	-0.009	0.004	-0.002	0.008

Actual settings M = 0.8, 0.9, 0.98 Port 5.9° down; Starboard 5.8° up
M = 1.42, 1.82 Port 5.1° down; Starboard 4.6° up

TABLE 8(d)

Aerodynamic Coefficients of the Model with Ailerons Represented

(Nominal settings Port 5° down, Starboard 10° up)

M	α	C_N	C_m	C_Y	C_n	C_ℓ
0.80	-1.12	-0.137	-0.015	-0.003	+0.004	+0.0345
	-0.05	-0.054	+0.000	-0.001	+0.003	+0.034
	+1.03	+0.032	+0.014	0	+0.002	+0.034
	+2.10	+0.116	+0.029	+0.002	+0.002	+0.035
	+3.18	+0.202	+0.044	+0.003	+0.001	+0.036
	+4.26	+0.291	+0.060	+0.003	+0.001	+0.0365
	+5.33	+0.380	+0.077	+0.004	0	+0.0365
	+6.41	+0.473	+0.072	+0.005	0	+0.036
	+7.46	+0.545	+0.057	+0.006	0	+0.0355
0.90	-1.13	-0.142	-0.016	-0.003	+0.004	+0.0345
	-0.05	-0.052	-0.001	-0.002	+0.003	+0.034
	+1.04	+0.042	+0.012	0	+0.002	+0.034
	+2.13	+0.137	+0.026	+0.002	+0.002	+0.035
	+3.22	+0.228	+0.042	+0.003	+0.001	+0.036
	+4.31	+0.326	+0.060	+0.004	+0.001	+0.0355
	+5.40	+0.427	+0.073	+0.006	0	+0.0355
	+6.49	+0.524	+0.080	+0.007	-0.001	+0.033
	+7.56	+0.610	+0.082	+0.008	0	+0.030
0.98	-1.15	-0.159	-0.005	-0.003	+0.004	+0.0345
	-0.06	-0.063	+0.004	-0.002	+0.003	+0.0345
	+1.04	+0.039	+0.012	0	+0.002	+0.034
	+2.14	+0.147	+0.022	+0.002	+0.002	+0.035
	+3.25	+0.262	+0.027	+0.003	+0.001	+0.035
	+4.36	+0.384	+0.026	+0.005	0	+0.035
	+5.46	+0.495	+0.021	+0.007	-0.001	+0.0345
	+6.56	+0.598	+0.019	+0.009	-0.001	+0.0335
	+7.65	+0.702	+0.018	+0.010	-0.002	+0.032

M	α	C_N	C_m	C_Y	C_n	C_ℓ
1.42	-2.34	-0.213	0.005	-0.003	+0.003	0.018
	-0.18	-0.060	0.003	-0.001	+0.002	0.0175
	1.98	+0.090	0.003	0	0.001	0.0175
	4.14	0.244	0.004	+0.002	0	0.018
	6.30	0.401	0.005	0.003	-0.001	0.018
	8.46	0.550	0.010	0.005	-0.002	0.018
1.82	-2.17	-0.166	0.008	-0.003	+0.003	0.012
	-0.06	-0.044	0.005	-0.001	0.002	0.012
	+2.06	+0.074	0.003	0	0	0.0125
	4.17	0.201	0.000	+0.002	-0.001	0.0125
	6.29	0.324	0.001	0.003	-0.002	0.0125
	8.41	0.454	0.001	0.004	-0.002	0.013
	9.47	0.516	0.001	0.006	-0.003	0.0135

Actual settings M = 0.8, 0.9, 0.98 Port 5.9° down Starboard 9.9° up
M = 1.42, 1.82 Port 5.1° down Starboard 9.9° up

TABLE 8(e)

Aerodynamic Coefficients of the Model with Ailerons Represented

(Nominal settings Port 10° down, Starboard 10° up)

M	α	C_N	C_m	C_Y	C_n	C_ℓ
0.80	-1.09	-0.102	-0.027	-0.004	+0.003	+0.043
	-0.02	-0.020	-0.013	-0.002	+0.002	+0.0425
	+1.05	+0.066	+0.002	0	+0.001	+0.0425
	+2.13	+0.152	+0.016	+0.001	0	+0.0435
	+3.20	+0.235	+0.031	+0.003	0	+0.045
	+4.28	+0.319	+0.048	+0.003	-0.001	+0.0435
	+5.35	+0.407	+0.059	+0.005	-0.001	+0.0435
	+6.42	+0.499	+0.060	+0.006	-0.002	+0.043
	+7.47	+0.567	+0.042	+0.007	-0.002	+0.042
0.90	-1.11	-0.111	-0.027	-0.004	+0.003	+0.041
	-0.02	-0.023	-0.013	-0.002	+0.002	+0.0415
	+1.06	+0.070	0	0	+0.001	+0.0415
	+2.15	+0.162	+0.014	+0.001	0	+0.042
	+3.23	+0.253	+0.030	+0.003	-0.001	+0.043
	+4.32	+0.346	+0.049	+0.005	-0.001	+0.0415
	+5.41	+0.439	+0.061	+0.006	-0.002	+0.039
	+6.50	+0.542	+0.066	+0.007	-0.002	+0.0385
	+7.57	+0.617	+0.076	+0.008	-0.002	+0.0345
0.98	-1.13	-0.128	-0.024	-0.005	+0.003	+0.0435
	-0.03	-0.026	-0.014	-0.003	+0.002	+0.044
	+1.07	+0.077	-0.005	0	+0.001	+0.044
	+2.16	+0.177	+0.004	+0.001	0	+0.0435
	+3.28	+0.296	+0.010	+0.003	0	+0.043
	+4.38	+0.410	+0.010	+0.006	-0.001	+0.043
	+5.48	+0.519	+0.008	+0.008	-0.002	+0.041
	+6.57	+0.621	+0.008	+0.010	-0.003	+0.0395
	+7.67	+0.727	+0.004	+0.011	-0.003	+0.038

M	α	C_N	C_m	C_Y	C_n	C_ℓ
1.42	-2.33	-0.200	-0.008	-0.005	+0.003	+0.023
	-0.17	-0.045	-0.008	-0.003	+0.002	+0.0235
	+1.99	+0.104	-0.009	-0.001	+0.001	+0.0235
	+4.15	+0.260	-0.005	+0.001	-0.003	+0.0235
	+6.32	+0.415	+0.005	+0.003	-0.002	+0.023
	+8.47	+0.568	-0.001	+0.005	-0.003	+0.023
1.82	-2.16	-0.152	0	-0.004	+0.003	+0.016
	-0.05	-0.032	-0.003	-0.002	+0.001	+0.016
	+2.06	+0.091	-0.006	0	0	+0.016
	+4.18	+0.213	0	+0.002	-0.002	+0.016

Actual settings: All Mach numbers Port 10.1° down, Starboard 9.9° up.

TABLE 9

Values of $\left(\frac{\partial C_L}{\partial \alpha}\right)_o$ for the tested Configurations

Mach No.	Basic Model	With Nacelles Off	With Nacelles Stopped	With Aileron Gaps	With Vortex Generators
0.70	0.072				0.072
0.80	0.075	0.075	0.074	0.074	0.074
0.85	0.078				0.077
0.90	0.081	0.081	0.081	0.081	0.080
0.94	0.085				0.085
0.96					0.086
0.98	0.091			0.088	0.089
1.00					0.094
1.02	0.101	0.088	0.101		0.099
1.42	0.071			0.069	0.069
1.61	0.063	0.060	0.061		0.062
1.82	0.059			0.054	0.057

TABLE 10

Values of $\left(\frac{\partial C_m}{\partial C_L}\right)_{C_L=0}$ for the tested Configurations

Mach No.	Basic Model	With Nacelles Off	With Nacelles Stopped	With Aileron Gaps	With Vortex Generators
0.70	0.20				0.22
0.80	0.20	0.125	0.195	0.20	0.21
0.85	0.19				0.20
0.90	0.18	0.115	0.170	0.185	0.19
0.94	0.16				0.165
0.96					0.145
0.98	0.10			0.12	0.11
1.00					0.14
1.02	0.035	0.025	0.025		0.045
1.42	0			-0.005	0.01
1.61	-0.005	-0.075	0		0.005
1.82	-0.015			-0.02	0

TABLE 11

Values of $\left(C_D\right)_o$ for the tested Configurations

Mach No.	Basic Model	With Nacelles Off	With Nacelles Stopped	With Vortex Generators
0.70	0.031			0.030
0.80	0.031	0.019	0.0315	0.030
0.85	0.031			0.0305
0.90	0.031	0.019	0.031	0.0305
0.94	0.032			0.0305
0.96				0.0345
0.98	0.0395			0.039
1.00				0.040
1.02	0.0415	0.0305	0.042	0.042
1.42	0.047			0.0465
1.61	0.046	0.030	0.0605	0.044
1.82	0.042			0.042

N.B. No drag measurements were made for the case of aileron gaps unsealed.

TABLE 12

Values of $\left(\frac{\partial C_L}{\partial \alpha}\right)_o$, $\left(\frac{\partial C_m}{\partial C_L}\right)_o$ and $\left(C_D\right)_o$ for the Body Alone

Mach No.	$\left(\frac{\partial C_L}{\partial \alpha}\right)_o$	$\left(\frac{\partial C_m}{\partial C_L}\right)_o$	$\left(C_D\right)_o$
0.70	0.004	1.95	0.010
0.80	0.004	2.00	0.010
0.85	0.004	2.00	0.010
0.90	0.004	1.95	0.011
0.94	0.004	1.80	0.0105
0.98	0.004	1.63	0.0105
1.02	0.004	1.58	0.014
1.42	0.004	2.35	0.019
1.61	0.004	2.45	0.0185
1.82	0.004	2.15	0.0165

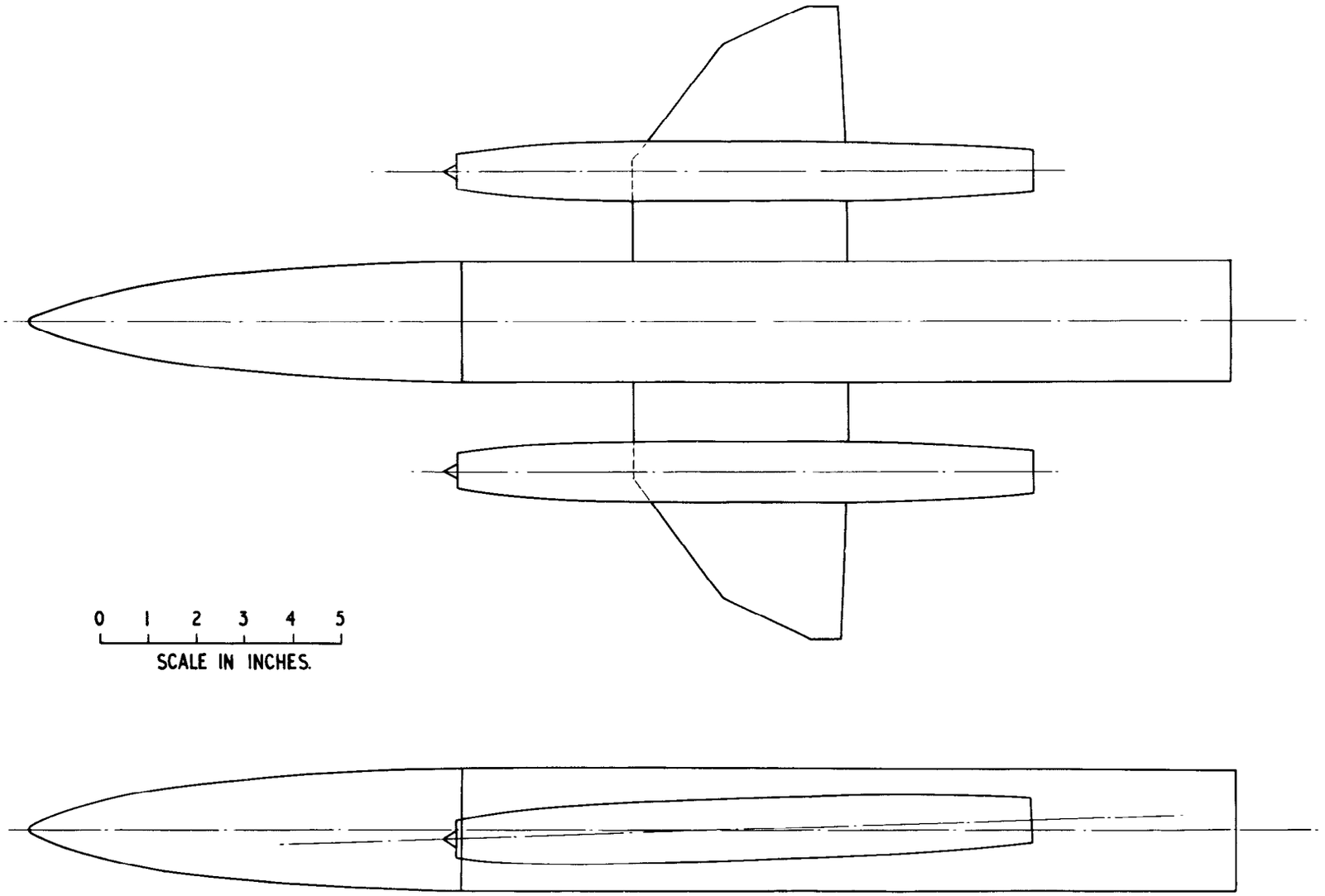

FIG. 1. GENERAL ARRANGEMENT OF THE MODEL.

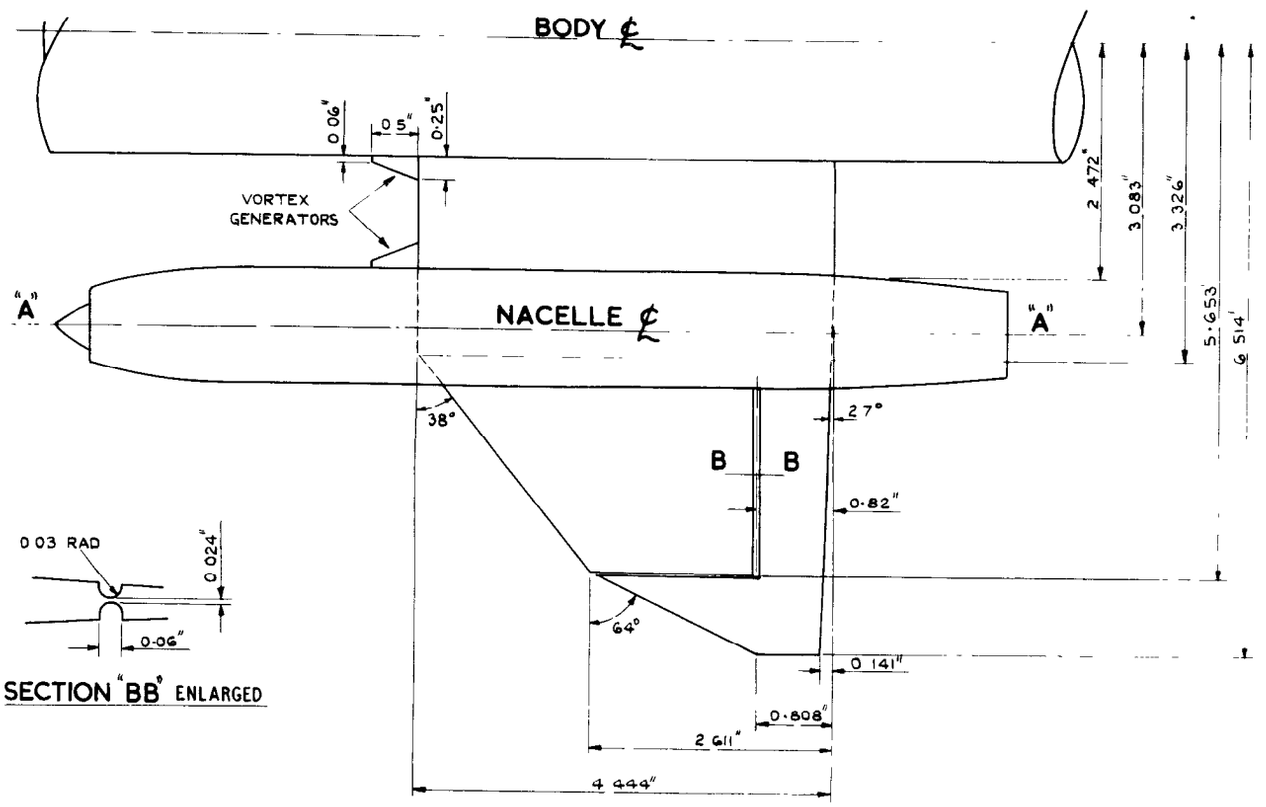

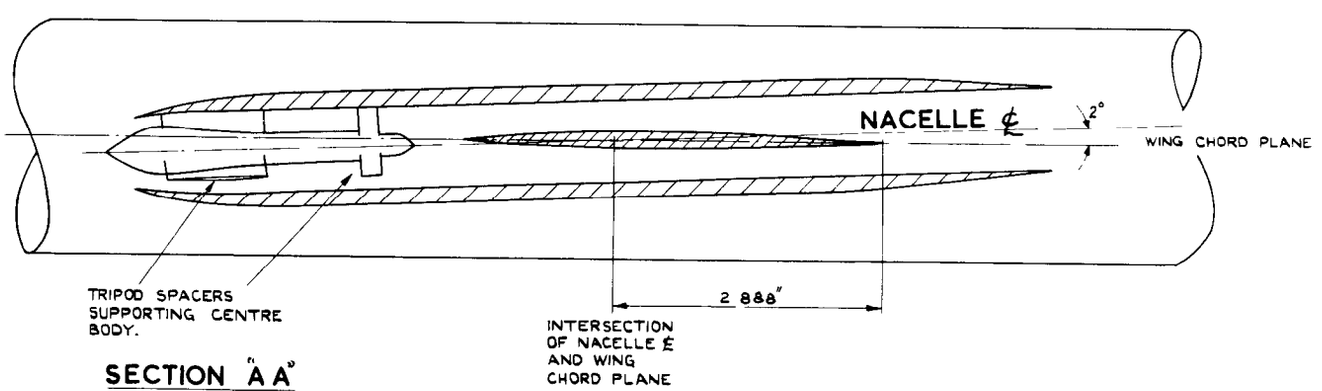

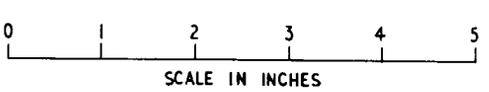

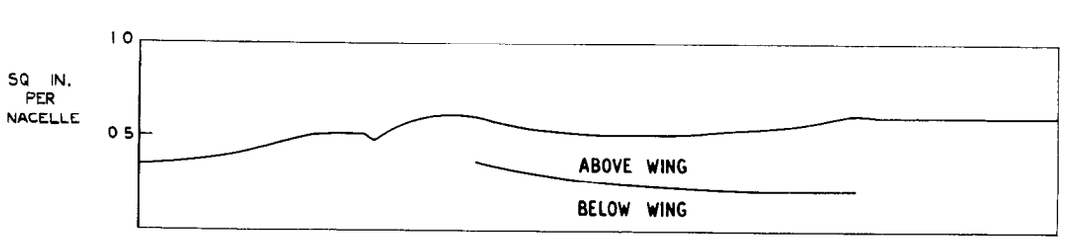

INTERNAL CROSS-SECTION AREA DISTRIBUTION OF NACELLE DUCT

FIG. 2. DETAILS OF THE WING AND NACELLE.

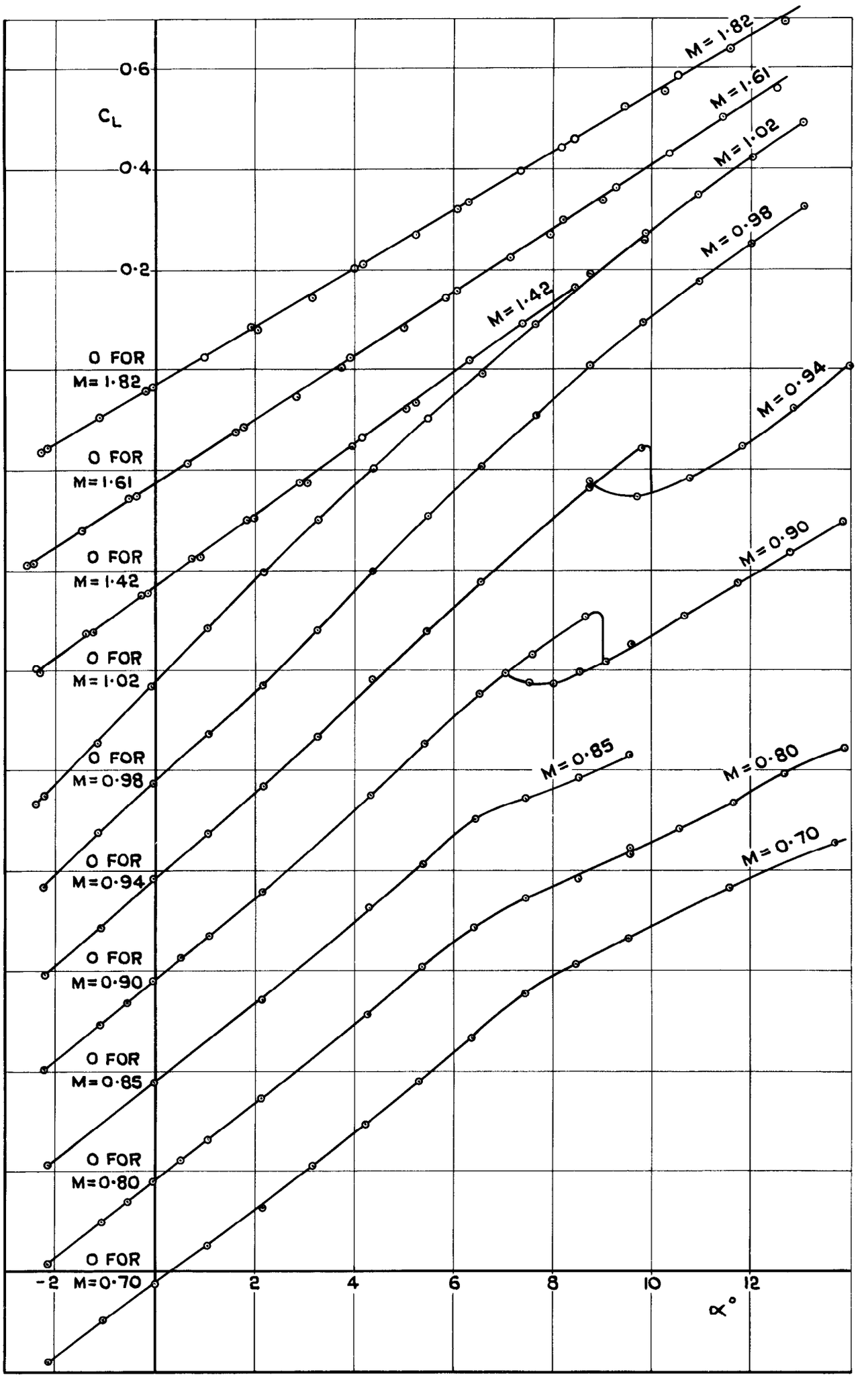

FIG. 3. VARIATION OF THE LIFT COEFFICIENT WITH INCIDENCE FOR THE BASIC MODEL.

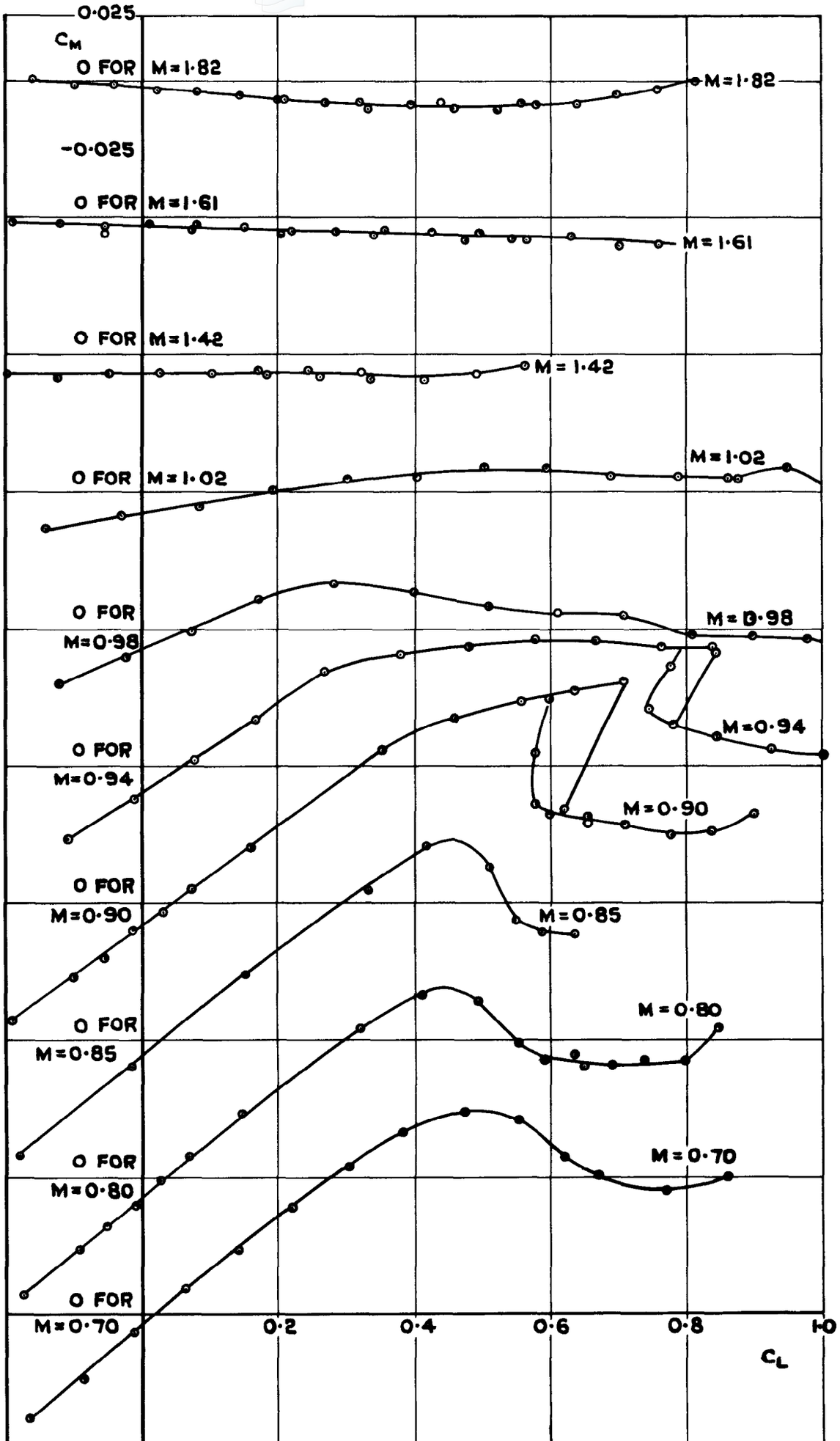

FIG. 4. VARIATION OF PITCHING MOMENT COEFFICIENT WITH LIFT COEFFICIENT FOR THE BASIC MODEL.

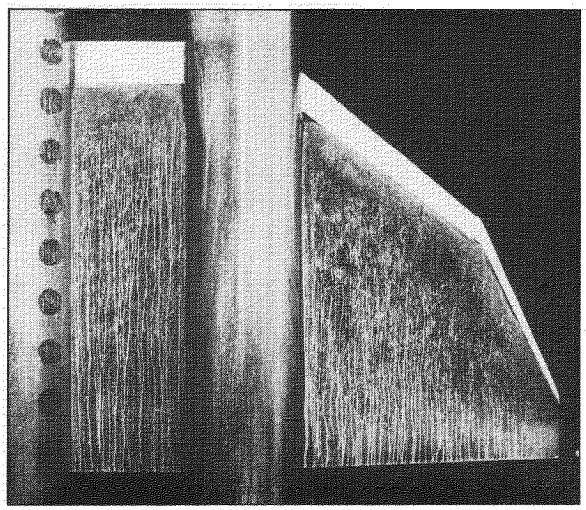

(a) $\alpha = 0$; $C_L = -0.02$

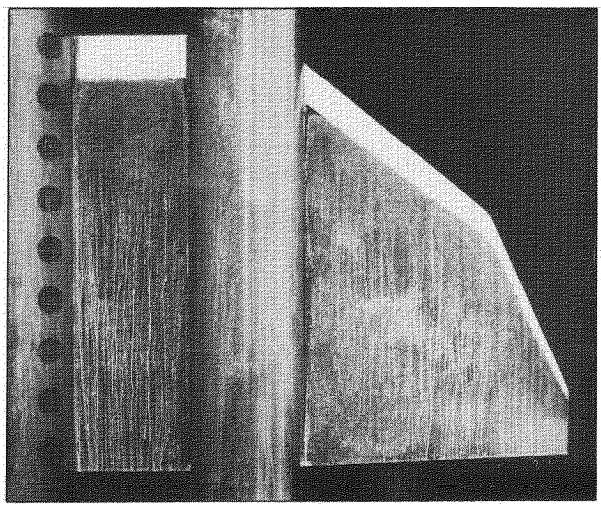

(b) $\alpha = 2.1^0$; $C_L = 0.14$

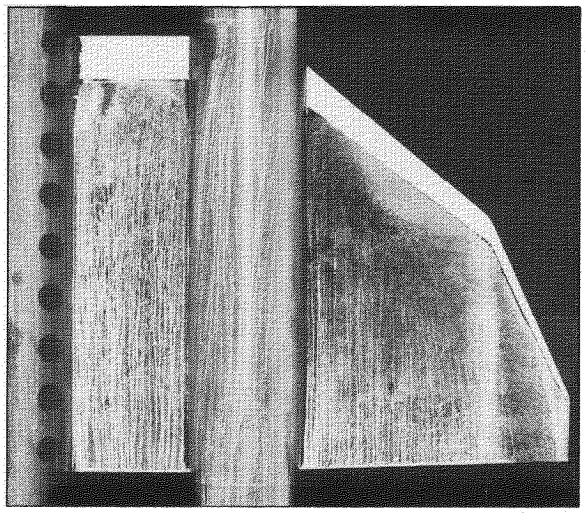

(c) $\alpha = 4.3^0$; $C_L = 0.32$

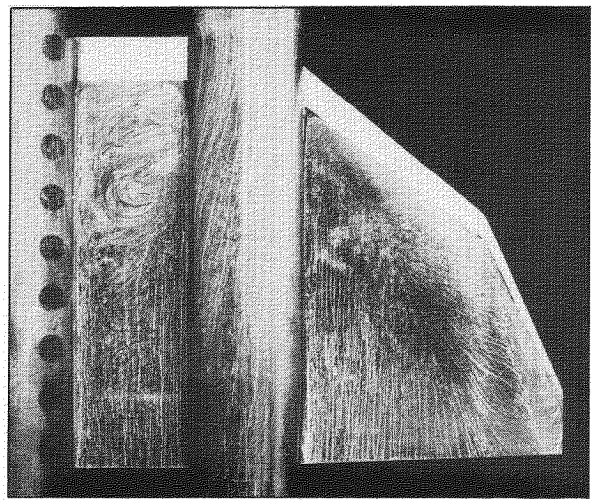

(d) $\alpha = 5.4^0$; $C_L = 0.41$

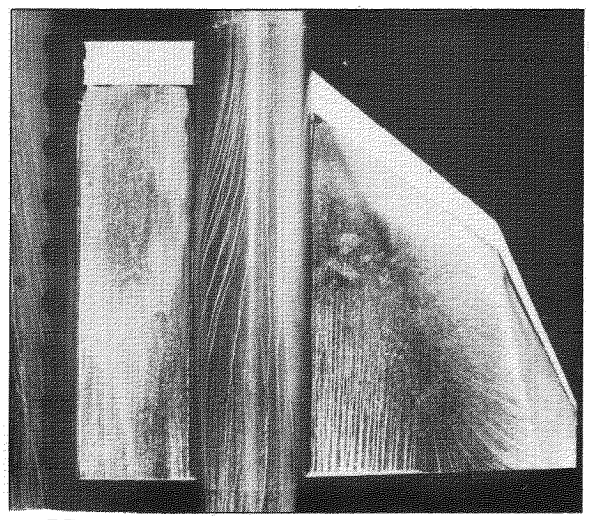

(e) $\alpha = 6.4^0$; $C_L = 0.49$

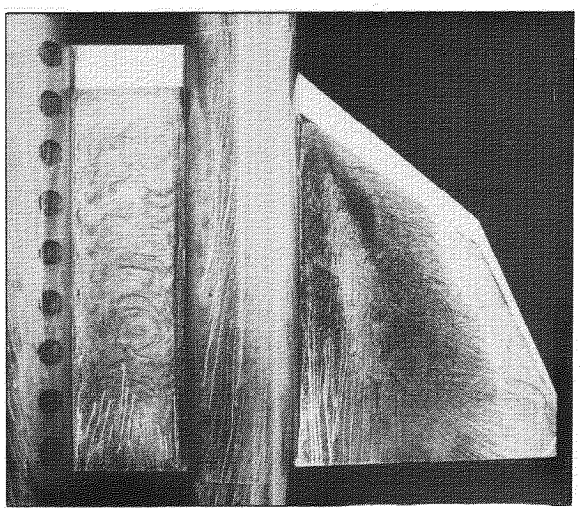

(f) $\alpha = 8.5^0$; $C_L = 0.59$

FIG.5. SURFACE OIL FLOW ON THE WING AT A

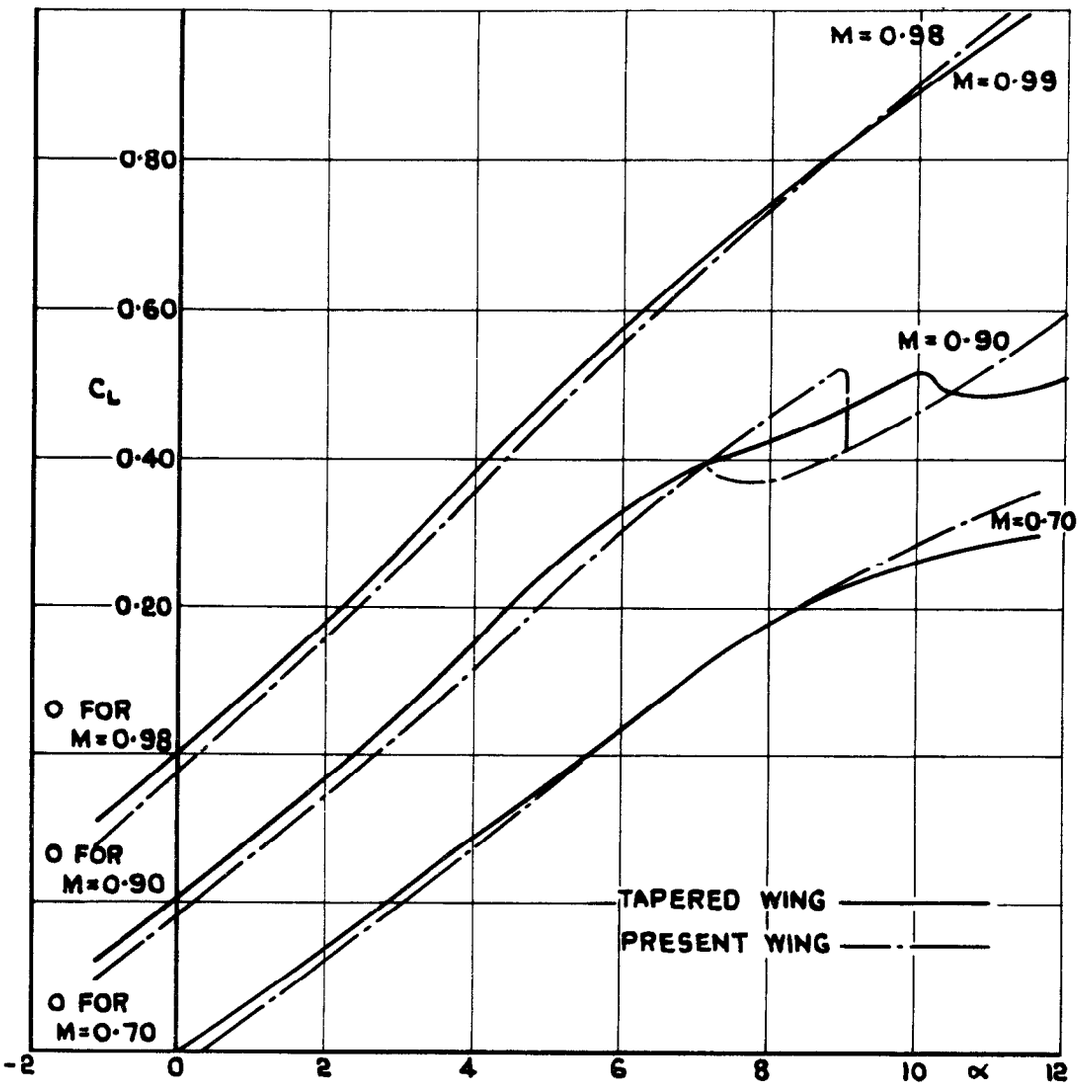

(a) VARIATION OF LIFT COEFFICIENT WITH INCIDENCE.

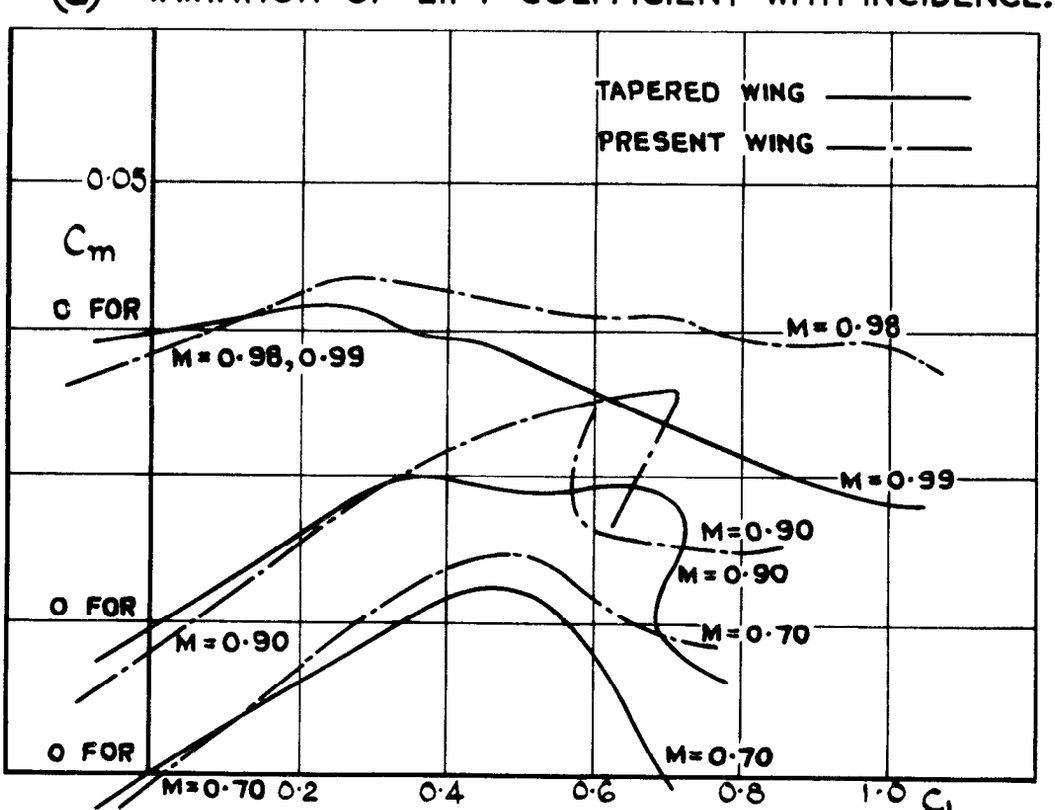

(b) VARIATION OF PITCHING MOMENT COEFFICIENT WITH LIFT COEFFICIENT.

FIG. 6 (a & b). COMPARISON OF THE LIFT AND PITCHING MOMENT OF THE BASIC MODEL WITH THOSE OF THE WING OF REFERENCE 5.

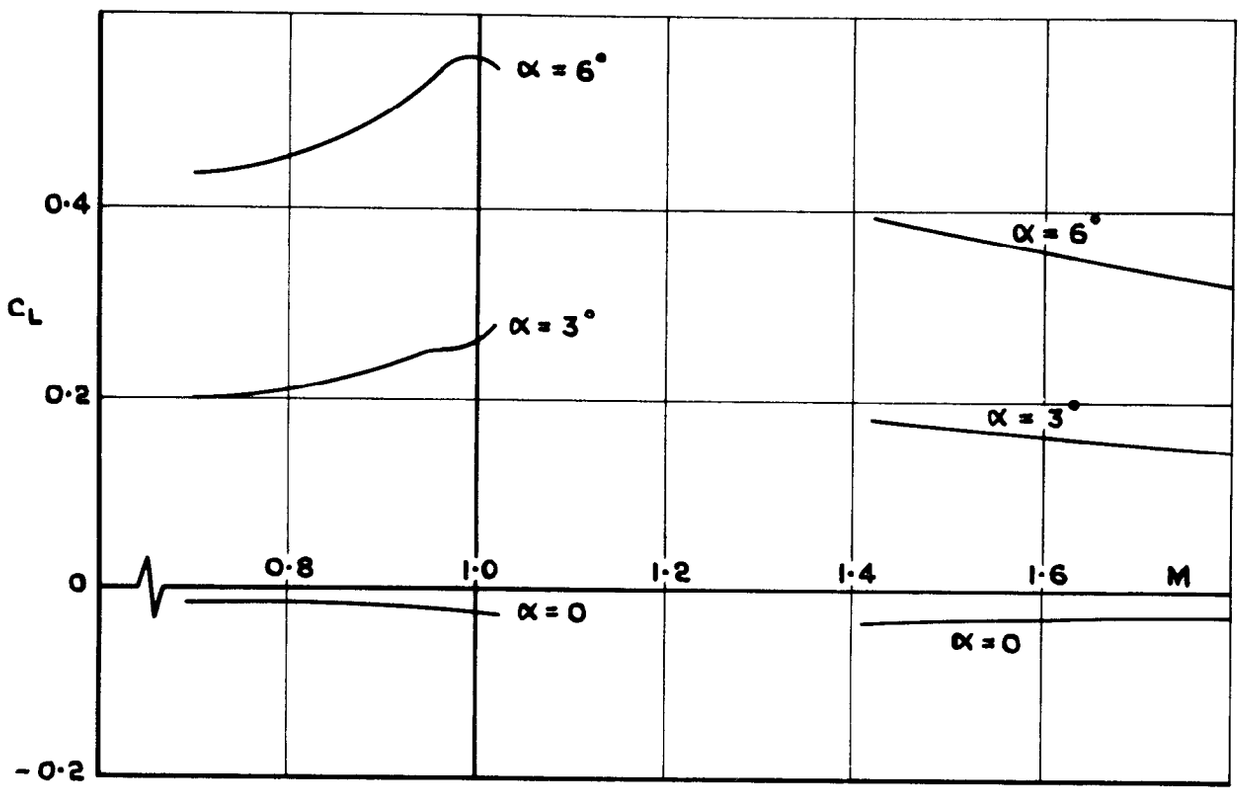

FIG. 7. VARIATION OF LIFT COEFFICIENT WITH MACH NUMBER AT CONSTANT INCIDENCE FOR THE BASIC MODEL.

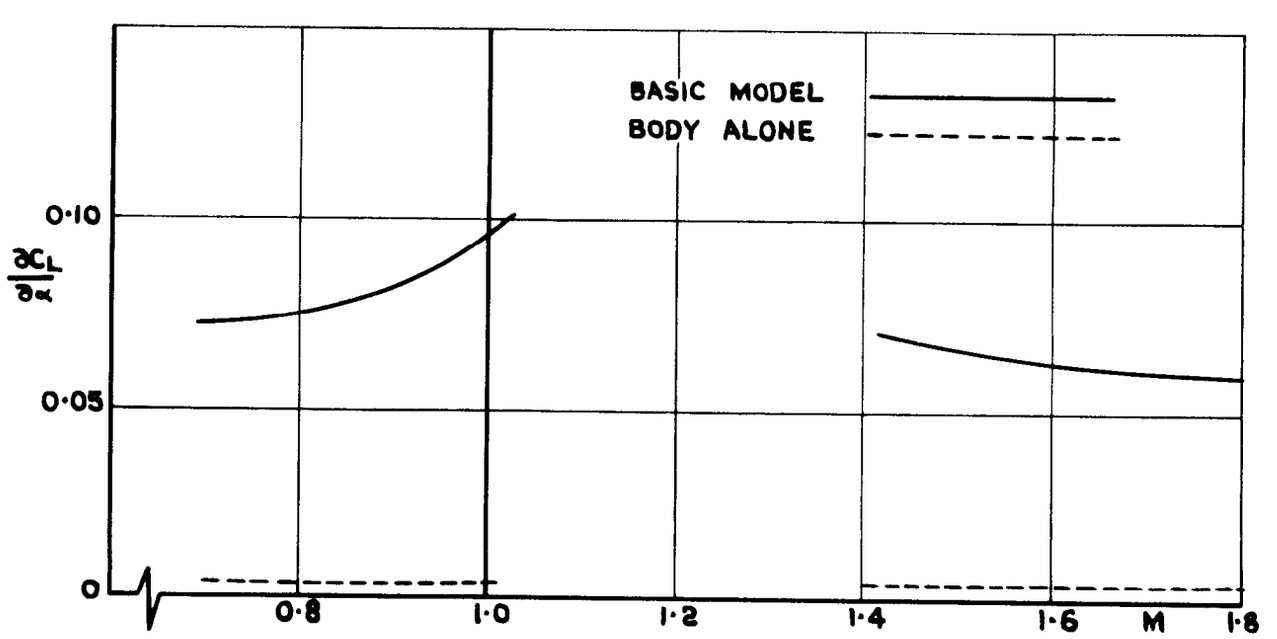

FIG. 8. VARIATION OF THE LIFT CURVE SLOPE $\left(\frac{\partial C_L}{\partial \alpha}\right)$ WITH MACH NUMBER.

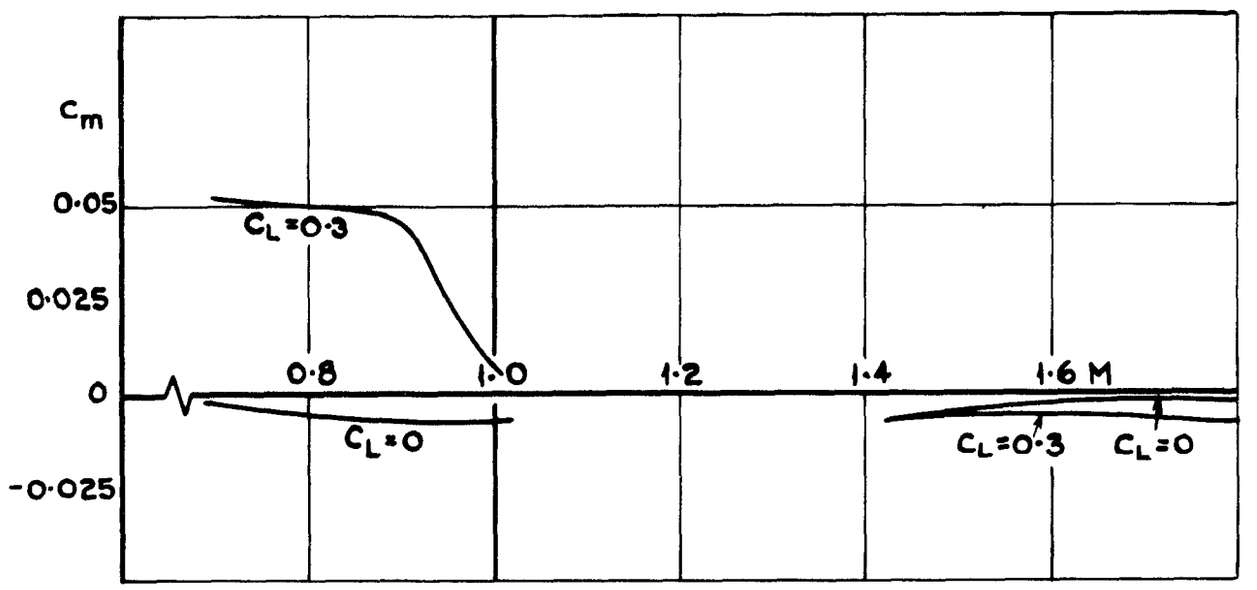

FIG. 9 . VARIATION OF PITCHING MOMENT COEFFICIENT WITH MACH NUMBER AT CONSTANT LIFT COEFFICIENT FOR THE BASIC MODEL.

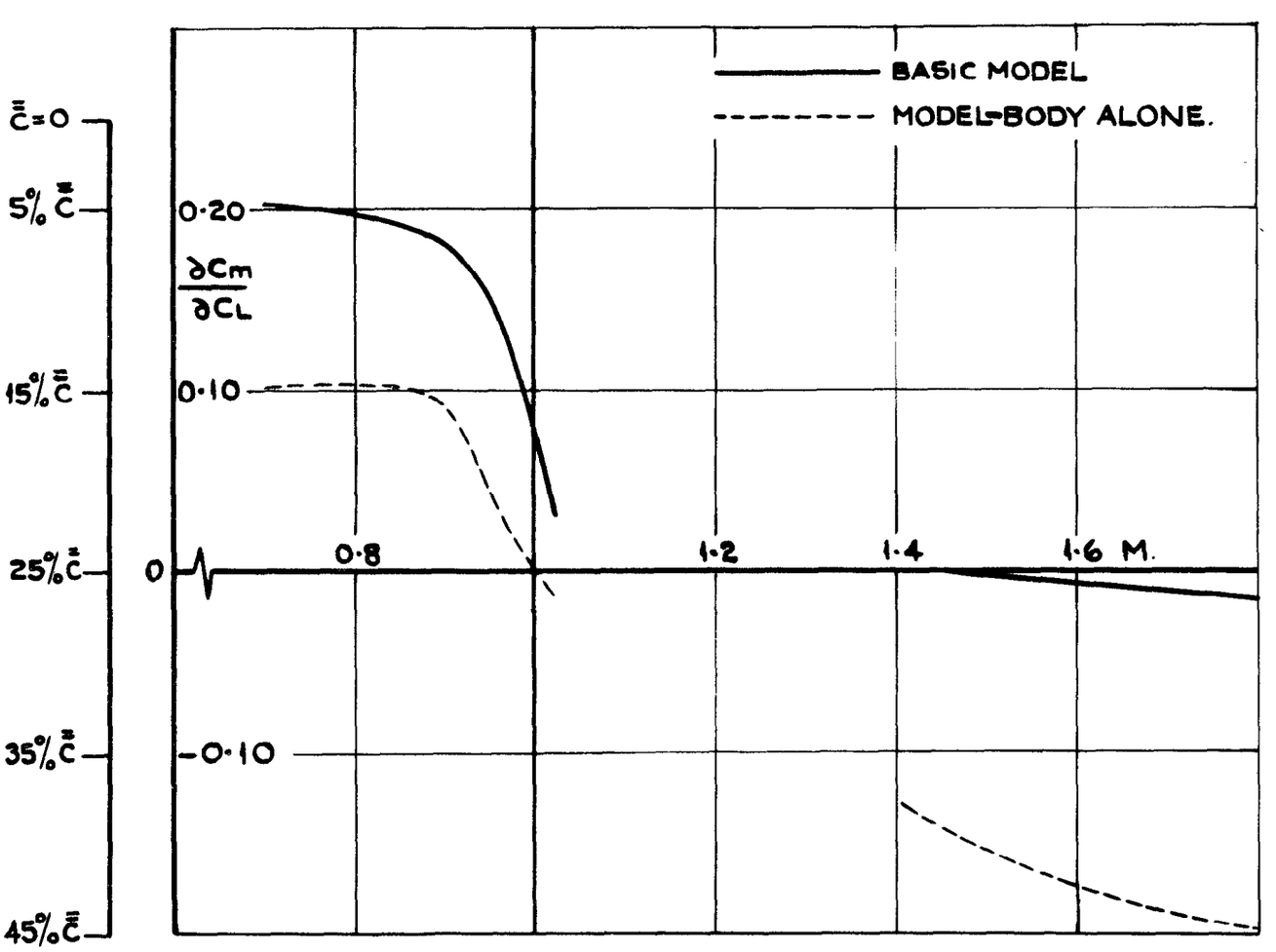

FIG. 10. VARIATION OF $\frac{\partial Cm}{\partial CL}$ WITH MACH NUMBER

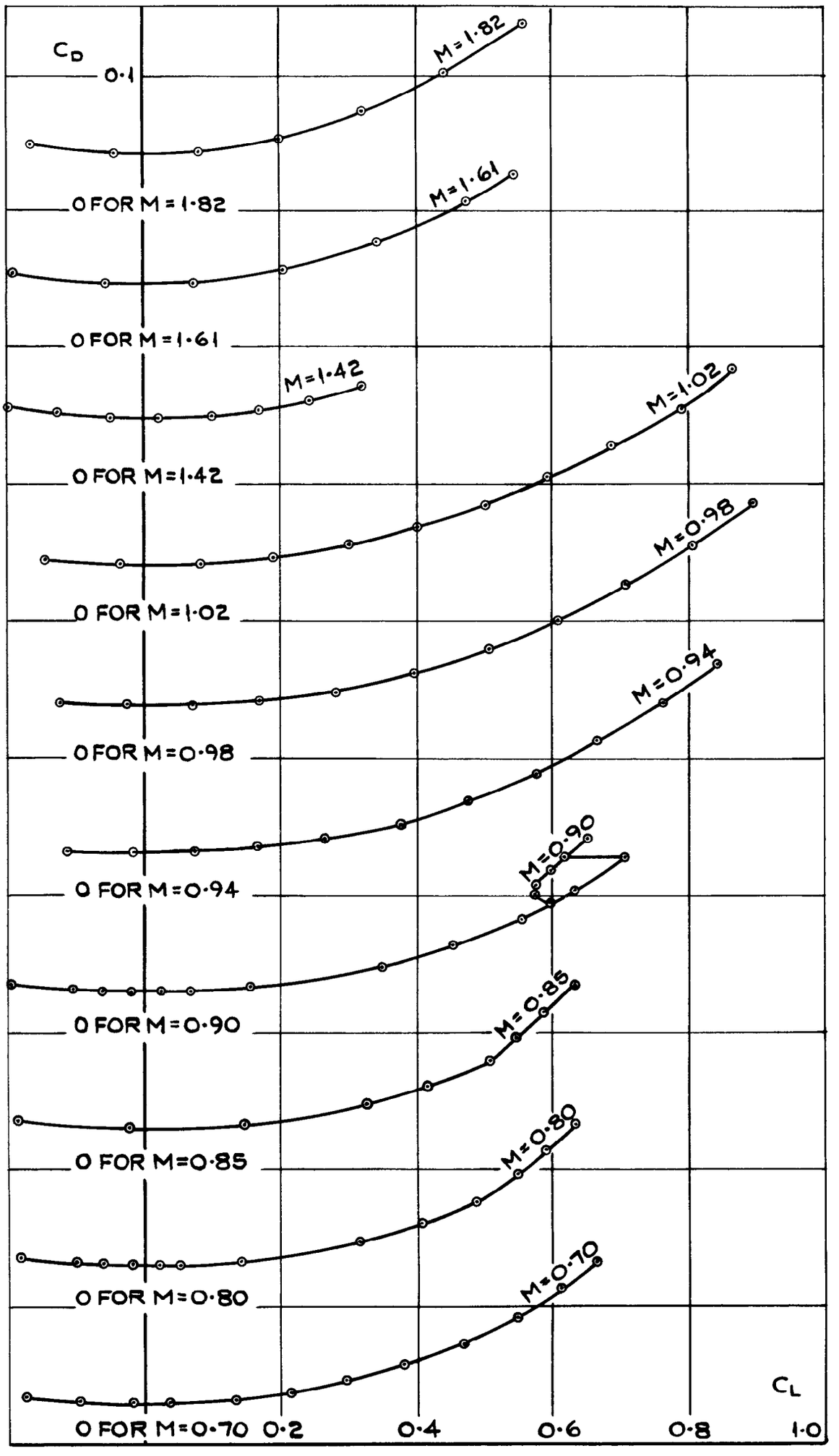

FIG. 11. VARIATION OF DRAG COEFFICIENT WITH LIFT COEFFICIENT FOR THE BASIC MODEL.

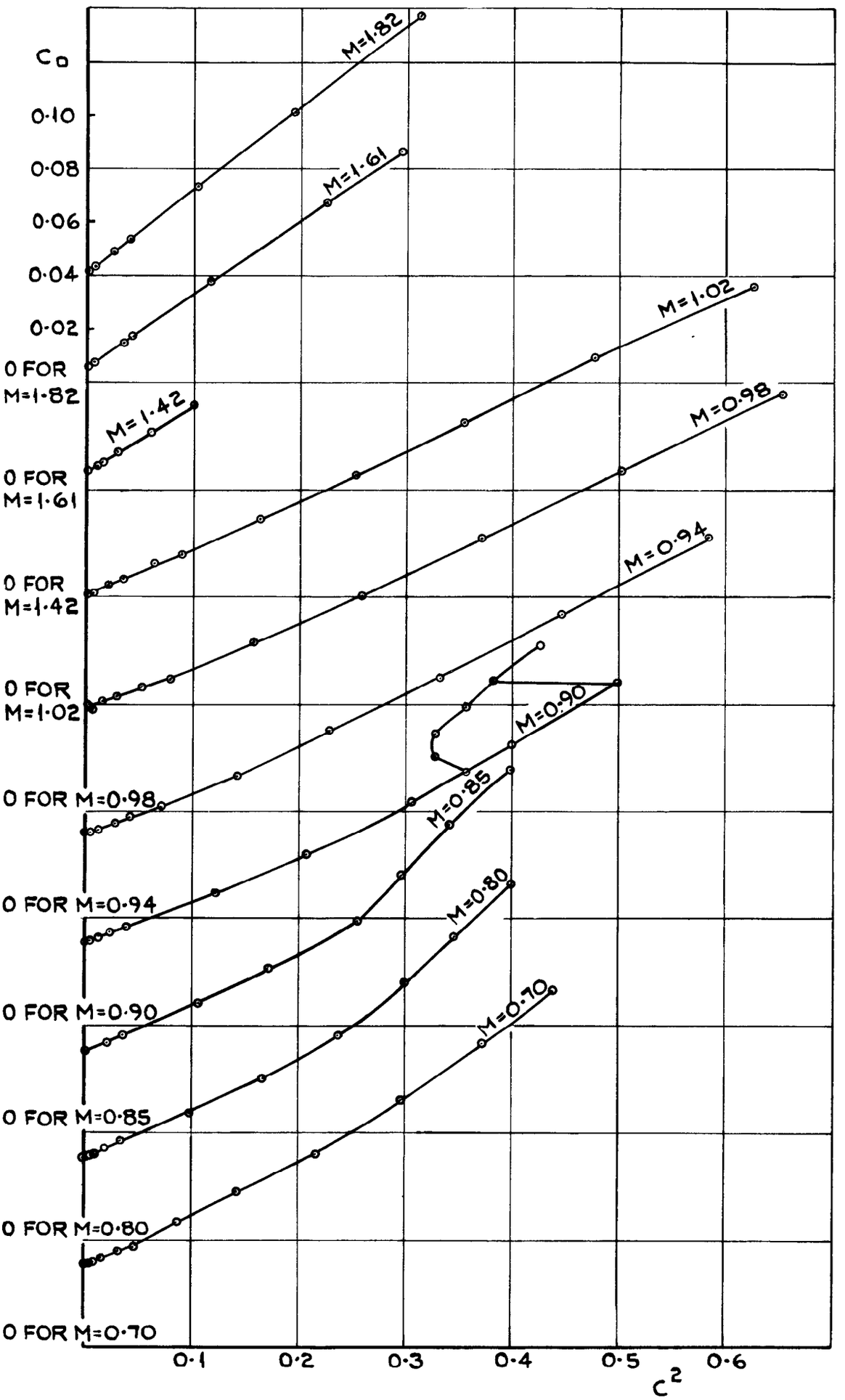

FIG.12. VARIATION OF DRAG COEFFICIENT WITH C_L^2 FOR THE BASIC MODEL.

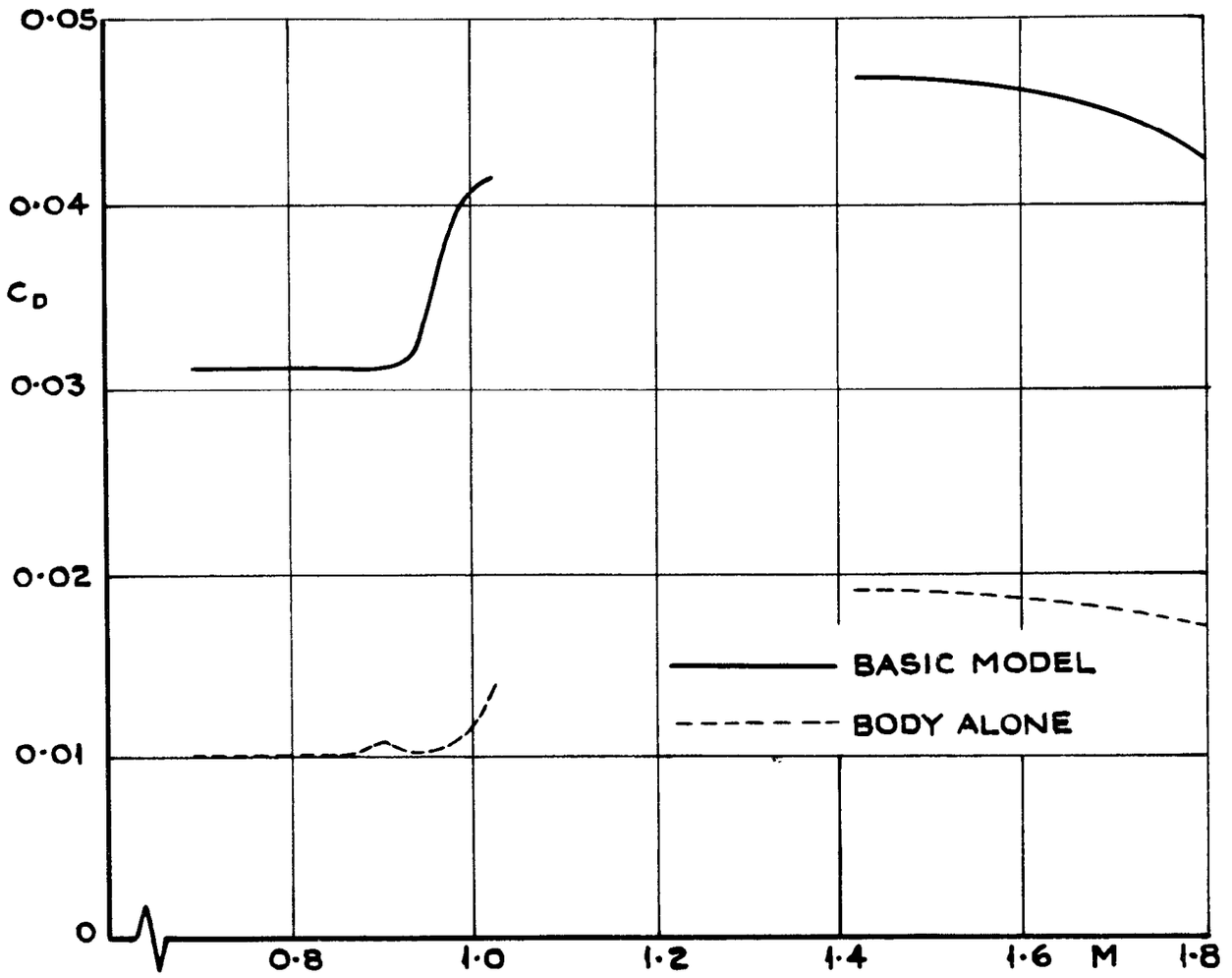

FIG. 13. VARIATION OF THE DRAG COEFFICIENT AT ZERO LIFT WITH MACH NUMBER.

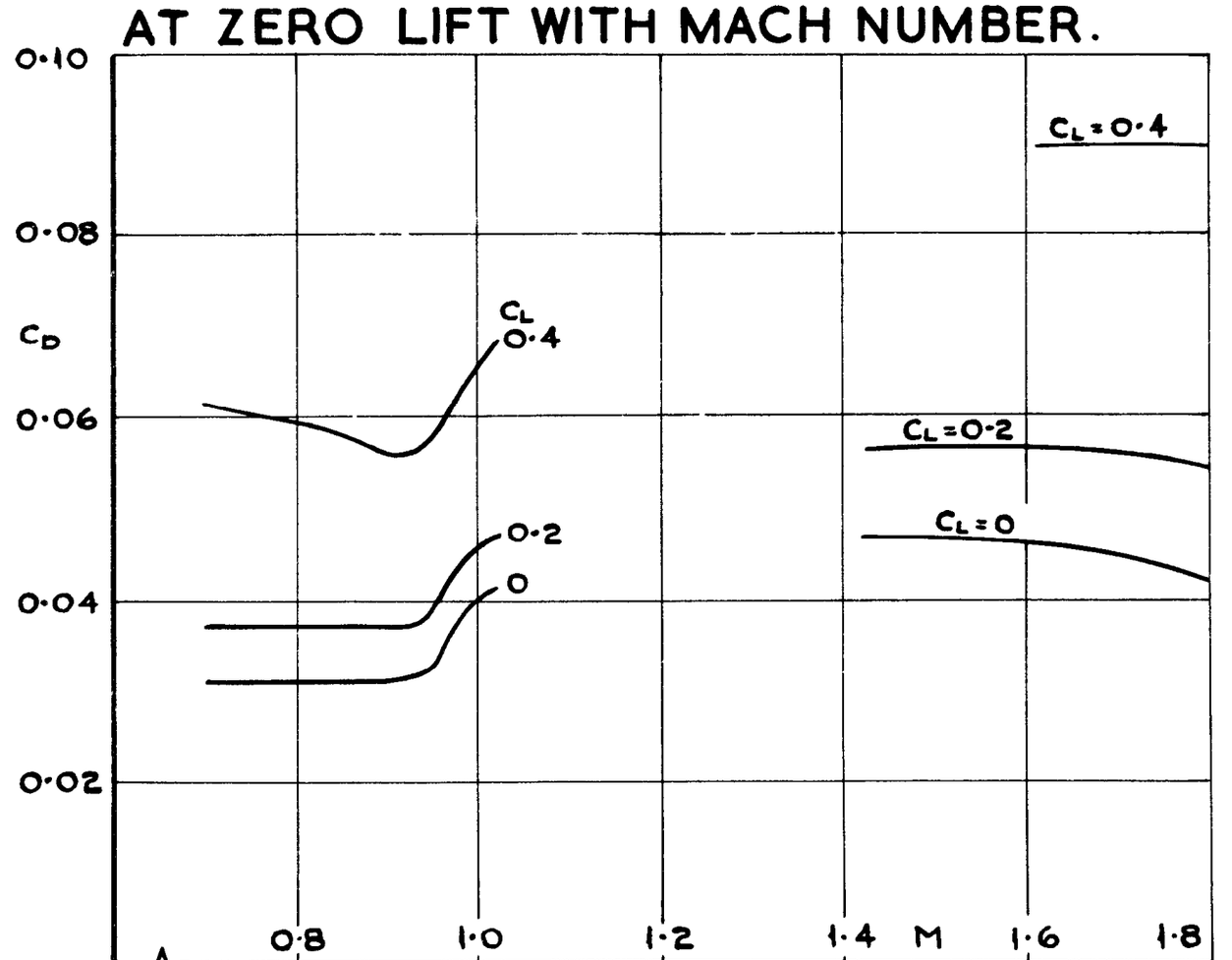

FIG. 14. VARIATION OF DRAG COEFFICIENT AT CONSTANT LIFT COEFFICIENT WITH MACH NUMBER.

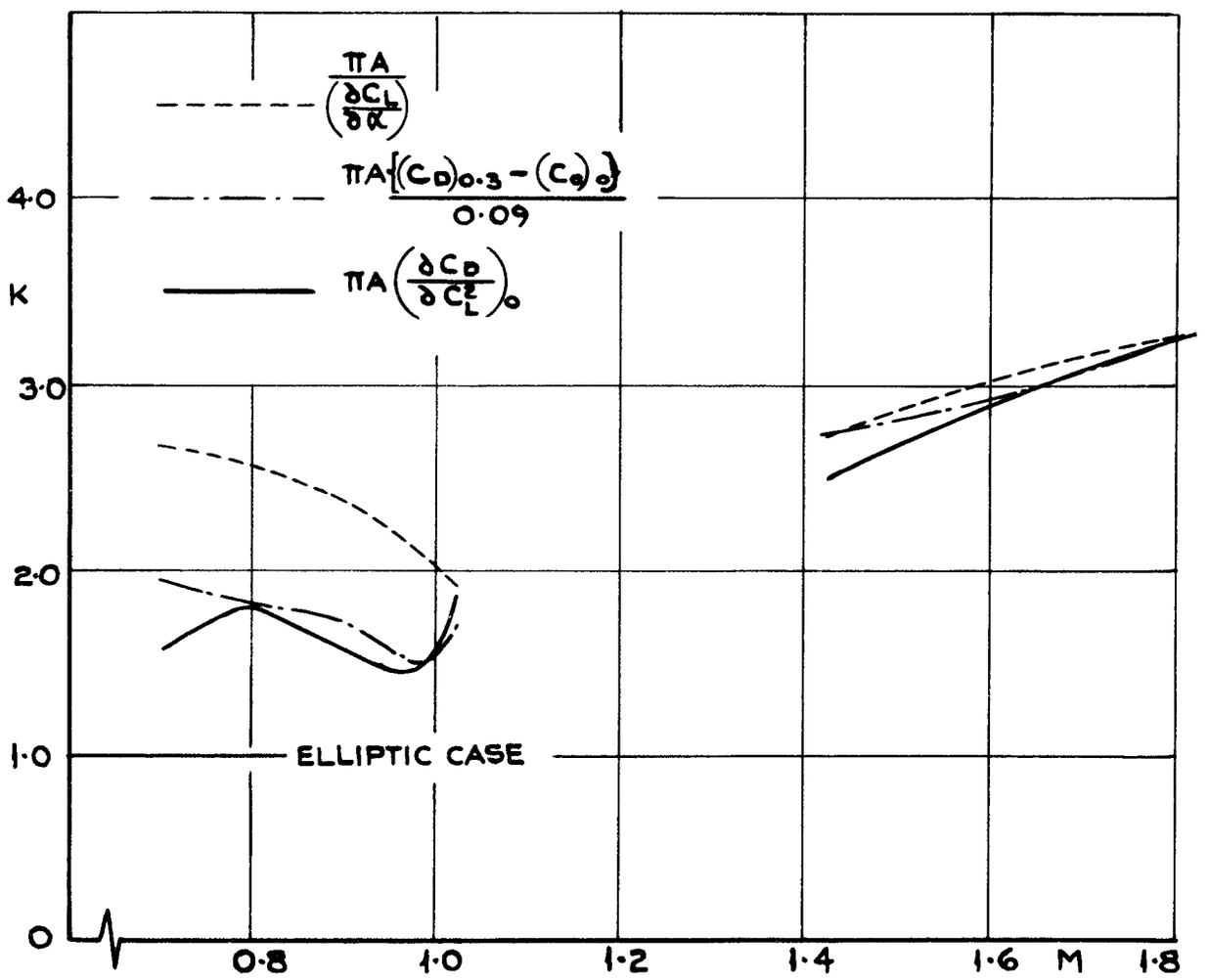

FIG. 15. VARIATION OF THE INDUCED DRAG FACTOR WITH MACH NUMBER.

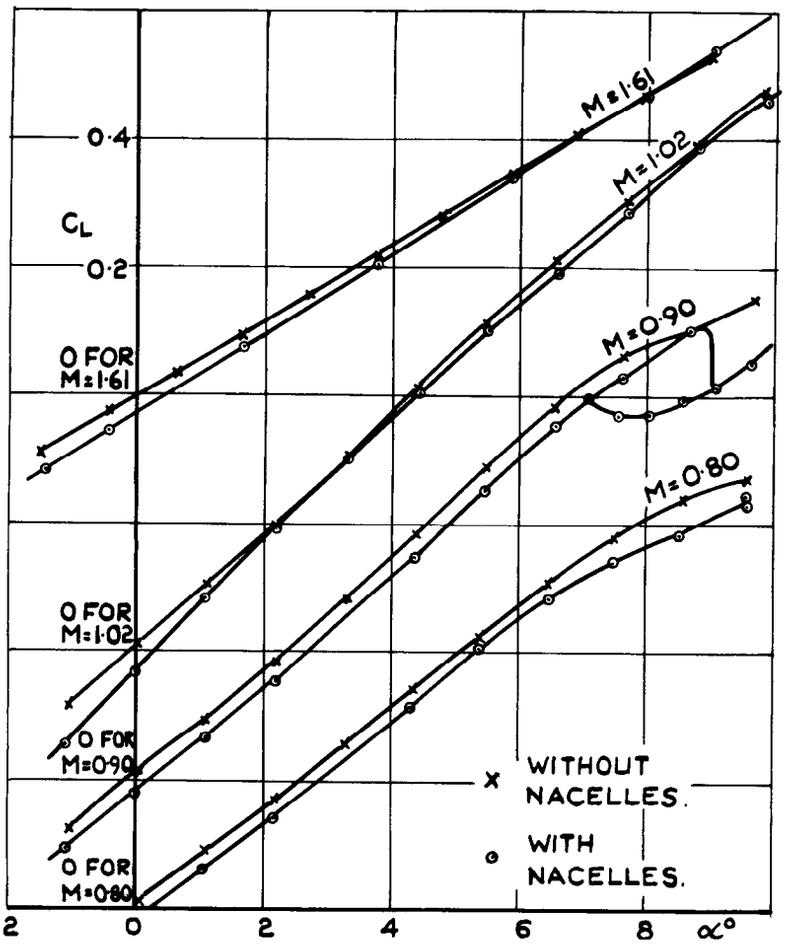

FIG. 16. VARIATION OF LIFT COEFFICIENT WITH INCIDENCE FOR THE MODEL WITH AND WITHOUT NACELLES.

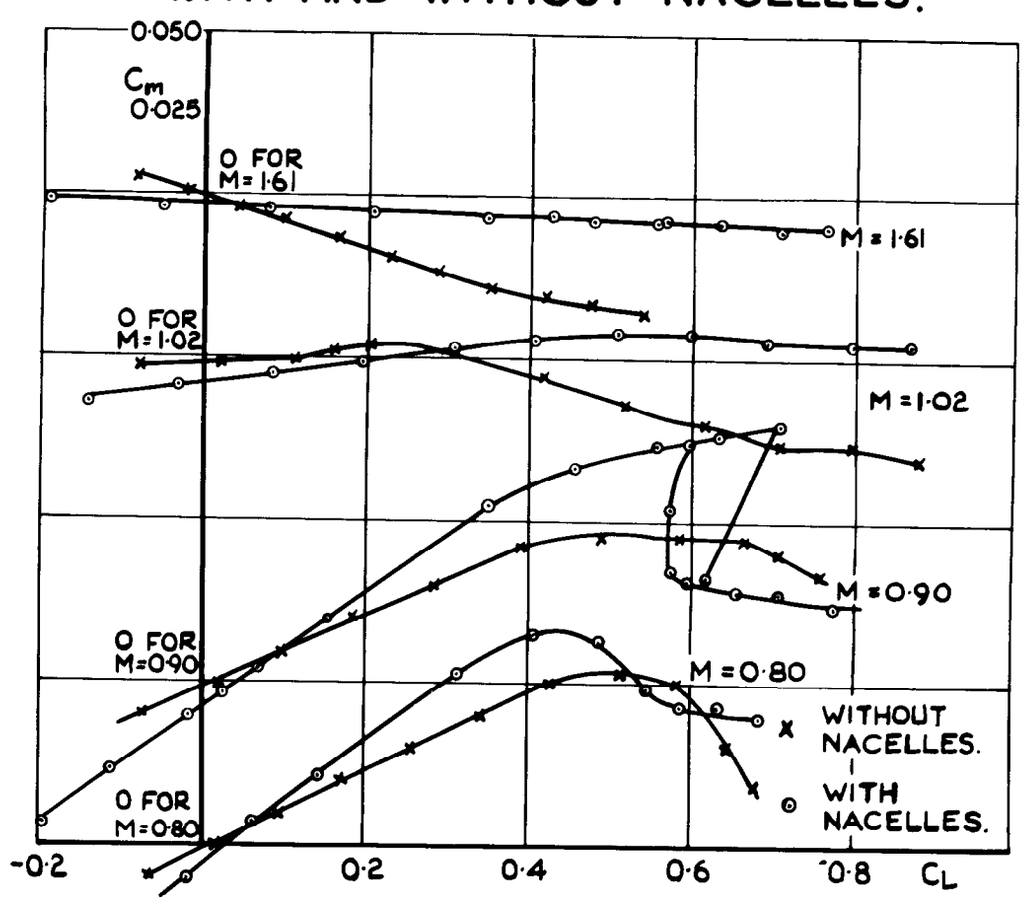

FIG. 17. VARIATION OF PITCHING MOMENT COEFFICIENT WITH LIFT COEFFICIENT FOR MODEL WITH AND WITHOUT NACELLES.

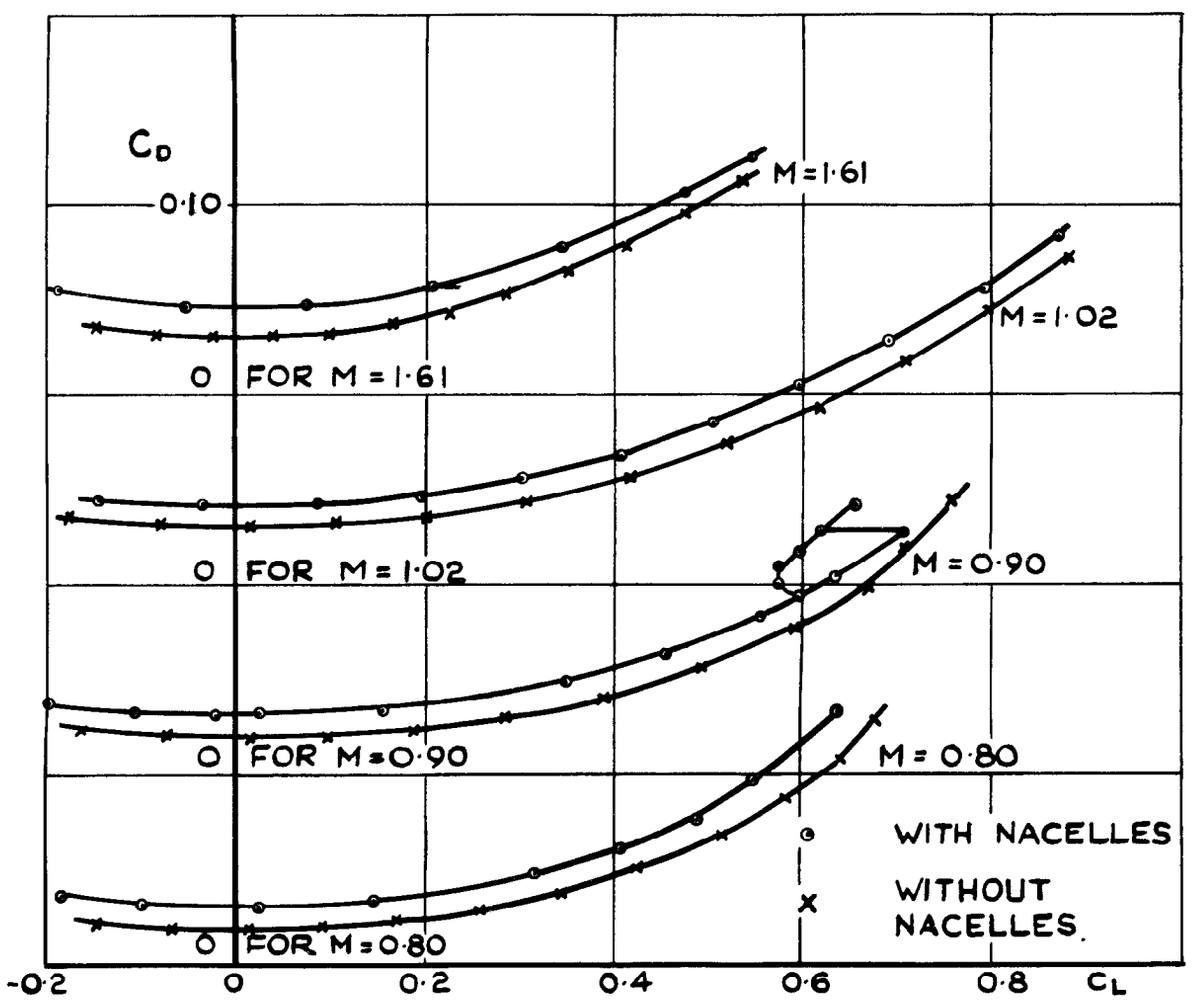

FIG. 18. VARIATION OF THE DRAG COEFFICIENT WITH LIFT COEFFICIENT FOR THE MODEL WITH AND WITHOUT NACELLES.

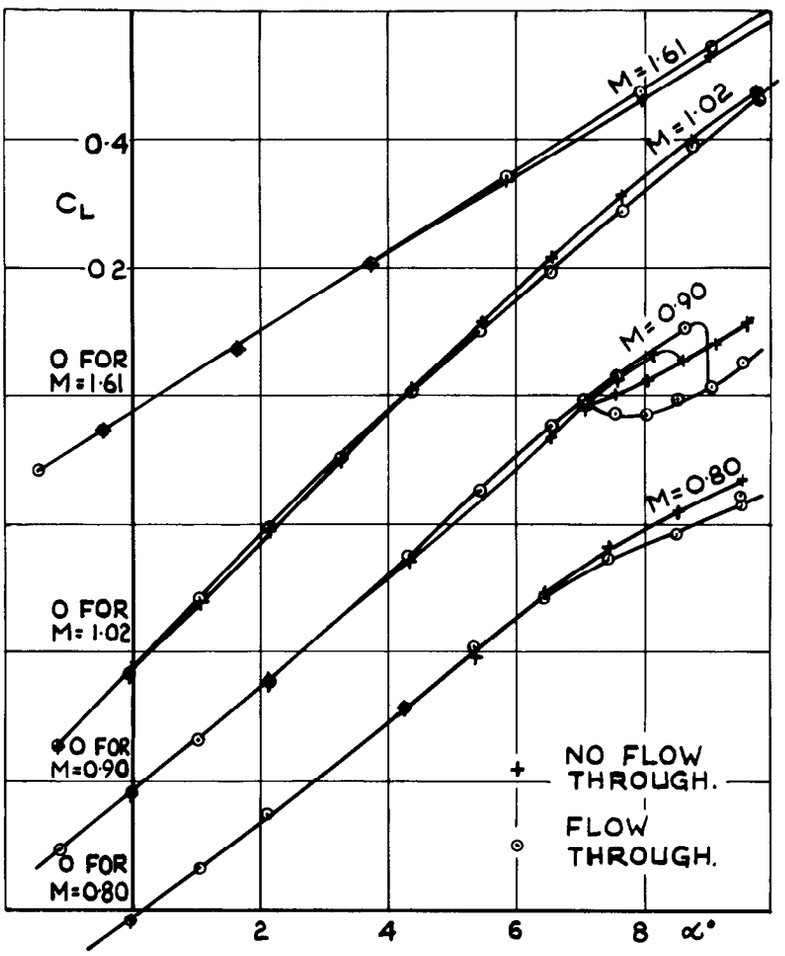

FIG. 19. VARIATION OF LIFT COEFFICIENT WITH INCIDENCE FOR THE MODEL WITH AND WITHOUT FLOW THROUGH THE NACELLES

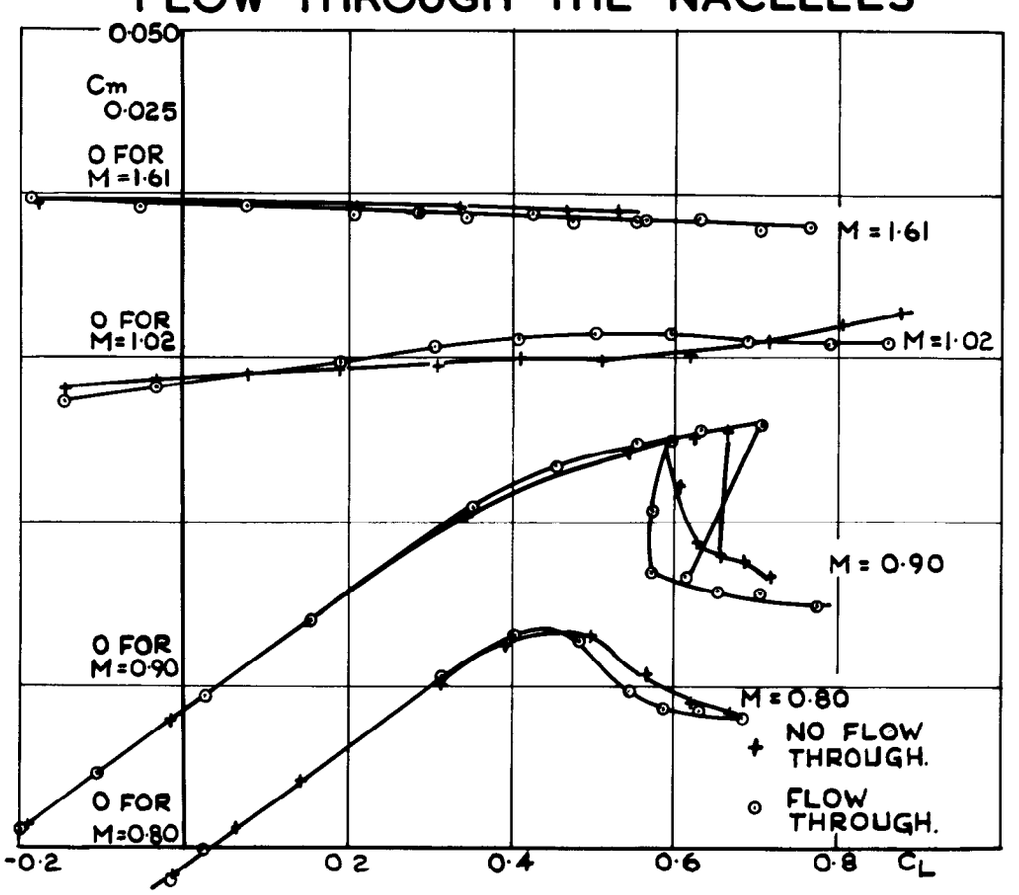

FIG. 20. VARIATION OF PITCHING MOMENT COEFFICIENT WITH LIFT COEFFICIENT FOR THE MODEL WITH AND WITHOUT FLOW THROUGH THE NACELLES.

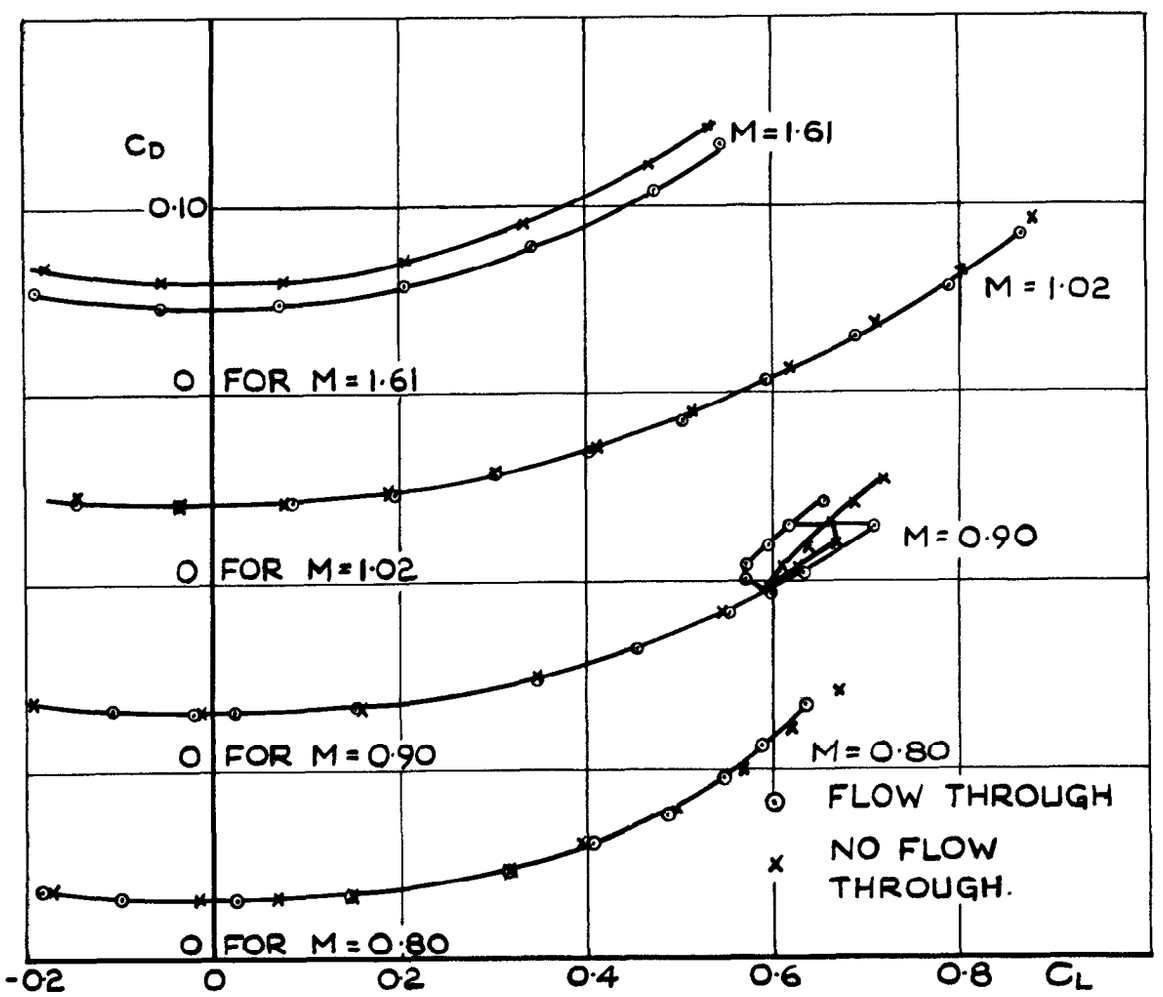

FIG. 21. VARIATION OF DRAG COEFFICIENT WITH LIFT COEFFICIENT FOR THE MODEL WITH AND WITHOUT FLOW THROUGH THE NACELLES.

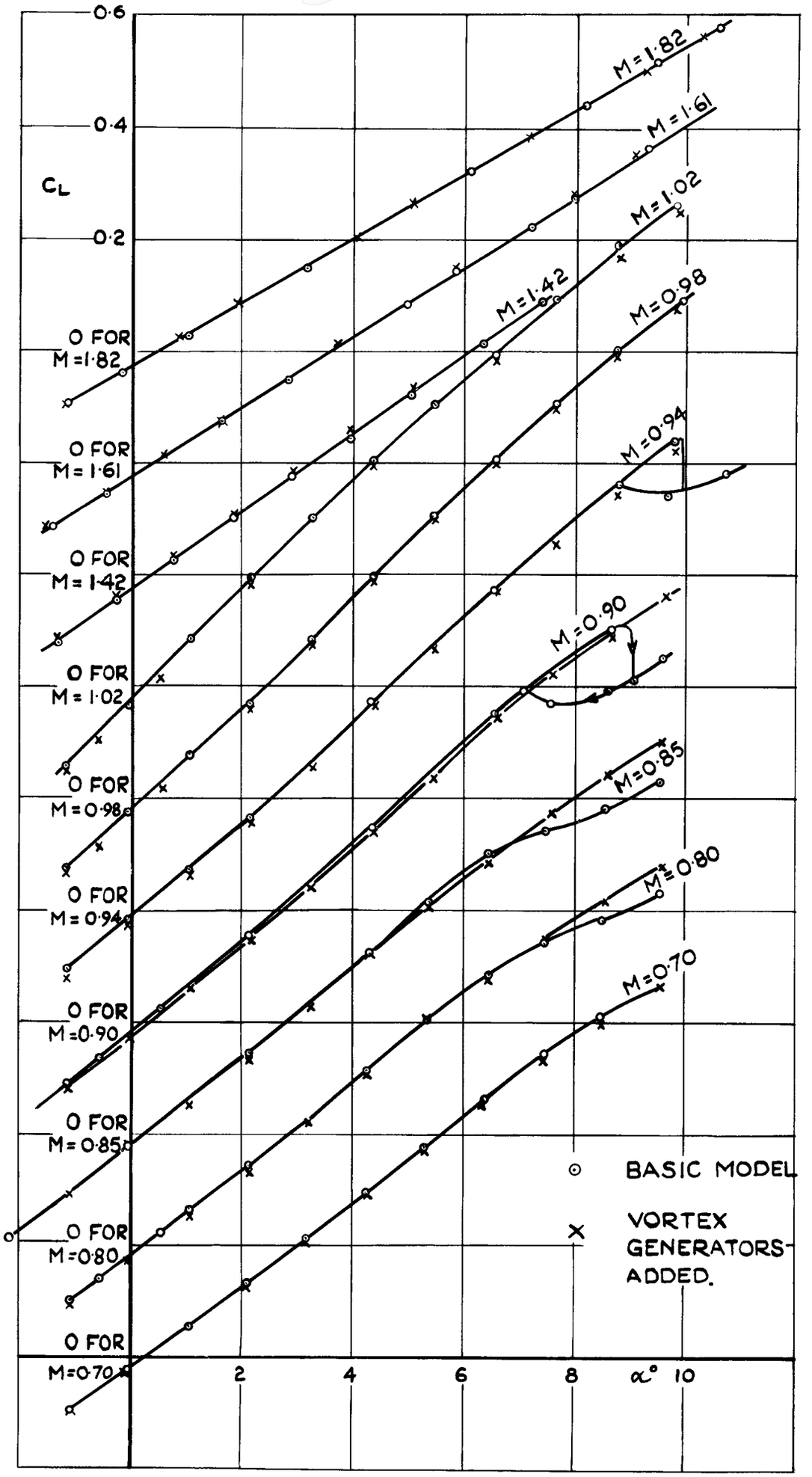

FIG. 22. EFFECT ON LIFT COEFFICIENT OF ADDING LEADING EDGE VORTEX GENERATORS.

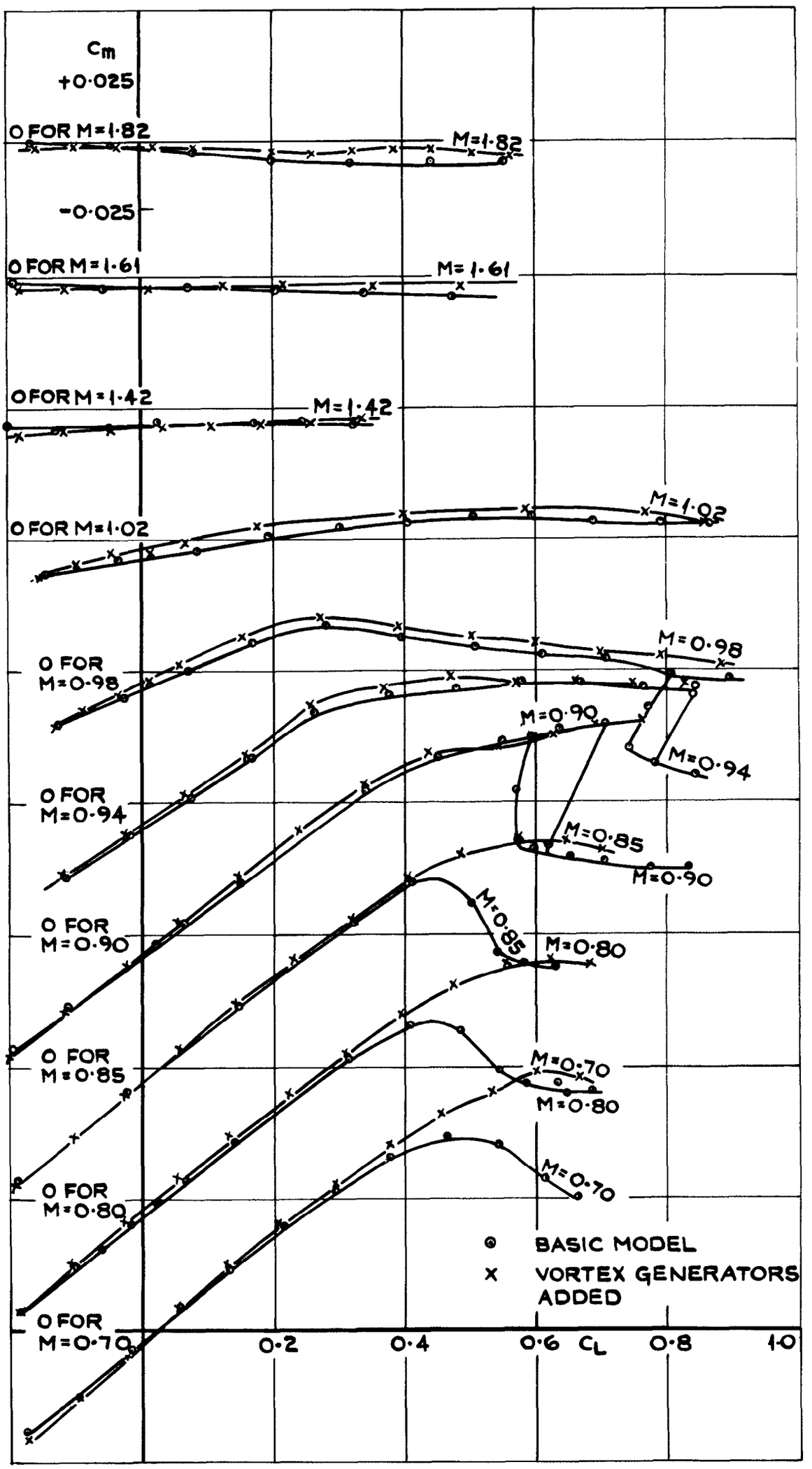

FIG. 23. EFFECT ON PITCHING MOMENT OF ADDING LEADING EDGE VORTEX GENERATORS.

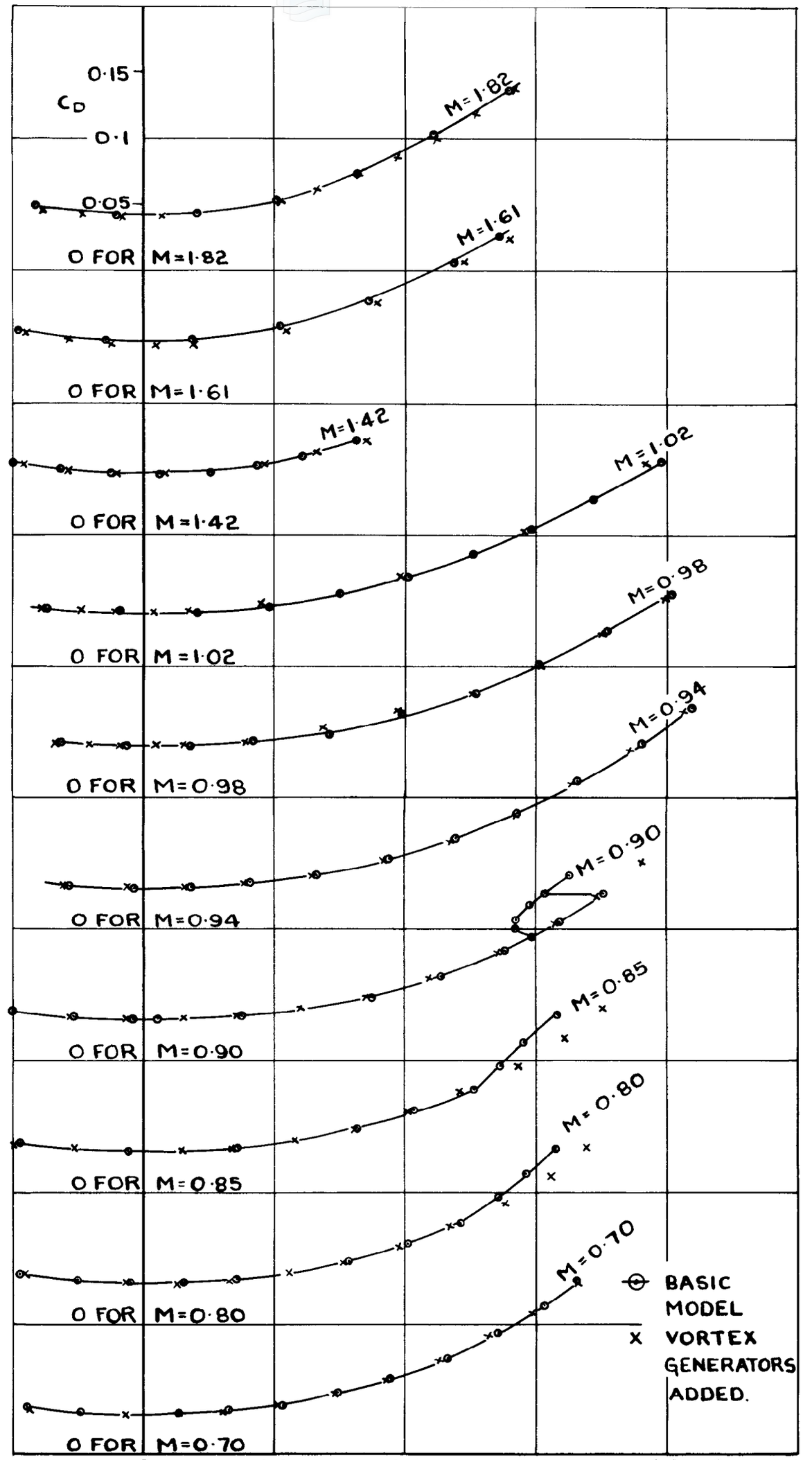

FIG. 24. EFFECT ON DRAG COEFFICIENT OF ADDING LEADING EDGE VORTEX GENERATORS.

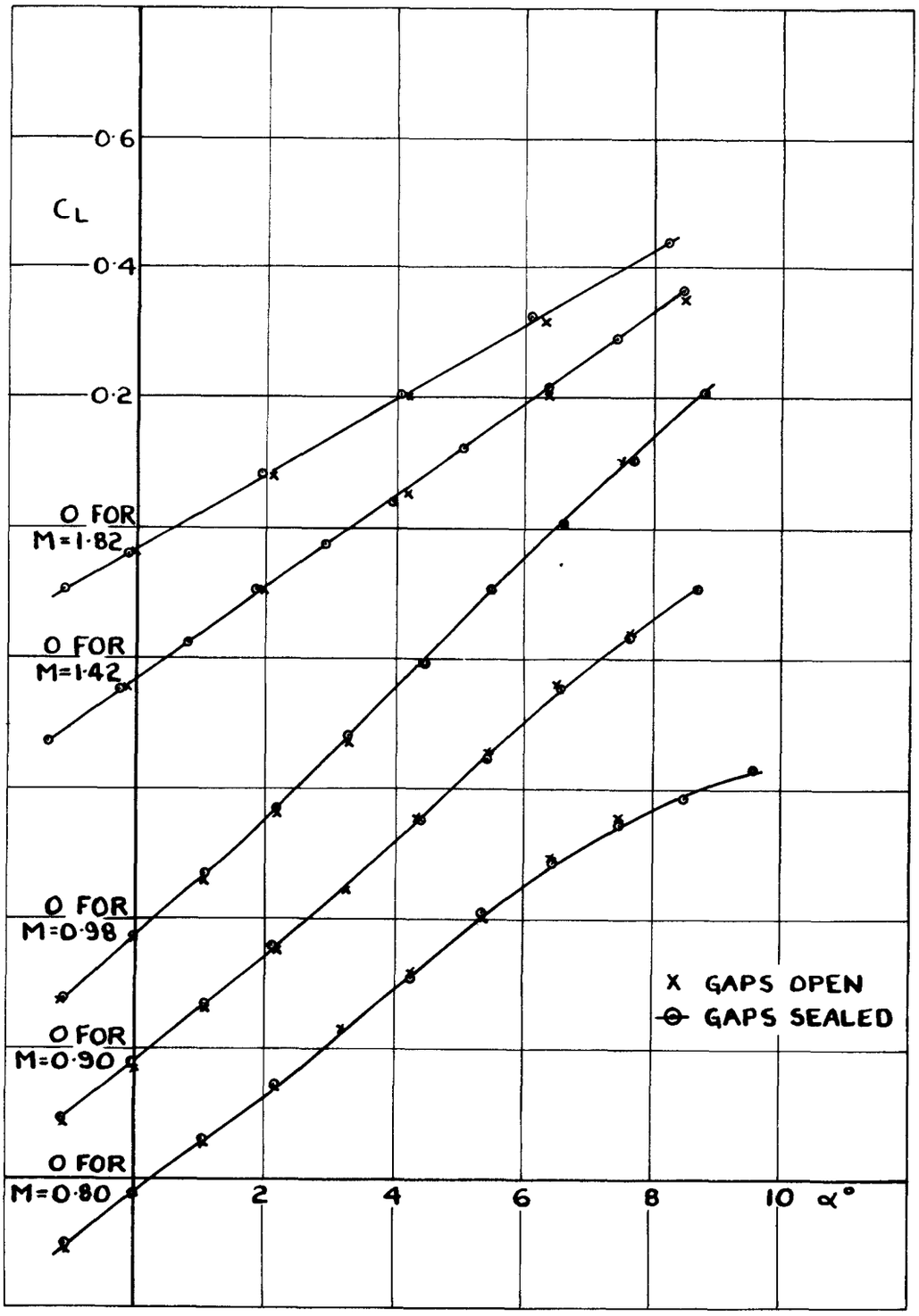

FIG. 25. EFFECT OF AILERON EDGE GAPS ON LIFT COEFFICIENT.

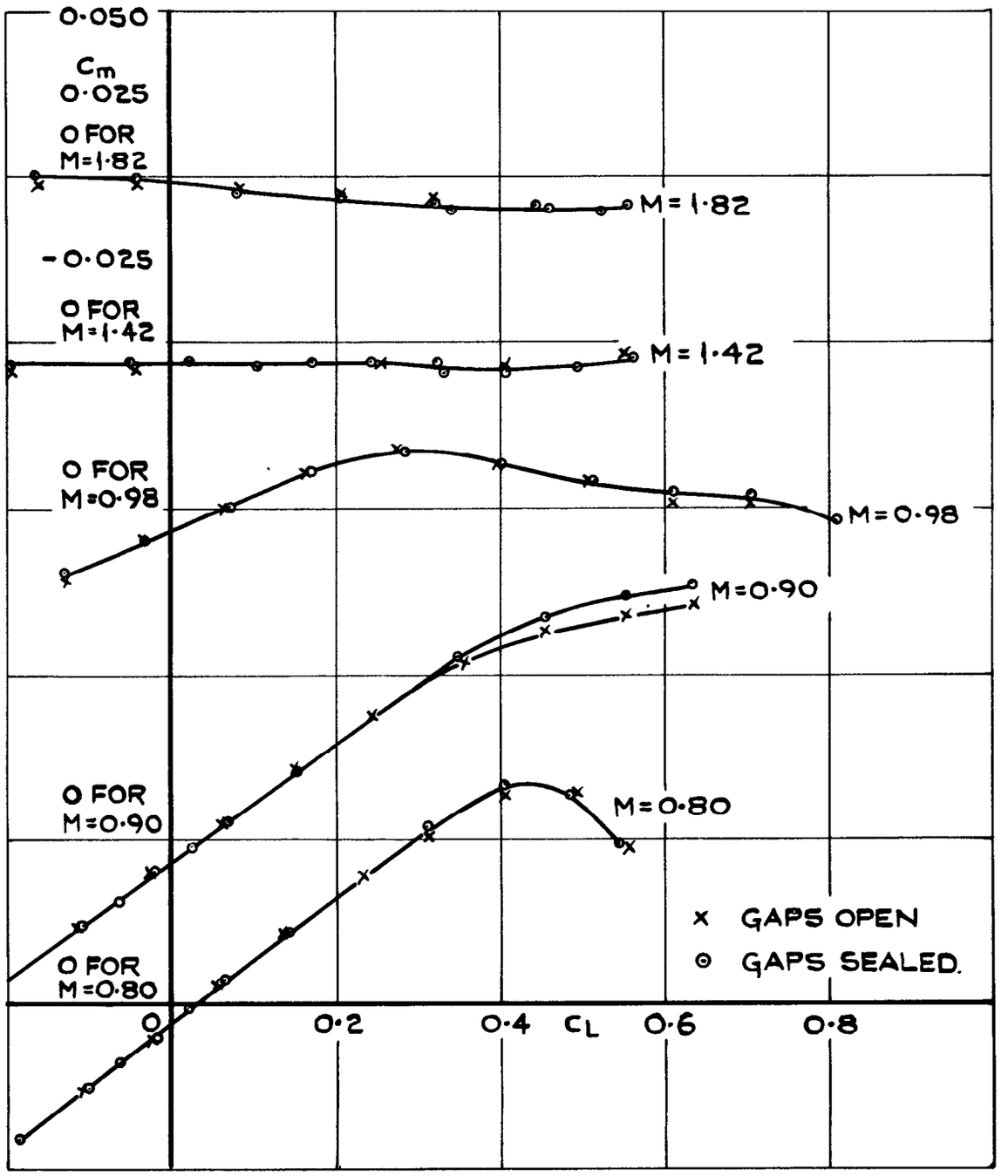

FIG. 26. EFFECT OF AILERON EDGE GAPS ON PITCHING MOMENT COEFFICIENT.

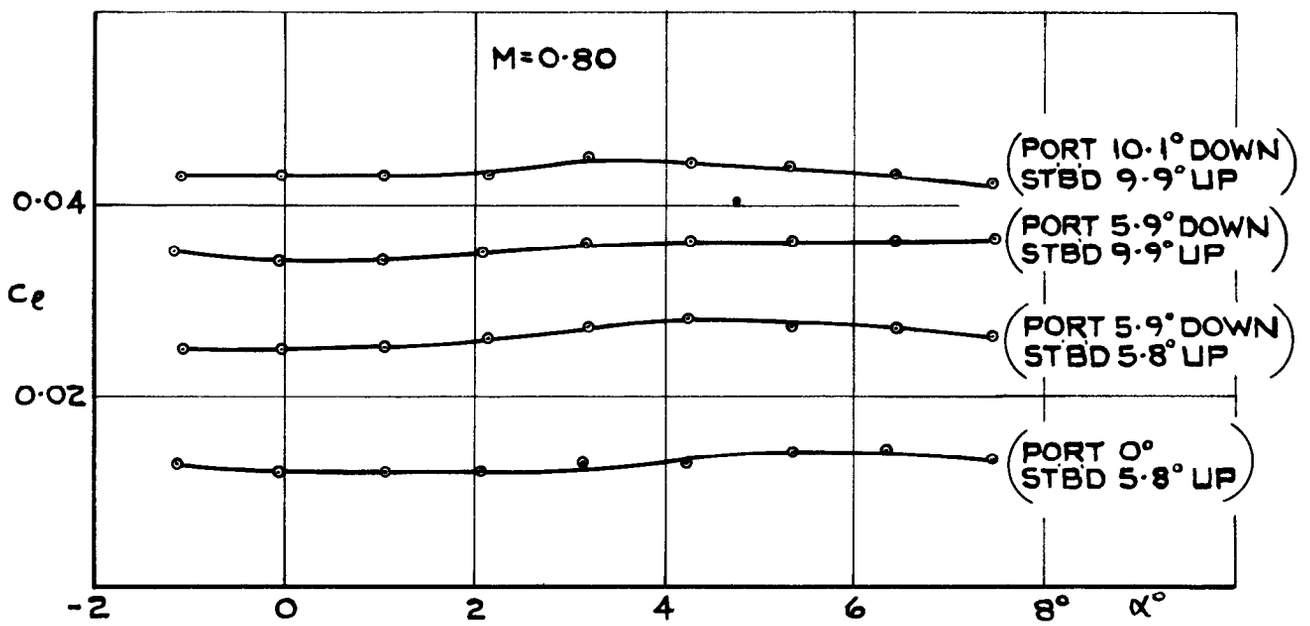

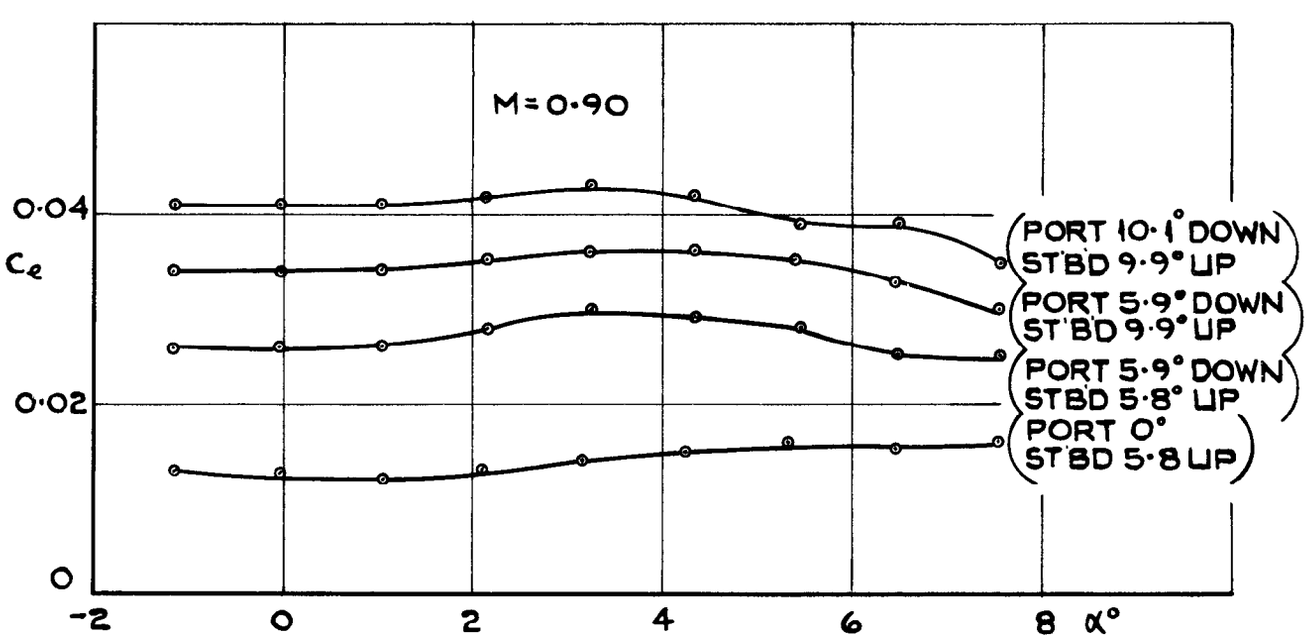

FIG.27(a) VARIATION OF ROLLING MOMENT COEFFICIENT WITH INCIDENCE FOR VARIOUS AILERON SETTINGS.

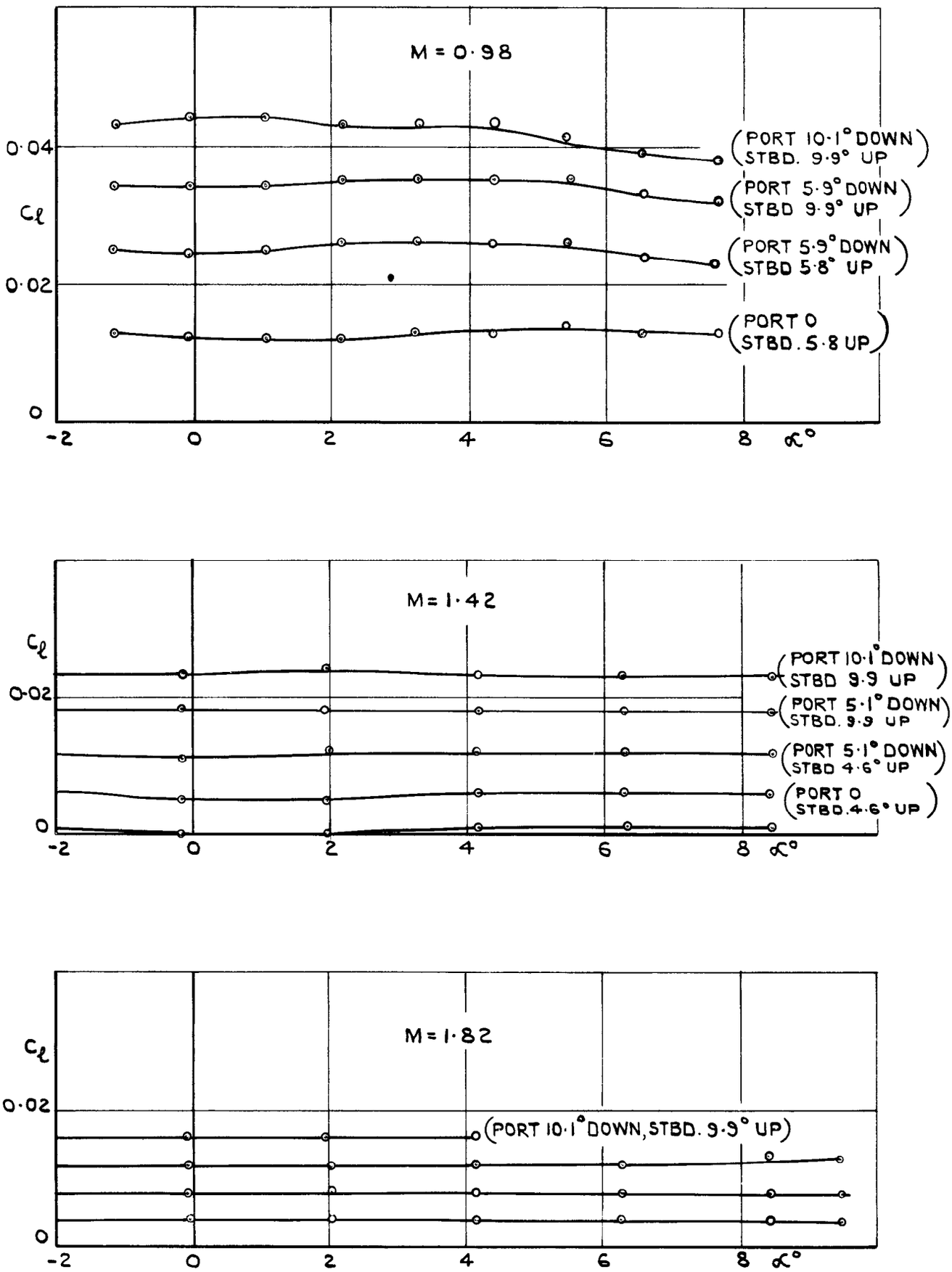

FIG. 27(b). VARIATION OF ROLLING MOMENT COEFFICIENT WITH INCIDENCE AT CONSTANT MACH NUMBER FOR VARIOUS AILERON SETTINGS.

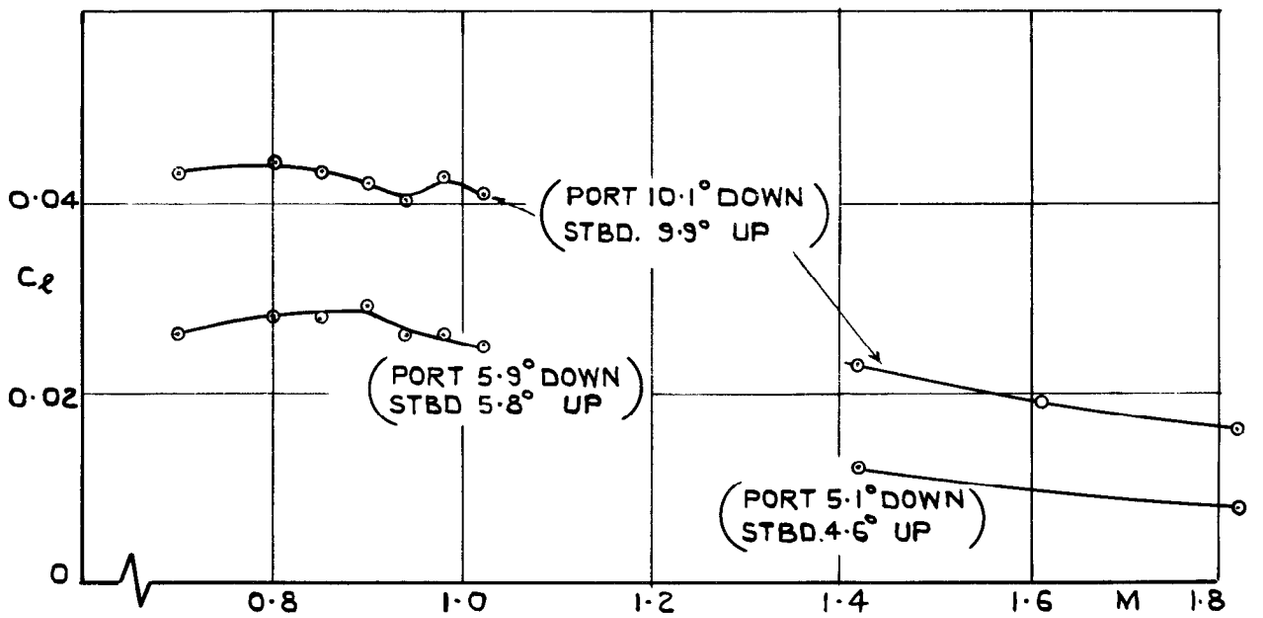

(a). AT APPROXIMATELY 4° INCIDENCE.

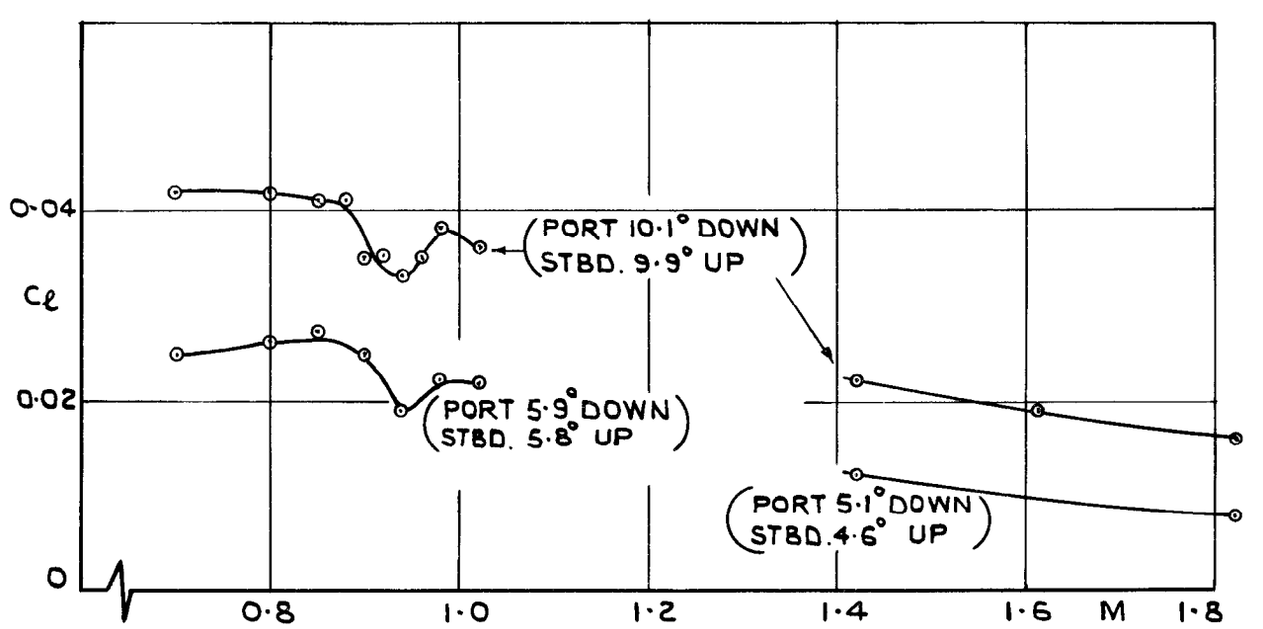

(b). AT APPROXIMATELY 7° INCIDENCE.

FIG. 28(a & b) VARIATION OF ROLLING MOMENT COEFFICIENT AT APPROXIMATELY CONSTANT INCIDENCE FOR VARIOUS AILERON SETTINGS.

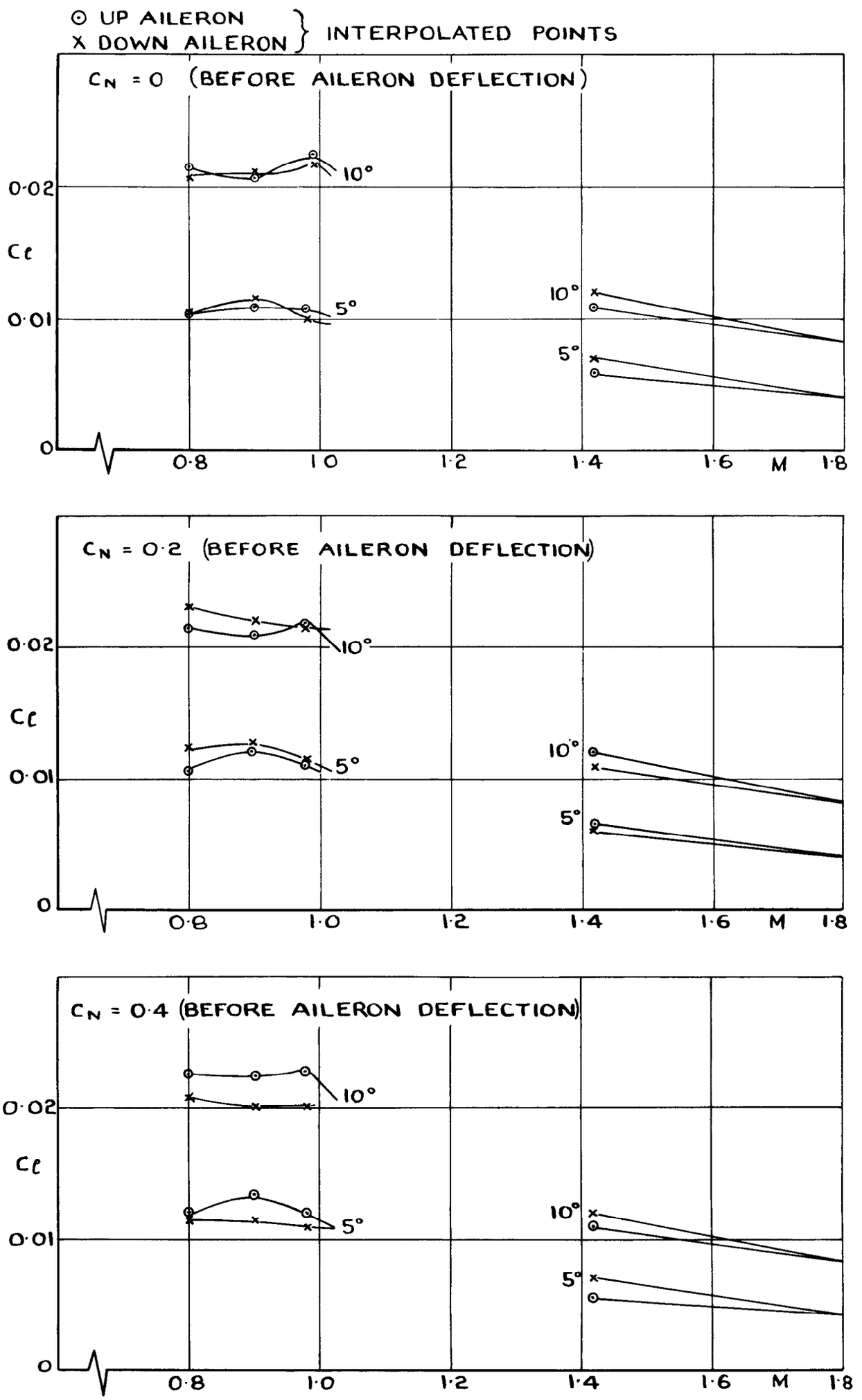

FIG. 29. VARIATION WITH MACH NUMBER OF THE ROLLING MOMENT DUE TO CONSTANT DEFLECTION OF ONE AILERON.

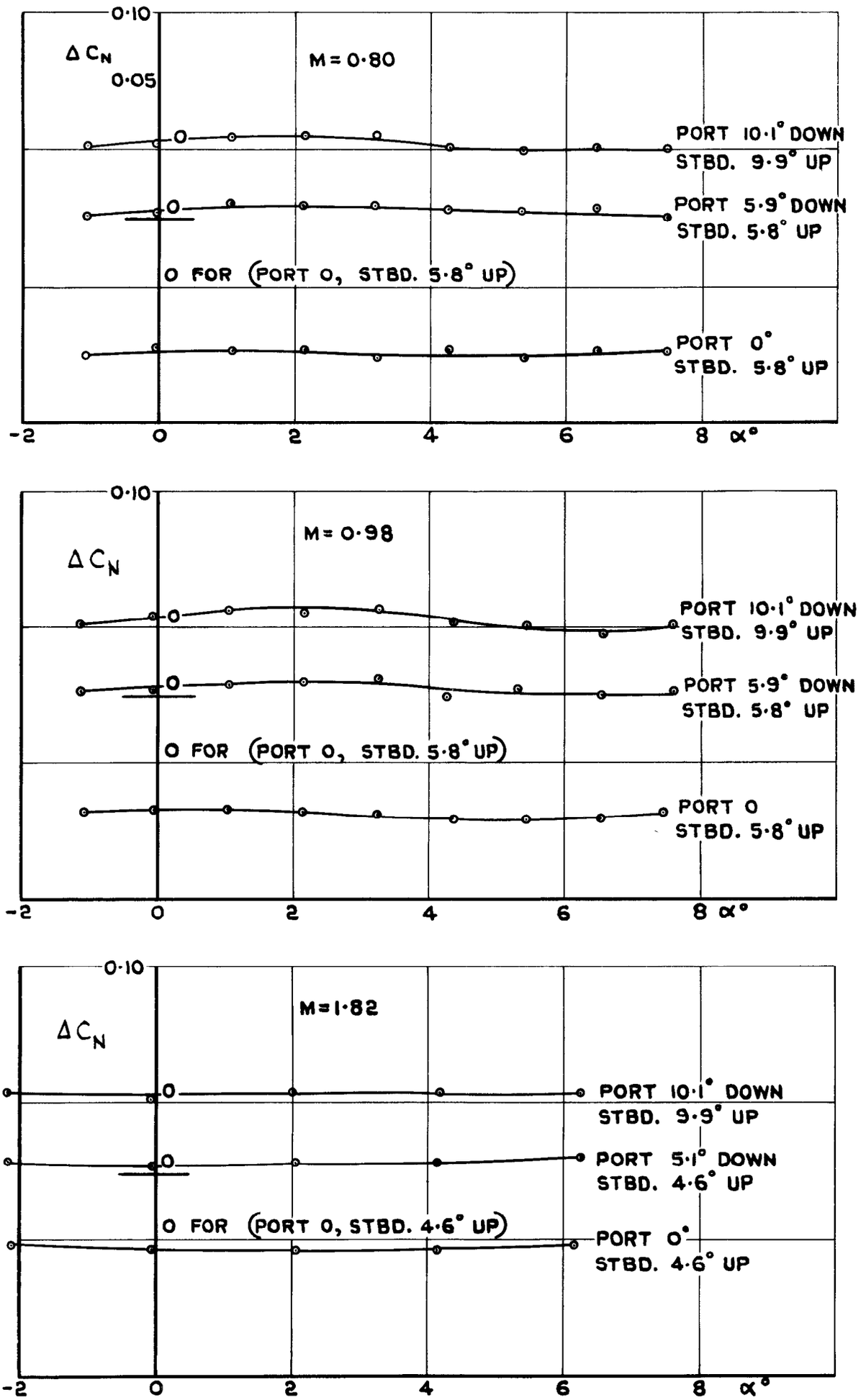

FIG. 30. CHANGE IN NORMAL FORCE COEFFICIENT DUE TO AILERON DEFLECTION.

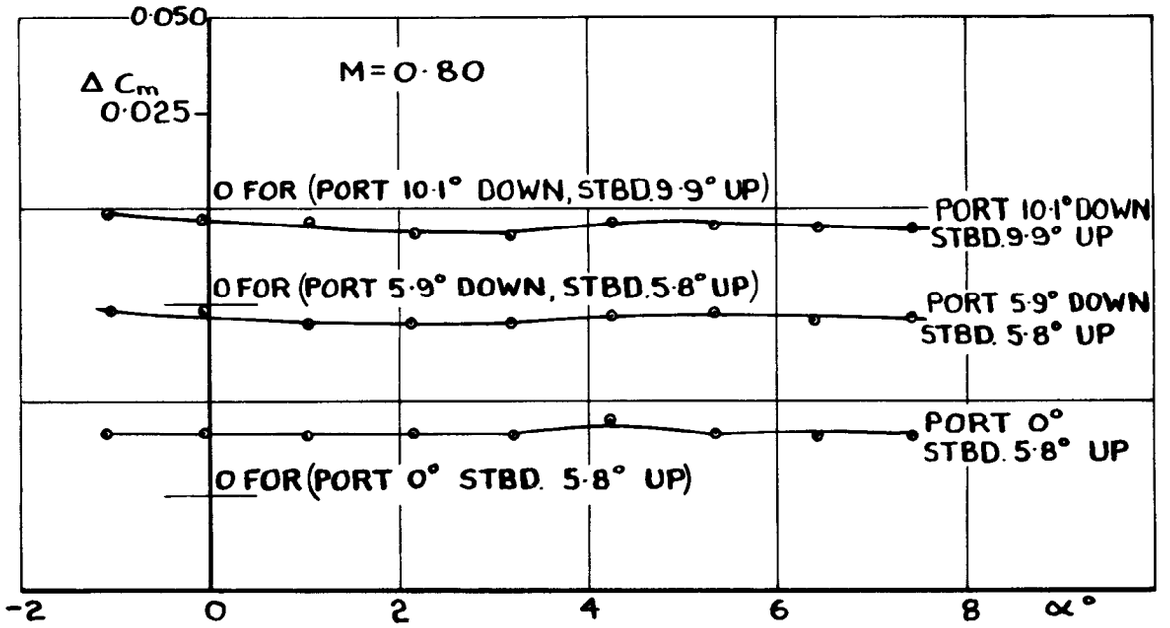

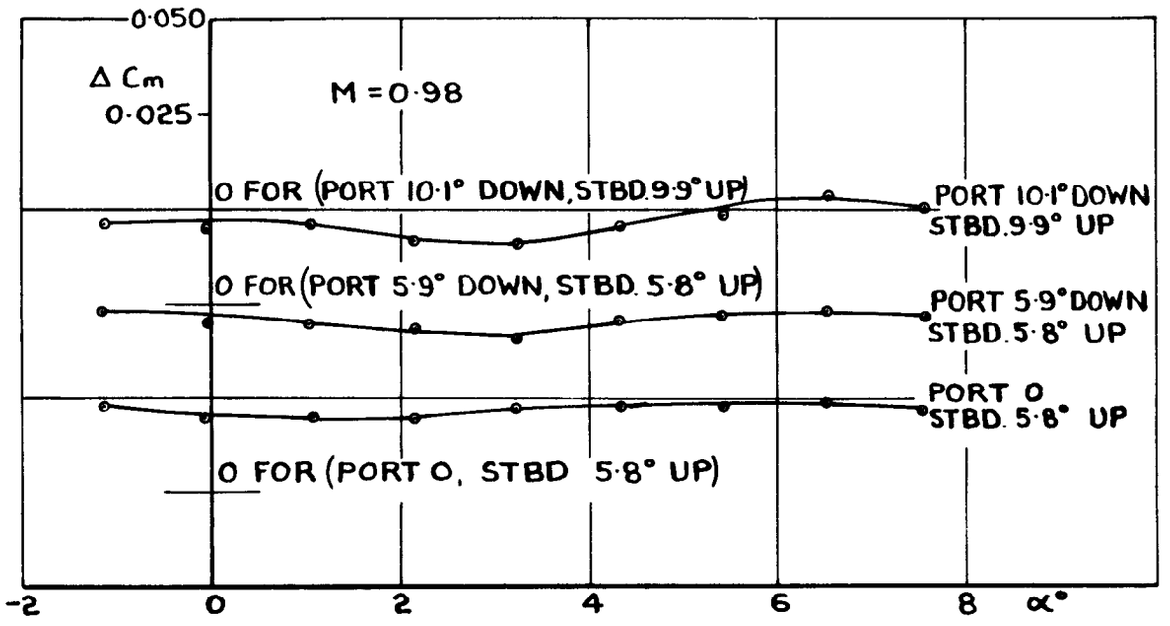

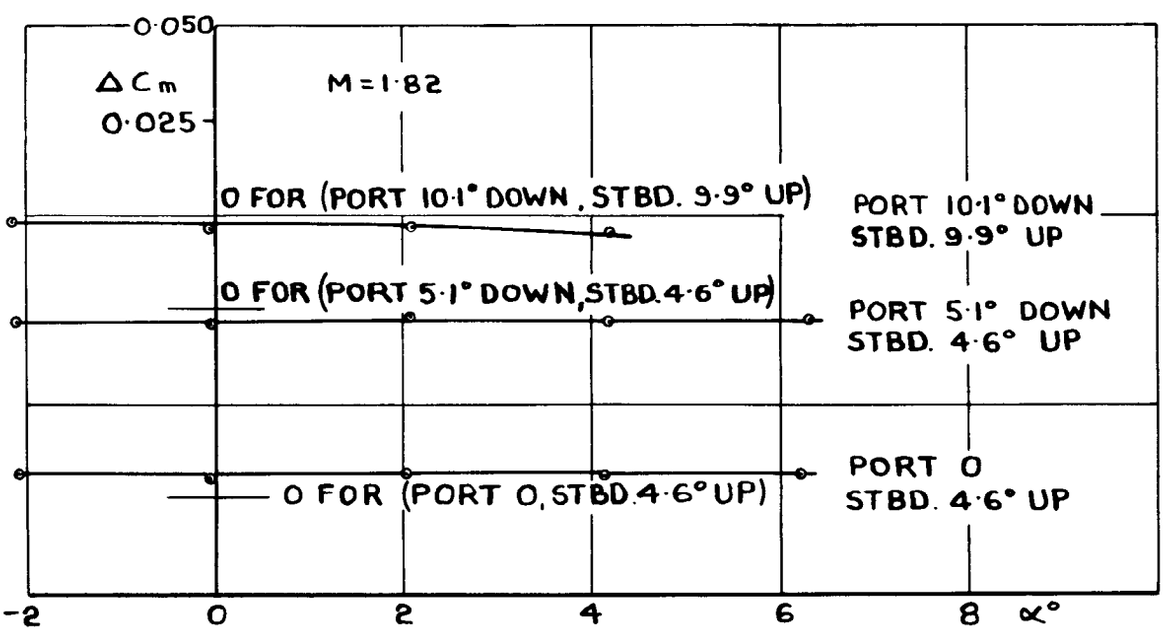

FIG. 31. CHANGE IN PITCHING MOMENT COEFFICIENT DUE TO AILERON DEFLECTION.

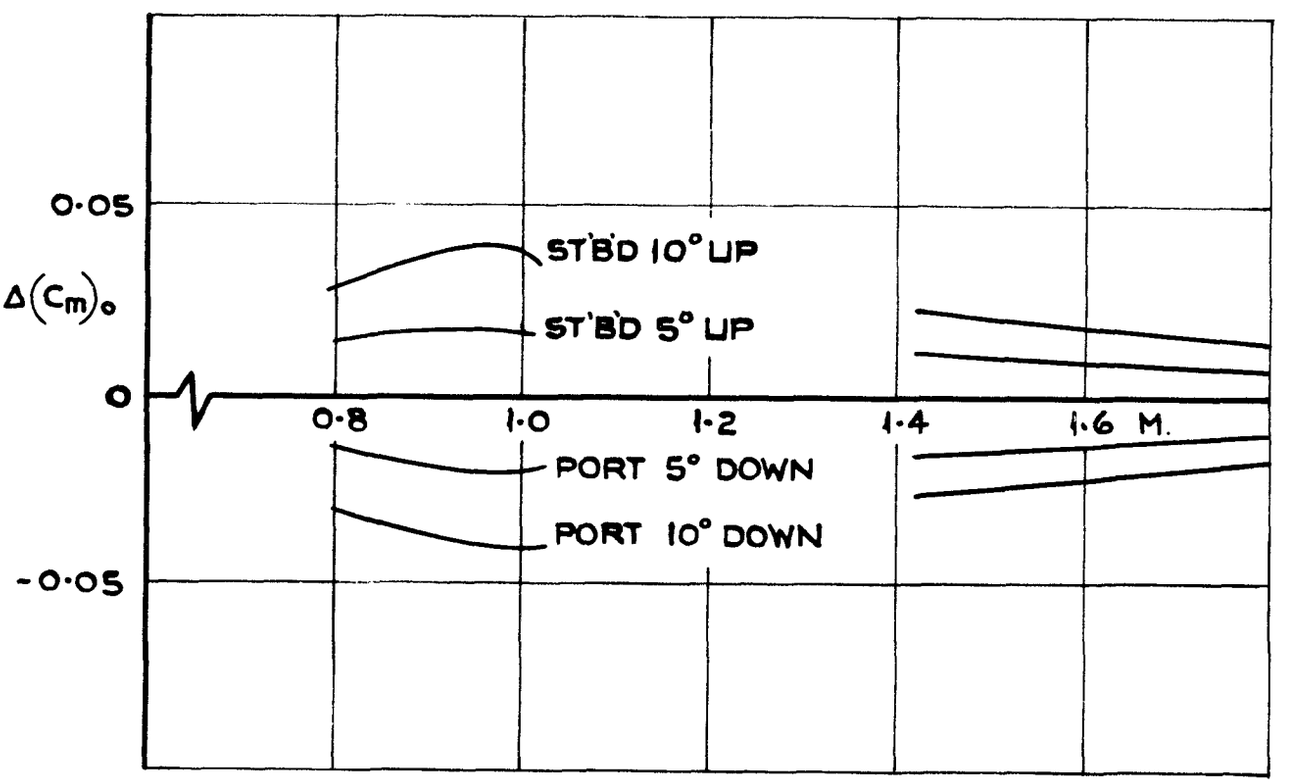

FIG.32. VARIATION WITH MACH NUMBER OF ΔC_m DUE TO AILERON DEFLECTION AT ZERO INCIDENCE

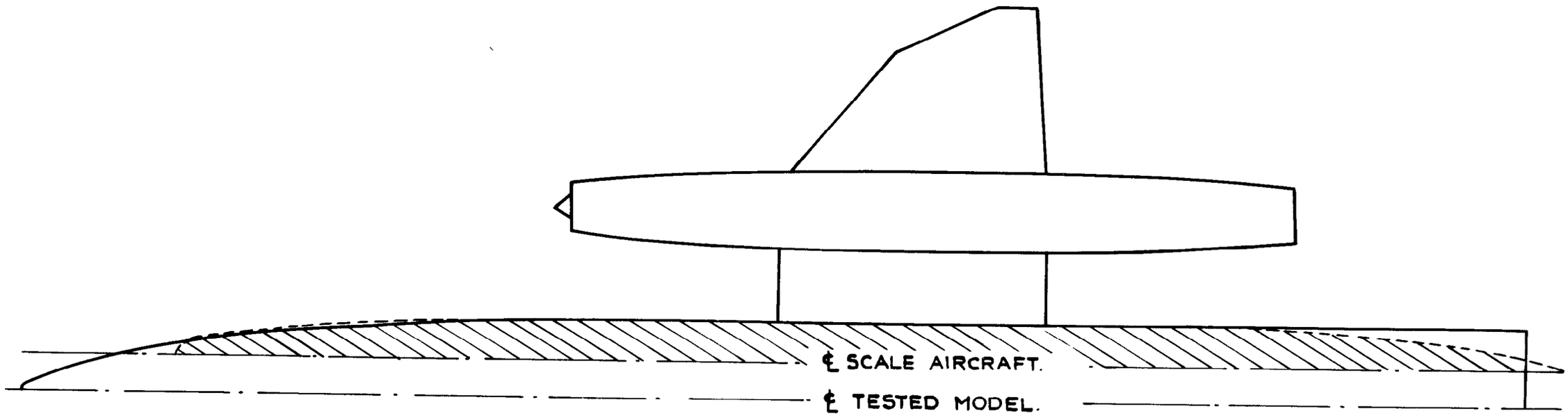

FIG. 33. COMPARISON OF BODY SIZES OF THE SCALE AIRCRAFT AND THE TESTED MODEL.

Printed in England for Her Majesty's Stationery Office by the Royal Aircraft Establishment, Farnborough. W.T.60. K.4.

A.R.C. C.P. No. 798 533.6.011.35/5 Bristol 188

WIND TUNNEL TESTS AT MACH NUMBERS UP TO 1.8 ON A MODEL WITH 1/36 SCALE WINGS AND NACELLES OF A TWIN-ENGINED SUPERSONIC AIRCRAFT (BRISTOL 188). Sutton, E.P., Hutton, P.G. and Squire, L.C. February 1958.

Tests have been made in the R.A.E. Bedford 3 foot tunnel on a model representing the exposed wing and nacelles of the Bristol 188 aircraft, mounted on an ogive-cylinder body. The wing was unswept inboard but had a swept-back leading edge outboard of the nacelles. Lift, drag, and pitching moment, and rolling moment due to aileron deflection, were measured at Mach numbers between 0.7 and 1.02 and between 1.4 and 1.8 at a Reynolds number of 1.7×10^6 based on mean aerodynamic chord.

At high subsonic speeds separations on the unswept inner wing dominate the characteristics of the model at incidence. Fitting leading edge vortex generators delays the effects of leading edge separation. The horn-balanced ailerons are effective throughout the test range.

The surface oil-flow technique was used as an aid to interpretation of the measurements.

A.R.C. C.P. No. 798 533.6.011.35/5 Bristol 188

WIND TUNNEL TESTS AT MACH NUMBERS UP TO 1.8 ON A MODEL WITH 1/36 SCALE WINGS AND NACELLES OF A TWIN-ENGINED SUPERSONIC AIRCRAFT (BRISTOL 188). Sutton, E.P., Hutton, P.G. and Squire, L.C. February 1958.

Tests have been made in the R.A.E. Bedford 3 foot tunnel on a model representing the exposed wing and nacelles of the Bristol 188 aircraft, mounted on an ogive-cylinder body. The wing was unswept inboard but had a swept-back leading edge outboard of the nacelles. Lift, drag, and pitching moment, and rolling moment due to aileron deflection, were measured at Mach numbers between 0.7 and 1.02 and between 1.4 and 1.8 at a Reynolds number of 1.7×10^6 based on mean aerodynamic chord.

At high subsonic speeds separations on the unswept inner wing dominate the characteristics of the model at incidence. Fitting leading edge vortex generators delays the effects of leading edge separation. The horn-balanced ailerons are effective throughout the test range.

The surface oil-flow technique was used as an aid to interpretation of the measurements.

A.R.C. C.P. No. 798 533.6.011.35/5 Bristol 188

WIND TUNNEL TESTS AT MACH NUMBERS UP TO 1.8 ON A MODEL WITH 1/36 SCALE WINGS AND NACELLES OF A TWIN-ENGINED SUPERSONIC AIRCRAFT (BRISTOL 188). Sutton, E.P., Hutton, P.G. and Squire, L.C. February 1958.

Tests have been made in the R.A.E. Bedford 3 foot tunnel on a model representing the exposed wing and nacelles of the Bristol 188 aircraft, mounted on an ogive-cylinder body. The wing was unswept inboard, but had a swept-back leading edge outboard of the nacelles. Lift, drag, and pitching moment, and rolling moment due to aileron deflection, were measured at Mach numbers between 0.7 and 1.02 and between 1.4 and 1.8 at a Reynolds number of 1.7×10^6 based on mean aerodynamic chord.

At high subsonic speeds separations on the unswept inner wing dominate the characteristics of the model at incidence. Fitting leading edge vortex generators delays the effects of leading edge separation. The horn-balanced ailerons are effective throughout the test range.

The surface oil-flow technique was used as an aid to interpretation of the measurements.

Published by
HER MAJESTY'S STATIONERY OFFICE

To be purchased from
York House, Kingsway, London w.c.2
423 Oxford Street, London w.1
13A Castle Street, Edinburgh 2
109 St. Mary Street, Cardiff
39 King Street, Manchester 2
50 Fairfax Street, Bristol 1
35 Smallbrook, Ringway, Birmingham 5
80 Chichester Street, Belfast 1
or through any bookseller

S.O. CODE No. 23-9015-98